PROCEEDINGS
OF THE
INTERNATIONAL
CONFERENCE
ON
MARTENSITIC
TRANSFORMATIONS
ICOMAT 1979

CAMBRIDGE, MASSACHUSETTS
USA

24-29 JUNE 1979

International Committee

G. S. Ansell (USA)
J. S. Bowles (Australia)
J. W. Christian (Great Britain)
M. Cohen (USA)
L. Delaey (Belgium)
F. E. Fujita (Japan)
E. Hornbogen (W. Germany)
P. M. Kelly (Australia)
L. G. Khandros (USSR)

G. V. Kurdjumov (USSR)
Z. Nishiyama (Japan)
J. Nutting (Great Britain)
W. S. Owen (USA)
V. D. Sadovsky (USSR)
K. Shimizu (Japan)
I. Tamura (Japan)
H. Warlimont (W. Germany)
C. M. Wayman (USA)

United States Organizing Committee

G. S. Ansell
P. C. Clapp
M. Cohen
R. F. Hehemann
D. S. Lieberman
G. Krauss

G. B. Olson
J. Perkins
G. Thomas
C. M. Wayman
P. G. Winchell
W. S. Owen, Chairman

Program Committee

G. S. Ansell
P. C. Clapp
G. B. Olson
J. Perkins

K. Shimizu
G. Thomas
P. G. Winchell
C. M. Wayman, Chairman

Arrangements Committee

M. Cohen
M. A. Meyer
W. S. Owen

Finance Committee

M. Cohen
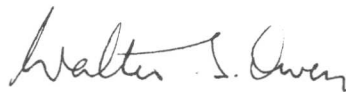W. S. Owen
G. S. Ansell, Chairman

Editorial Office

Department of Materials Science and Engineering
Massachusetts Institute of Technology
Cambridge, Massachusetts 02139

PREFACE

The papers collected together in this volume constitute the Proceedings of the International Conference on Martensitic Transformations (ICOMAT-79) held at the Massachusetts Institute of Technology, Cambridge, Massachusetts, U.S.A. on 24-29 June 1979. The conference was the third in a series of international conferences on martensitic transformations. The first was held at Kobe, Japan on 10-12 May 1976 and the second (ICOMAT 77) in Kiev, U.S.S.R. on 15-20 May 1977. The central theme in all three was martensitic transformation, but each conference emphasized different aspects of this broad and perplexing subject. At ICOMAT-79 attention was directed towards the basic scientific understanding of this class of transformations. Thus, whereas in these Proceedings there are many papers dealing with transformation mechanisms, papers dealing with the mechanical properties of the products of martensitic transformations are included only when they shed some light on the nature of the transformations.

In recent years an amazing variety of crystallographically displacive transformations have been described and studied. It is clear that martensitic transformations must be included in the general classification of displacive transformations; it is far from clear whether or not all displacive transformations are martensitic. In the first paper Drs. Cohen, Olson and Clapp discuss this dilemma in some detail and propose a classification scheme which reveals the interrelationships between different types of displacive transformation. This paper is an extended version of the keynote address which Professor Morris Cohen delivered at the opening of the conference. Throughout the conference, many speakers approached aspects of this theme from many different individual points of view. In this way a primary objective of the conference – to approach a synthesis of the work in physics on displacive transformations with that in metallurgy on martensitic transformations – was achieved. On reading the papers here collected, it is evident that the synthesis is incomplete. Much work remains for future conferences to bring into being a homogeneous, self-consistent theoretical framework embracing all displacive transformations.

The conference was attended by 146 scientists from 19 different countries. All who attended recognize that the success of the conference was in large measure due to the excellent work of the secretariat directed by Ms. Marguerite A. Meyer, who also saw this volume through publication, and of the different organizing committees. Membership of the latter and a list of the agencies which financially supported the conference will be found on pages ii and v. Special mention must be made of the work of Professor C. M. Wayman who was Chairman of the Program Committee. To him and to all the people and organizations who contributed we offer our special thanks.

Walter S. Owen
Chairman, ICOMAT-79

Cooperating Societies

American Society for Metals

Associazione Italiana di Metallurgia

The Australasian Institute of Metals

Dansk Metallurgisk Selskab

Deutsche Gesellschaft für Metallkunde

The Institute of Scientific and Industrial Research

The Iron and Steel Institute of Japan

The Japan Institute of Metals

The Metallurgical Society of AIME

Verein Deutscher Eisenhüttenleute

The Metals Society (Great Britain)

ACKNOWLEDGMENTS

CONTENTS

II. THERMODYNAMICS AND KINETICS

Keynote

- x -

III. PRETRANSFORMATION EFFECTS

Keynote

IV.   AGING PHENOMENA

Keynote

On the Classification of Displacive Phase Transformations

Morris Cohen,[*] G. B. Olson,[*] and P. C. Clapp[**]

Our objective is to arrive at a set of necessary and sufficient characteristics for defining a martensitic transformation, keeping in mind the traditional usage of this term in metallurgical circles as well as its growing application to displacive phase transformations more generally. We start with the full class of displacive/diffusionless transformations, and then establish a scheme of categories and subcategories with increasing constraints until a logical and useful characterization of a martensitic transformation emerges. While this classification approach is based on the nature of the atomic displacements at play between the parent and product phases, operational emphasis is given to the consequences of these displacements reflecting the extent to which elastic strain energy controls the kinetics and morphology of the transformation. Thus, we conclude that: (1) within the overall class of displacive/diffusionless phase transformations, martensitic transformations are dominated, not by atom shuffling, but by homogeneous lattice deformations; (2) within the latter category, martensitic transformations are dominated, not by dilatational displacements, but by deviatoric (shear) displacements; and (3) within the latter subcategory, the resulting shape-change must be sufficiently large so that the associated strain energy exerts a dominant influence on the kinetics and morphology of the transformation. For those transformations which qualify for criteria (1) and (2) above, but not for (3), we introduce the term quasimartensitic. We also consider the implications of concomitant diffusion phenomena, and propose that incidental diffusion occurring in an otherwise-martensitic transformation should not disqualify the transformation from being called martensitic, inasmuch as such diffusion is not required for the transformation. When, however, concomitant diffusion is required for a displacive transformation, as in the case of bainites, we do not advise applying the term martensitic.

I. Introduction

A significant part of scientific understanding is based on the classification of natural phenomena -- the placing of entities into hierarchical categories. This is the approach we now take in attempting to reassess, and hence possibly to redefine, the essential nature of a martensitic transformation. It is a fitting subject, indeed, for opening an International Conference on Martensitic Transformations, particularly in the light of (a) the rapidly advancing knowledge-base concerning this type of solid-state reaction, and (b) the increasing application of the name "martensitic" to many transformations occurring in nonmetallic systems. Perhaps we have

---

* Department of Materials Science and Engineering, Massachusetts Institute of Technology, Cambridge, MA 02139, USA.

** Department of Metallurgy, University of Connecticut, Storrs, CT 06268, USA.

reached a further stage in our understanding of structural changes when, again, the definition of martensitic transformations should be broadened. But if so, we may be in danger of stretching this term so out-of-shape that another name will have to be coined for the traditional class of martensitic transformations.

Phase transformations[+] in the solid state have been classified in various ways by Christian [1], Lieberman [2], and Warlimont [3]. References [1] and [2] include martensitic transformations, while reference [3] is directed to martensitic transformations primarily. Our approach is similar to the latter, but starts with the "universe" of displacive phase transformations because martensitic transformations are fully contained in this set. Moreover, it is not our intent here to deal with the entire array of solid-state reactions. We propose to develop a classification scheme which identifies broad categories of displacive transformations having features in common with martensitic transformations, but yet being usefully distinct from the martensitic class. In so doing, we want to arrive at the necessary and sufficient characteristics which qualify a solid-state phase transformation to be called <u>martensitic</u>.

The scheme in question arises from an attempt to classify displacive transformations solely from knowledge of (a) the crystal structures of the parent and product phases, and (b) the relation between these two structures during the transformation (i.e., the lattice correspondence, as may be deduced from shape-change measurements [4]). With this information it is possible to describe in quantitative terms the nature of the atomic displacements which produce the transformation and which, in effect, constitute the root cause of its character. When one differentiates among atomic displacements of different types, however, it appears that a spectrum of displacive transformations may exist wherein the relative magnitudes of these displacements will vary almost continuously from system-to-system; any important changes in the macroscopic character of the transformations will depend not only on the magnitudes of the atomic displacements, but also on the physical properties (of both phases) that determine the energetic consequences of the displacements. Unfortunately, the various energies at play (interfacial energy, strain energy, transformational driving force, etc.) are generally not known in the same quantitative detail as are the atomic displacements. Consequently, it was decided to link our proposed classification demarcations to the macroscopic kinetic and morphological character of a transformation (controlled in principle by the various energies at play), and all this within a framework based conceptually on the nature of the atomic displacements.

+ In the literature, the terms "phase transformation" and "phase transition" are sometimes used interchangeably. We prefer the former as the more inclusive set, and we are inclined to reserve the latter for the subset of higher-order or continuous (not nucleation and growth) transformations. However, this distinction is not a real issue in the present paper.

Although we shall later consider the complication of various types of diffusion taking place during the transformation, we first restrict our attention to the classification of displacive transformations which are diffusionless, meaning there is no random-walk mixing of atoms during the transformation.

II. Classification of Displacive/Diffusionless Phase Transformations

We define a displacive phase transformation as a structural change in the solid state which occurs by coordinated shifts of atoms. Any such transformation can be described as a combination of a homogeneous lattice deformation (or distortion) and shuffles [5].

A lattice deformation is a homogeneous strain which converts one Bravais lattice to another [6]. This is the same as a Bain strain or Bain distortion - the term originally adopted for the fcc→bcc and fcc→bct lattice deformations in iron-base martensitic transformations.

A shuffle is a coordinated shift of atoms within a unit cell which, in itself, does not produce a homogeneous lattice-distortive strain [7]. Shuffle displacements may be planar, linear, or more complex (e.g., coordinated rotations of atomic groupings within unit cells).

Hence, we can distinguish between two kinds of atomic displacements in displacive phase transformations: lattice-distortive displacements and shuffle displacements. These are illustrated in Figure 1.
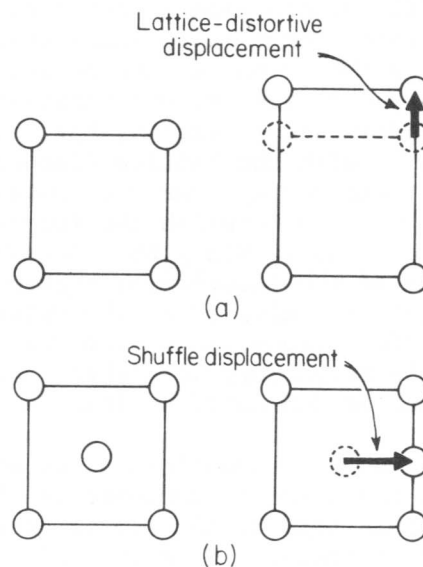
Schematic illustration of simple lattice-distortive
and shuffle displacements

Figure 1

While lattice-distortive displacements will give rise to elastic strain energy, the shuffle displacements per se will influence interfacial energy only. Therefore, we may expect major differences in the kinetic and morphological character of transformations that consist of only one type of displacement or the other. For transformations comprising both types of displacement, expressing the lattice distortion in terms of relative displacements within a unit cell, as illustrated in Figure 1, allows a direct comparison of the most prominent largest displacements of each kind; this then may provide an indication of which kind of displacement will dominate the transformation.

The idea that either lattice-distortive or shuffle displacements may dominate the character of a displacive phase transformation brings us to the first division in the classification scheme for displacive/diffusionless transformations represented in Figure 2. While the relative magnitudes of the largest shuffle and lattice-distortive displacements or the relative magnitudes of interfacial energy and strain energy accompanying the transformation can provide a rough guide as to which type of displacement is more important, we are presently adopting an operational separation between shuffle transformations and lattice-distortive transformations based on the single criterion as to whether or not the kinetics and morphology during transformation are dominated by shuffle displacements. Shuffle transformations then include not only those transformations which occur solely by shuffle displacements, but also those involving additional lattice-distortive displacements as long as these displacements are small enough not to significantly alter the kinetic and morphological character of the transformation. Examples of shuffle transformations include the ferroelastic displacive transformation in strontium titanate [8] which is described entirely in terms of shuffle displacements (rotation of oxygen tetrahedra); indeed, the associated strain energy is so small that the transformation can occur continuously from the parent to the product phase. The familiar $\beta \rightarrow \omega$ transformation in Ti- and Zr-base alloys entails a small lattice distortion in addition to shuffle displacements, but the mechanism and kinetics are dominated by shuffles -- with the lattice distortion playing such a secondary role that the strain energy does not control the morphology [9]. The shuffle displacements which accomplish the ferroelectric transformations in KH_2PO_4 [10] and high-resistivity $KTa_{.65}Nb_{.35}O_3$ (KTN) [11] cause a large electrostatic contribution to the interfacial energy which, in turn, results in a transformation morphology dominated by the anisotropy of interfacial energy. For shuffle transformations, then, the role of strain energy is sufficiently small that the morphology is either that of a continuous transformation or one which is dominated by interfacial energy.

In contrast, displacive transformations in which shuffles are either absent or insufficient in magnitude to dominate the kinetics and morphology fall into the class of lattice-distortive transformations in Figure 2. These are further divided according to the type of lattice deformation. A starting point in the crystallographic theories of martensitic transformations is the assumption that the lattice deformation itself produces an undistorted line which, if unrotated, becomes an invariant line during the transformation [12, 13]. Hence, a necessary condition for a transformation that might ultimately fall into the class of martensitic transformations
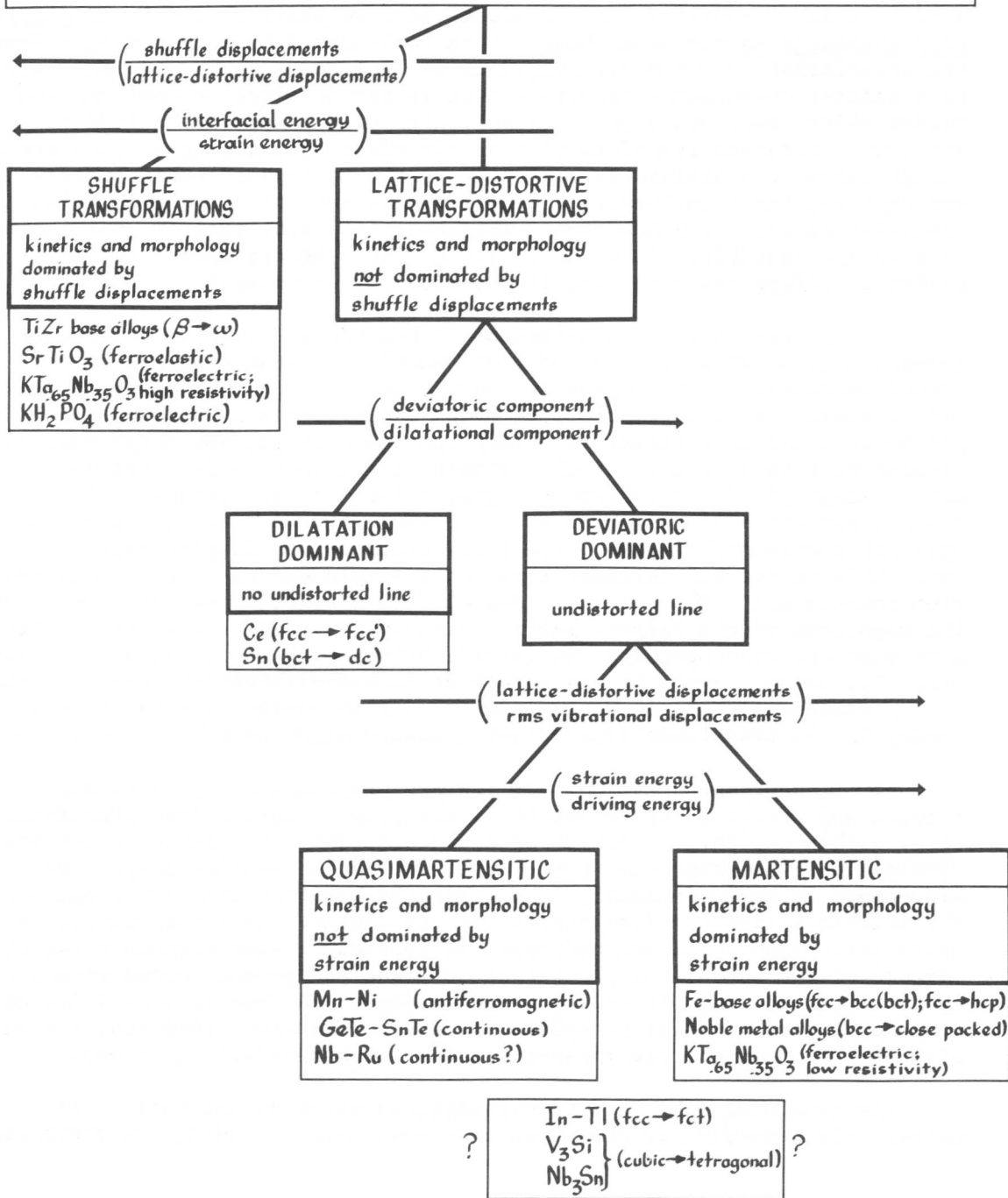
Proposed classification scheme for displacive/diffusionless phase
transformations

Figure 2

is for the lattice deformation to yield an undistorted line. Separating the lattice deformation into dilatational and deviatoric (shear) components, the relative magnitudes of these two components will determine whether or not there is an undistorted line. Accordingly, if there is no undistorted line in a lattice-distortive transformation, we shall regard it as <u>dilatation dominant</u>; on the other hand, if an undistorted line does result from the transformation, we shall regard it as <u>deviatoric dominant</u>. An example of a dilatation-dominant transformation is the fcc→fcc' transformation in cerium which undergoes a pure volume contraction of 16% below 100K [14]. The low-temperature transformation in tin might also belong to this class[+]; though there is a deviatoric component in the tetragonal→cubic lattice deformation, the transformation appears to be dominated by a 12% volume expansion on cooling below room temperature [15] such that an undistorted line is not possible. There is evidence that some transformations in plutonium alloys may also fall in the dilatation-dominant class [16].

An important point now arises as to whether all lattice-distortive transformations with undistorted lines should be classed as martensitic transformations. In our opinion, those cases in which the displacements are so small that the transformation can occur continuously should certainly not be regarded as martensitic. Then the question is, how large must the displacement be in order for the transformation to fall into the martensitic category? In discussing the displacive transformations in A15 compounds, Barrett [17] has noted that, in these transformations which nearly approach continuous behavior, the lattice-distortive displacements are comparable to the rms lattice-vibrational displacements at the transformation temperature. Thus, as an index of displacement size, one might compare the magnitude of the largest lattice-distortive transformational displacement with the corresponding rms lattice-vibrational displacement. Alternatively, because a major consequence of lattice-distortive displacements is the associated (shape-change-induced) strain energy, the ratio of strain energy to the transformational driving energy might be adopted as an index.

For present purposes, however, we are proposing a fairly straightforward and practical criterion for identifying a martensitic transformation, within the larger context of deviatoric-dominant, lattice-distortive displacive transformations; namely, we require the lattice-distortive displacements to be sufficiently large that the kinetics and morphology during the transformation are dominated by strain energy. As a consequence, a martensitic transformation undergoes nucleation, passes through a two-phase mixture of the parent and product phases, and the product grows with a transformation front in a plate-like or lath-like shape that is indicative of a tendency toward an invariant-plane interface. In these respects, martensitic transformations are first-order (not higher-order) reactions.

The remaining subset of transformations which do not qualify as martensitic according to the above criterion, and including the previously

---

+ If the kinetics of this transformation in tin are controlled by thermally-activated shuffle displacements, it might better be classed as a shuffle transformation; enough information is not available to settle this point at the present time.

mentioned continuous cases, is designated as <u>quasimartensitic</u> in Figure 2. Examples in this class include various continuous magnetic transitions accompanied by deviatoric-dominant lattice distortions, such as the anti-ferromagnetic transition in Mn-Ni alloys [18]. The fcc→rhombohedral transformation in the GeTe-SnTe system is clearly continuous [19] as well as lattice-distortive and diffusionless. There is some evidence that a lattice-distortive transformation in Nb-Ru alloys also occurs in a continuous manner [20] and so can be tentatively classed as quasimartensitic.

Examples of true martensitic transformations include, of course, the classicial fcc→bcc (bct) and fcc→hcp transformations [21] in Fe-base alloys as well as many transformations from bcc to close-packed structures in noble-metal alloys [22]. The transformation in low-resistivity $KTa_{.65}Nb_{.35}O_3$ (KTN) [11] provides an interesting case illustrating that, although the classification scheme is grounded conceptually on the nature of the atomic displacements, the actual classification criteria adopted here depend sensitively on the energetic consequences of these displacements. The transformation in high-resistivity KTN (mentioned previously) is dominated by the highly anisotropic electrostatic contribution to the interfacial energy [11] arising from the shuffle displacements, and so we can classify that transformation as a shuffle transformation. However, when the same structural transformation occurs in lower-resistivity material, electronic conduction eliminates these charge effects [11]. The strain energy associated with the lattice distortion then dominates and results in an invariant-plane interface. Under these conditions, the transformation is properly classed not only as lattice-distortive, but also as martensitic.

The box at the bottom of Figure 2 indicates some interesting possible "borderline" cases in the distinction between martensitic and quasimarten-sitic transformations. It is to be expected that a given structural transformation which occurs over a range of temperatures or thermodynamic conditions might exhibit more than one mode of transformation. While the fcc→"fct" transformation in uniformly-cooled In-Tl alloys apparently proceeds initially by the formation of martensitic plates [23], there is some evidence that else-where in the specimen the transformation on further cooling takes place by a continuous quasimartensitic mode [24]. It is possible that the cubic→tetragonal transformations in A15 compounds such as V_3Si and Nb_3Sn may also occur either continuously or by some mixture of martensitic and quasimarten-sitic modes [25, 26]. Available information with respect to the morphologi-cal changes <u>during</u> these transformations is inadequate to classify them con-clusively at this time. Nevertheless, these cases serve to emphasize that classification of a displacive transformation according to the proposed scheme cannot be made simply by noting the final morphology of the transforma-tion <u>product</u>; rather, knowledge is required concerning the morphological relations between parent and product phases <u>during</u> the transformation. It is, after all, the transformation itself that is being classified.

III. Some Variations of Martensitic Transformations

It will be evident now that in developing the suggested classification criteria emerging primarily from structural considerations, we have delib-

erately avoided many distinctions among subtypes of martensitic transformations. As a case in point, we have not been concerned with the origin of thermodynamic driving forces (e.g., electronic, ferromagnetic, ferroelectric, ferroelastic, applied stress, etc.) or with transformation micromechanisms (e.g., heterophase-fluctuation/phonon vs. dislocation modes, etc.). These, or any other aspects of displacive transformations, could be used to subdivide any of the classes shown in Figure 2. For example, there are interesting subsets of martensitic transformations according to thermoelastic vs. nonthermoelastic behavior, or lath vs. plate morphology, or isothermal vs. athermal vs. anisothermal kinetics, or thermally-induced vs. deformation-induced transformations.

Other martensitic subclasses stem from twinning vs. slip processes in the lattice-invariant deformations which often accompany martensitic transformations. The nature of the lattice-invariant deformations exerts a significant influence on the habit and fine structure of the martensitic product (and, in turn, on its properties), but these deformations per se are not a defining characteristic of martensitic transformations as a class. In fact, they need not occur at all in martensitic fcc→hcp transformations.

Shuffle transformations might also be usefully subdivided depending on the nature of the shuffle displacements (e.g., linear, planar, rotational, etc.). But in view of our overall objective toward a precise definition of martensitic transformations, the scheme represented by Figure 2 is intended to emphasize only what is _essential_ to martensitic transformations, and what characteristics set them apart from other broad classes of displacive diffusionless transformations.

IV. Diffusion in Displacive Transformations

The classification chart in Figure 2 is restricted to diffusionless categories, but diffusion is not necessarily excluded from displacive transformations. We now allow diffusional processes to enter the classification scheme in a manner orthogonal to the plane of Figure 2. Thermally-activated atomic mixing may operate to varying extents in any of the structural changes that we have considered here, and so new questions arise regarding the terminology that we have developed thus far for diffusionless transformations.

We can visualize two levels of diffusion which have a bearing on the definition of martensitic and other displacive transformations:

(1) The diffusion in question may occur incidentally to a martensitic transformation without being essential to the displacive changes in any way. Diffusion of this sort is only a happenstance, as in the self-aging of iron-carbon martensitic products, and should not in itself remove a transformation from the martensitic category, even though such inadvertent diffusion may have occurred concomitantly. Consequently, it now seems realistic and justifiable to relax somewhat the "diffusionless" requirement of a martensitic transformation from "absolutely" diffusionless to "virtually" diffusionless.

(2) On the other hand, diffusion may function in a major, even rate-controlling, way during a lattice-distortive transformation. This diffusion may be short-range, as in the order-disorder transformation which generates a superlattice with surface reliefs in AuCu [27]; or it may be long-range, as in bainitic-types of transformations [28]. Among the latter, we can include the isothermal non-pearlitic transformations in steel, the formation of Widmanstätten ferrite from austenite [29], and the intermediate $\beta \rightarrow \alpha$ transformation in copper-zinc alloys [30], all of which are lattice-distortive but require long-range compositional changes to attain enough driving force for their operation. Because diffusion is vital to the occurrence of these displacive transformations, they cannot be described as virtually diffusionless and, hence, are not classed as martensitic in our proposed terminology.

The lattice-distortive transformations which are controlled by long-range diffusion shed further light on the nature of lattice deformations in structural changes. When the diffusing species is interstitial as with carbon or nitrogen in fcc iron, one can readily imagine that a fixed array of host atoms in the parent phase is carried over into a corresponding array of host atoms in the product phase, no matter how the interstitial atoms may happen to rearrange themselves. But this is not feasible in the copper-zinc case wherein both atomic species are diffusing substitutionally in opposite directions, and so a fixed array of the respective atomic species cannot be identified. Instead, the observed surface upheavals suggest that a lattice network tends to be preserved during the lattice deformation despite the uncoordinated jumping of atoms among the lattice points. This indicates that the lattice as such may have more significance than do the atoms themselves in the maintenance of correspondence during a lattice-distortive phase change.

These concepts then allow a further extension of our classification scheme for displacive transformations in general. While the displacive character of a transformation can be classified according to the criteria represented in Figure 2, each category can be further subdivided according to whether diffusion which might accompany the transformation is incidental or necessary. Cases in the latter group can be further subdivided as to whether a particular "sublattice" of atoms is preserved during diffusion, or whether only a lattice network is maintained to account for the displacive character.

V. What, Then, Is a Martensitic Transformation?

Our logic in this paper has been (a) to select an hierarchical system of structural changes in the solid state, encompassing the martensitic transformations we wish to define, and then (b) to follow down through more and more restricted categories, justifying the decisions we have made at the several "forks in the road", and finally arriving at the necessary and sufficient characteristics for classifying a phase transformation as martensitic. The pathways traced out in this process have been guided primarily by crystallographic concepts and related operationally-accessible phenomena rather than by solid-state theories and transformation mechanisms. The latter two arenas of scientific thought are

-9-

exciting and challenging, but our present purpose is best served by not allowing the martensitic definition being sought to depend on theories and mechanisms. Putting this point the other way around, the essential features of a martensitic transformation, once identified, are what the theorists and mechanicians should then strive to explain.

We conclude that: "A martensitic transformation is a lattice-distortive, virtually diffusionless structural change having a dominant deviatoric component and associated shape change such that strain energy dominates the kinetics and morphology during the transformation."

These characteristics are typified by a course of transformation which involves nucleation, a parent/product two-phase regime, and a growth front tending toward an invariant-plane interface. It becomes evident that the morphological features, which are so important in identifying martensitic transformations, cannot be reliably disclosed by bulk measurements; microstructural techniques (especially applied during the course of the transformation) are indispensable. One can also see that the commonly-ascribed combination of "displaciveness and diffusionlessness" is neither necessary nor sufficient for rigorously defining a martensitic transformation.

The above definition retains a secure place for the well-known martensitic transformations familiar to the metallurgists, but also incorporates many of the newer transformations appearing in nonmetals and compounds. This growing profusion of phase changes which can now be rigorously classed as martensitic transformations will surely lead to a new symbiotic inter-mixing of the disciplines that intersect in materials science, and all of this should pave the way toward a much deeper understanding of the nature and cause of martensitic transformations. Thus, the proposed definition has the prospect of being both useful and intellectually stimulating.

Acknowledgments

REFERENCES

[1] J. W. Christian: The Theory of Transformations in Metals and Alloys, Part I. Equilibrium and General Kinetic Theory, Pergamon Press, Oxford (1975).
[2] D. S. Lieberman: Phase Transformations, ASM, Metals Park, Ohio (1970), Ch. 1.
[3] H. Warlimont: J. Microsc. Spectrosc. Electron., 2 (1977), 333.
[4] H. M. Clark and C. M. Wayman: Phase Transformations, ASM, Metals Park, Ohio (1970), Ch. 2.
[5] J. W. Christian: ibid. p. 55.
[6] J. W. Christian: ibid. p. 40.

[7] J. W. Christian: ibid. p. 50.

[8] J. F. Scott: Rev. Mod. Phys., 46 (1974), 83.

[9] D. deFontaine, N. E. Paton, and J. C. Williams: Acta Met., 19 (1971), 1153

[10] J. Bornarel and J. Lajzerowicz: J. Phys. Soc. Japan, 28 Suppl. (1970), 360; J. F. Scott; ibid. p. 113.

[11] M. DiDomenico, Jr. and S. H. Wemple: Phys. Rev., 155 (1967), 539.

[12] J. S. Bowles and J. K. Mackenzie: Acta Met., 2 (1954), 129.

[13] M. S. Wechsler, D. S. Lieberman, and T. A. Read: Trans. AIME, 197 (1953), 1503.

[14] M. S. Rashid and C. J. Alstetter: Trans. TMS-AIME, 236 (1966), 1649.

[15] E. O. Hall: The Mechanism of Phase Transformation in Metals, Inst of Metals Monograph No. 18, London (1956), 87.

[16] S. F. Hecker, Los Alamos Scientific Laboratory, private communication, 1979.

[17] C. S. Barrett: Trans. Japan Inst. Metals, 17 (1976), 465.

[18] V. Hocke and H. Warlimont: J. Phys. F.: Metal Phys., 7 (1977), 1145.

[19] J. N. Bierly, L. Muldawer, and O. Beckman: Acta Met., 11 (1963), 447.

[20] B. K. Das and D. S. Lieberman: Acta Met., 23 (1975), 579.

[21] Z. Nishiyama: Martensitic Transformations, Academic Press, N. Y. (1978), Table 2.4, 115.

[22] H. Warlimont and L. Delaey: Prog. Matr. Sci., 18 (1974), 1.

[23] L. Guttman: Trans. AIME, 188 (1950), 1472.

[24] L. Guttman: ibid. Fig. 5, 1475.

[25] L. R. Testardi and T. B. Bateman: Phys. Rev., 154 (1967), 402.

[26] R. Mialfert, B. W. Batterman, and J. J. Havak: Phys. Stat. Sold., 32 (1969), K67.

[27] R. Smith and J. S. Bowles: Acta Met., 21 (1973), 961.

[28] R. F. Hehemann: Phase Transformations, ASM, Metals Park, Ohio (1970) Ch. 9.

[29] J. D. Watson and P. G. McDougall: Acta Met., 21 (1973), 961.

[30] R. D. Garwood: Physical Properties of Martensite and Bainite, Special Report 93, Iron and Steel Inst., London (1965), 90.

TRANSMISSION ELECTRON MICROSCOPY CHARACTERIZATION OF

DISLOCATED "LATH" MARTENSITE

B. V. Narasimha Rao and G. Thomas
University of California

Department of
Materials Science and Mineral Engineering
and
Materials and Molecular Research Division
Lawrence Berkeley Laboratory
Berkeley, California 94720

ABSTRACT

In this paper, a summary of the recent observations made with high resolution transmission electron microscopy on the morphology, crystallography and formation of "lath" martensite is presented. The present work has confirmed earlier observations that within each packet the adjacent "laths" are separated by rotation boundaries, such that a $180°$ rotation of the reference shear vector is achieved in a group of adjacent laths. The number of laths required to achieve this rotation decreases as the carbon content is increased from 0 to 0.4 wt.%. Concomitant with this, the tendency for adjacent twin related laths increases with carbon content. Retained austenite is found only in carbon containing alloys and even in these alloys it is found only if the adjacent laths are not twin related. High resolution lattice imaging at the retained austenite/lath martensite interface has revealed substantial carbon segregation in austenite during the shear transformation and this raises fundamental questions in regard to whether "lath" martensites are truly martensitic. Lattice imaging also revealed the presence of interfacial ledges at the retained austenite/lath martensite interface.

Introduction

There are two basic morphologies of bulk martensite in ferrous alloys (1-3): dislocated lath martensite and twinned plate martensite. The former is usually associated with steels for carbon contents of less than about 0.4 wt.% with a total alloy content such that the M_s is not far below about $250°C$. Plate martensites occurring in steels of high alloy concentrations have been extensively studied (1,4) and the crystallography of this transformation is well understood (1,5). However, as has been pointed out previously (6) a complete understanding of the crystallography, the transformation mechanism and the precise morphology of the technologically more important lath martensite is lacking. As a result of detecting austenite in these steels (7,8) however, it has been shown (6) that direct crystallographic analysis on austenite serves to

-12-

eliminate scatter in the published crystallographic data (9,10) for the lath martensite transformation.

Several important questions remain unanswered regarding the mechanism of the lath martensite formation. For example, the independent nucleation and growth events of this transformation are not clearly established (11-14). Studies using two adjacent lath orientations yielded no concrete results on the accommodation of shape strain for this transformation (15,16). In particular, the above aspects have to be re-examined in the light of the identification of retained austenite. This paper is a summary of a detailed characterization of lath martensite using conventional, high resolution and high voltage transmission electron microscopy to be reported in full elsewhere (17) and is a continuation of the work first reported at the Kiev Conference in 1977 (6).

Experimental Procedures

Compositions of the alloys used in this investigation are listed in Table I. The iron-nickel alloys available in the form of thin sheets were first encapsulated in evacuated quartz tubes and austenitized for 1 hour followed by quenching into iced water. The quartz capsule was broken immediately after its contact with the quenching medium. The medium carbon (0.3 wt.%) steels were austenitized in bulk at $1100^{\circ}C$ for 1 hour followed by quenching into iced water or oil. However, for alloy 5 and for the 0.4%C alloy interrupted quenching in the M_s-M_f range was necessary in order to avoid intergranular quench cracking (18). Some of the medium carbon steels were also subjected to grain refining double treatments. Details about these heat-treatments and specimen preparation are discussed elsewhere (18,19). Thin foils made by jet polishing were examined in a Philips EM 301 microscope at 100 KV and also in a Hitachi HU 650 high voltage microscope at 500 KV. The latter was used to utilize the higher resolution capabilities for selected area diffraction (SAD) associated with higher voltages due to lower spherical aberration effects. Detailed SAD analyses were performed on arrays of packets in the alloys studied (Table I). Lattice imaging was done in the Philips EM 301 microscope using tilted beam illumination (20). Laser optical microdiffraction was subsequently conducted to analyze the lattice fringe images (21).

Results

(i) Morphology and Substructure of Martensite

Figures 1 and 2 show examples of a group of dislocated laths within a packet of the binary Fe-15%Ni and the Fe/3Cr/0.5Mo/2Mn/0.3%C alloys respectively. The laths in all the alloys are characterized by fairly straight boundaries except for the curvature at the packet boundaries. The average lath width of the carbon containing alloys is smaller than that of the carbon free alloys (cf. Figs. 1 and 2). Interlath retained austenite has been identified only in the carbon containing alloys, Fig. 3, but not in Fe/Mo/C steels in agreement with previous studies (6, 22). In addition, in the 0.3%C and 0.4%C alloys, quite frequently interweaving packets belonging to two different variants of the habit plane and interference from nucleation of the laths belonging to other variants has been observed.

-13-

(ii) <u>Orientation Analysis of a Group of Adjacent Laths in the Packets</u>

Analysis of many alloys show that two main types of lath orientation occur. In carbon-less alloys, the martensite packets generally consist of groups of parallel laths each lath being separated by successive rotations about $\langle 110 \rangle_m$ or occasionally $\langle 100 \rangle_m$ until the nth lath is 180° rotated from the first (6). The value of n varies but on the average it is five or more (Fig. 1) for the binary Fe-Ni alloys. On the other hand, in the carbon containing alloys, the laths are often twin related. In this case, of course, n=2. Figure 4 shows twin related laths in a 0.3%C steel. The bright-field image contrast clearly shows the identical orientations of laths 1, 3, 5 etc. and of the alternate twin laths 2, 4 etc. This is also confirmed by the SAD patterns. On the average n=3 for the medium carbon steels, Fig. 2.

It is important to emphasize here that the interface twinning plane for adjacent twin related laths in 0.3%C alloys is frequently $\{110\}_m$ and not the $\{112\}_m$. However, the latter has been observed occasionally in 0.3%C alloys and quite extensively in the 0.4%C steel (alloy 9). Associated with $\{112\}_m$ twin related laths is the change in habit plane for the transformation from the widely observed (6) $\{110\}_m$ to the $\{112\}_m$. Also when the interface plane is $\{110\}_m$, then the two adjacent laths, twin related, have identical $\langle 111 \rangle_m$ SAD patterns which superimpose as one pattern if the SAD records both. This point is an important one since this effect has been universally overlooked by other investigators.

(iii) <u>Morphology, Occurrence and Crystallography of Retained Austenite</u>

Figure 3 shows a typical example of the continuous, thin interlath films of retained austenite in the carbon containing alloys. The dark-field micrograph of this figure also reveals retained austenite at packet boundaries. Significantly, retained austenite is absent at those lath boundaries for which the adjacent lath orientations correspond to a twin relation, Fig. 4. This is true for both $\{110\}_m$ and $\{112\}_m$ twins.

Both Kurdjumov-Sachs (K-S) and Nishiyama-Wasserman (N-W) orientation relations are widely observed in the alloys used. In addition both K-S and N-W relations are found to be obeyed frequently within the same packet (10) (for example, the SAD pattern of Fig. 3 shows this). Also, a new result is found in a few instances viz., the Bain orientation relation between retained austenite and lath martensite. In this case, interestingly the lath rotation axis is observed to be $\langle 100 \rangle_m$, e.g., Fig. 1.

Direct habit plane analysis on retained austenite confirmed the $\{111\}_a$ habit plane for this transformation (6).

(iv) <u>Carbon Analysis</u>

High resolution lattice imaging can be performed to estimate the carbon content of retained austenite since carbon is below the resolution limits of x-ray STEM techniques. Details of the method are discussed elsewhere (17). Figure 5 shows an example of the simultaneous lattice imaging of $\{101\}_m$ and $\{111\}_a$ planes (an extremely difficult experiment).

From the fringe spacings, analyzed directly and by laser optical diffraction, the lattice parameters c and a were estimated from established formulae (23) as follows:

$$c(\mathring{A}) = 2.8664 + 0.1162(x) \tag{1}$$

$$a(\mathring{A}) = 2.8664 - 0.01303(x) \tag{2}$$

where x is weight % carbon. For calculating the room temperature lattice parameter of the austenite, the following equation is employed (23):

$$a_o(\mathring{A}) = 3.555 + 0.044(x) \tag{3}$$

The data are given in Table II; these are for alloy 5 only, but are typical.

The above results indicate significant carbon enrichment in austenite varying between a minimum of 0.41 wt.% and a maximum of 1.04 wt.%.

(v)   Structure of the Austenite-Martensite Interface

The lattice imaging (Fig. 5) experiments also provide detailed information about interfaces (20). In Fig. 5 there are three different fringes: (1) the {110} martensite fringes on either side of the austenite region, (2) the {111} austenite fringes and (3) the larger periodicity structural moiré fringes at the interface. Figure 5 shows that the retained austenite/lath martensite interface exhibits a high degree of coherence. Occasional terminating fringes in either phase have been observed indicating that some of the elastic strain is accommodated by interfacial dislocations. Interestingly, the lattice fringes in both phases are fairly straight right up to the interface but very close to the interface drastic bending takes place to maintain coherency. The structural moiré, Fig. 5, for the first time reveals the presence of interfacial ledges several unit cells high at the retained austenite/lath martensite interface. The presence of these ledges has already been proposed (6) to account for the scatter in the habit plane analysis. By changing the ledge density and morphology, a curved macroscopic lath boundary can be generated while maintaining a unique microscopic habit plane. This then accounts for the curved interfaces for the laths particularly close to their packet boundaries, for example in Fig. 4.

Discussion

The observations in this paper suggest that the following transformation paths are followed in the austenite-martensite lath situation:
1. Twin related laths grow cooperatively to minimize strain energy from a common interface plane -- the twinning plane in austenite {viz., $(111)_\gamma \rightarrow (110)_m$ or $(112)_m$}. No retained austenite should then ever occur between such laths (as is observed).
2. Non-twin related laths also nucleate successively and cooperatively. The principal shear direction is however rotated during successive nucleations. This explains the orientation relationships (each lath rotated from its precursor until a full 180° has been achieved, Fig. 6). The retained austenite is then trapped between these laths; it is highly deformed -- also

-15-

probably as a result of accommodation of the transformation strains. This austenite is so stabilized but as shown it is also chemically stabilized by carbon enrichment which will drive the M_s to very low temperatures. The resultant block of rotated laths is such that the net shear across the block is zero (analogous to the successive $1/6 [11\bar{2}] + 1/6 [1\bar{2}1] + 1/6 [\bar{2}11]$ shears to minimize strain and shape deformation in the fcc - hcp transformation; in this case the rotation is successively 60°).

For the carbonless alloys, twin related laths are rarely seen and the adjacent lath orientations correspond to case 2 above without the interlath retained austenite.

The observation that both K-S and N-W relations are found to be alternating within the same martensite packet of most of the alloys investigated needs explanation. If the transformation is nucleation limited, then it can be greatly aided if there are a larger number of variants available for martensite nucleation. This is explained by the stereographic analysis shown in Fig. 6. The number of orientations for nucleation increases from two for purely K-S to three for combined K-S and N-W, i.e., a 50% gain in nucleation flexibility (Path 1, Fig. 6). Path 2 indicates the alternate twin related nucleation path.

The observation of the Bain relation means that a different habit plane other than $\{110\}_m$ occurs and this is probably partly responsible for some scatter in the habit plane analysis by indirect methods. On the other hand, the Bain relation provides a different rotation axis for the laths in a packet, i.e., $<100>_m$ (Fig. 1) as opposed to the most frequently observed $<110>_m$, Figs. 2-4. This again provides for increased flexibility in the nucleation and shape accommodation.

Figure 4 shows a unique example of the degree of accommodation necessary at the impingement site of three packets in the medium carbon steels. First, the laths in the central packet are twin-related. Second, the rotation axes for the adjoining packets are rotated 70° and 110° with respect to $<110>_m$ rotation axes in the central packet. Further minimization of the volume dependent strain energy at the impingement sites can be discerned from the decrease in lath widths at the packet boundaries. In addition, some $\{112\}_m$ substructural (probably accommodation) twinning is seen in the packet at the upper right hand side, Fig. 4.

An interesting example of the rotation of the shear vector and the resultant upheavals in the lateral direction at a packet boundary is provided by the bright-field (BF) and dark-field (DF) micrographs of Fig. 3.

Summary and Conclusions

(1) Retained austenite has been observed only in carbon containing alloys. Direct analysis on the austenite yielded a single $\{111\}_a$ habit plane, i.e., a $\{110\}_m$ plane including the twin interface plane in twin related laths. The only exception to this is the $\{112\}_m$ twin interface

·plane and when the Bain relationship is seen.

(2)   In order to minimize the strain energy, the shear components in a group of laths must add up to a 180° rotation. Since the strain energy increases with %C, this rotation is most simply obtained by twinning. In non-twin related laths (lower %C) successive laths are rotated in varying degrees with stabilized retained austenite between them which also plays a part in accommodation.

It should be emphasized, however, that this model relies on a specific interpretation of the electron diffraction patterns, since in cubic crystals there is an inherent 180° ambiguity in spot patterns and in such cases it is impossible to distinguish between planes of the same {hkl} form. The interpretation presented here may not be unique, even though careful dark field analysis has also been carried out. For example, in Fig. 1(c) the patterns could be indexed in terms of alternating [130] and [120] orientations, i.e., n could equal $\sim$2. Thus, the establishment of exactly how many rotations are involved between laths in the packets clearly requires more detailed studies, especially in cubic lath martensites. At this present stage of the work we are assuming a systematic rotation across successive laths, since this is an attractive model to account for minimization of the shape deformation.

(3)   In the medium carbon alloys a high degree of accommodation of shape strain is also seen in the form of interweaving packets and reduced lath widths at the packet boundaries.

(4)   Lattice imaging revealed ledges at the retained austenite lath martensite interface confirming earlier predictions (6). In addition, lattice imaging indicates substantial carbon enrichment of austenite which is important in its stabilization. Except for the twin related laths, the presence of interlath retained austenite suggests that the individual laths are the fundamental nucleation and growth events.

(5)   The present study confirms the morphology of lath martensite proposed earlier; they are indeed thin platelets with their thickness undergoing a slight reduction at the packet boundaries.

(6)   The question should then be asked -- in the lath martensite containing interlath retained austenite, since carbon enrichment (and hence, diffusion) occurs, is the transformation really martensitic? The structure can be described as incomplete upper bainite (complete upper bainite contains interlath carbides, e.g., from a γ-Fe_3C type reaction at the lath interfaces

Acknowledgements

References

(1) C. M. Wayman: Metallography, 8(1975), 105.

(2) G. Thomas: Iron and Steel Intl., 46(1973), 451.

(3) G. Krauss and A. R. Marder: Met. Trans., 2(1971), 2343.

(4) A. B. Grenninger and A. R. Troiano: Trans. AIME, 140(1940), 307.

(5) M. Umemoto and C. M. Wayman: Aeta Met., 26(1978). 1529.

(6) G. Thomas and B. V. N. Rao: Proc. International Conf. on Martensite, ICOMAT-77, Kiev, USSR, (1978), 57.

(7) B. V. Narasimha Rao, J. Y. Koo and G. Thomas: Proc. EMSA, Ed. by G. W. Bailey, Claitors Pub. Div., Baton Rouge, Louisiana, (1975), 30.

(8) G. Thomas: Met. Trans. A., 9A(1978), 439.

(9) D. S. Sarma, J. A. Whiteman, and J. H. Woodhead: Metal. Sci. J., 10(1976), 391.

(10) B. V. Narasimha Rao: Met. Trans. A., (1979), in press.

(11) M. J. Roberts: Met. Trans., 1(1970), 3287.

(12) J. S. Pascover and S. V. Radcliffe: Acta Met., 17(1969) 321.

(13) J. M. Oblak and R. F. Heheman: Transformation and Hardenability in Steels, Climax Moly Co., Ann Arbor, Michigan, (1967), 15.

(14) F. J. Schoen and W. S. Owen: Metallography, 3(1970), 473.

(15) J. M. Chilton, C. J. Barton and G. R. Speich: JISI, 208(1970), 184.

(16) G. R. Speich and P. R. Swann: JISI, 203(1965), 480.

(17) B. V. Narasimha Rao and G. Thomas: Met. Trans. A., to be published.

(18) B. V. Narasimha Rao and G. Thomas: Mat. Sci. and Engin., 20(1975), 195.

(19) B. V. Narasimha Rao and G. Thomas: Met. Trans. A., in press.

(20) J. G. Allpress and J. V. Sanders: J. Appl. Cryst., 6(1973), 165.

(21) R. Sinclair and G. Thomas: Met. Trans. A., 9A(1978), 373.

(22) R. B. G.Yeo: Trans. AIME, 224(1962), 1222.

(23) J. M. Moyer and G. S. Ansell: Met. Trans. A., 6A(1975), 1785.
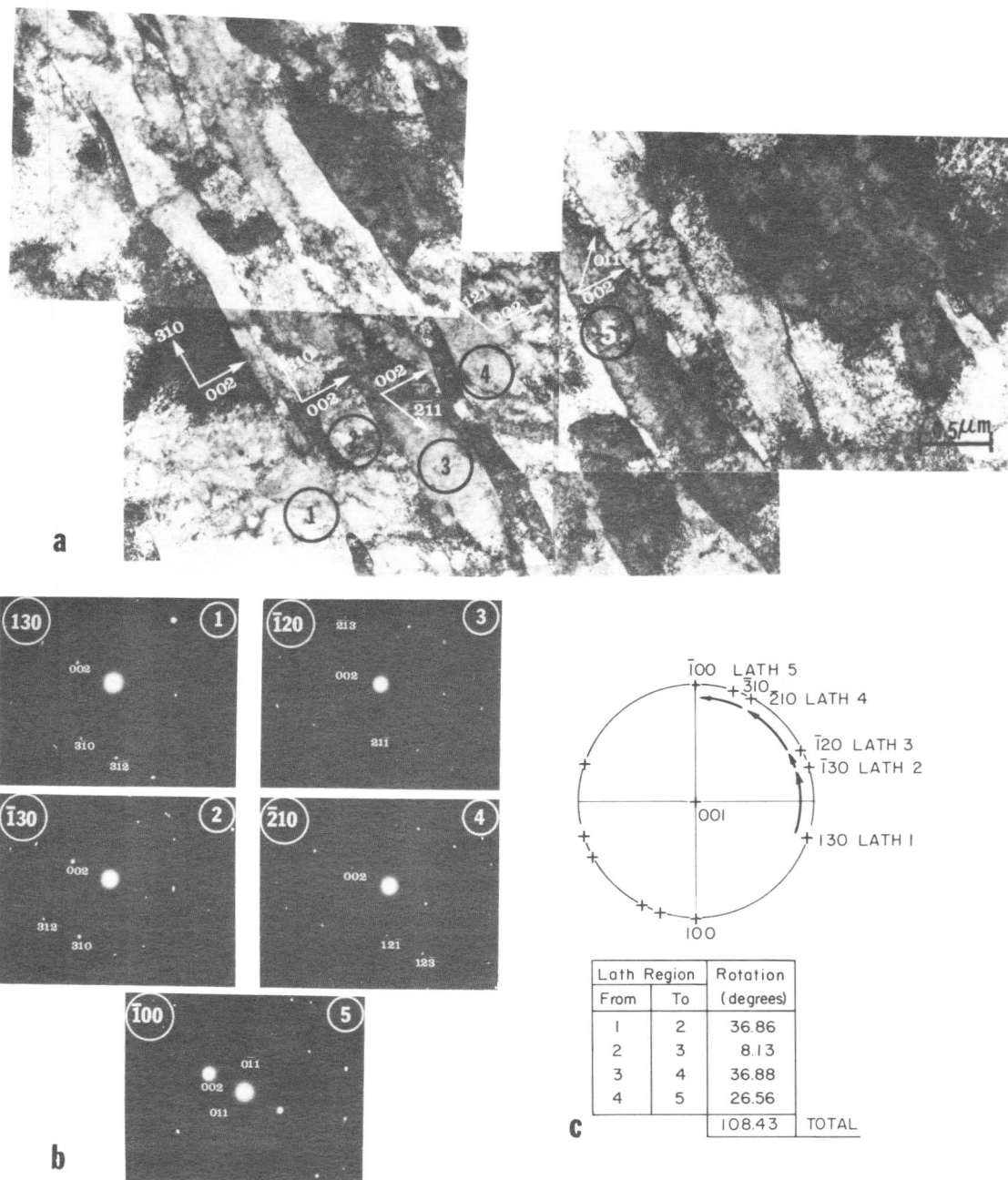
Fig. 1 Detailed analysis of orientations of martensite laths in a packet of the binary Fe-15Ni alloy.
   a. Bright-field micrograph with laths identified by 1, 2, 3 etc.
   b. SAD patterns from laths identified by 1, 2, 3 etc. in (a).
   c. Stereographic analysis showing rotations of laths 1 through 5.
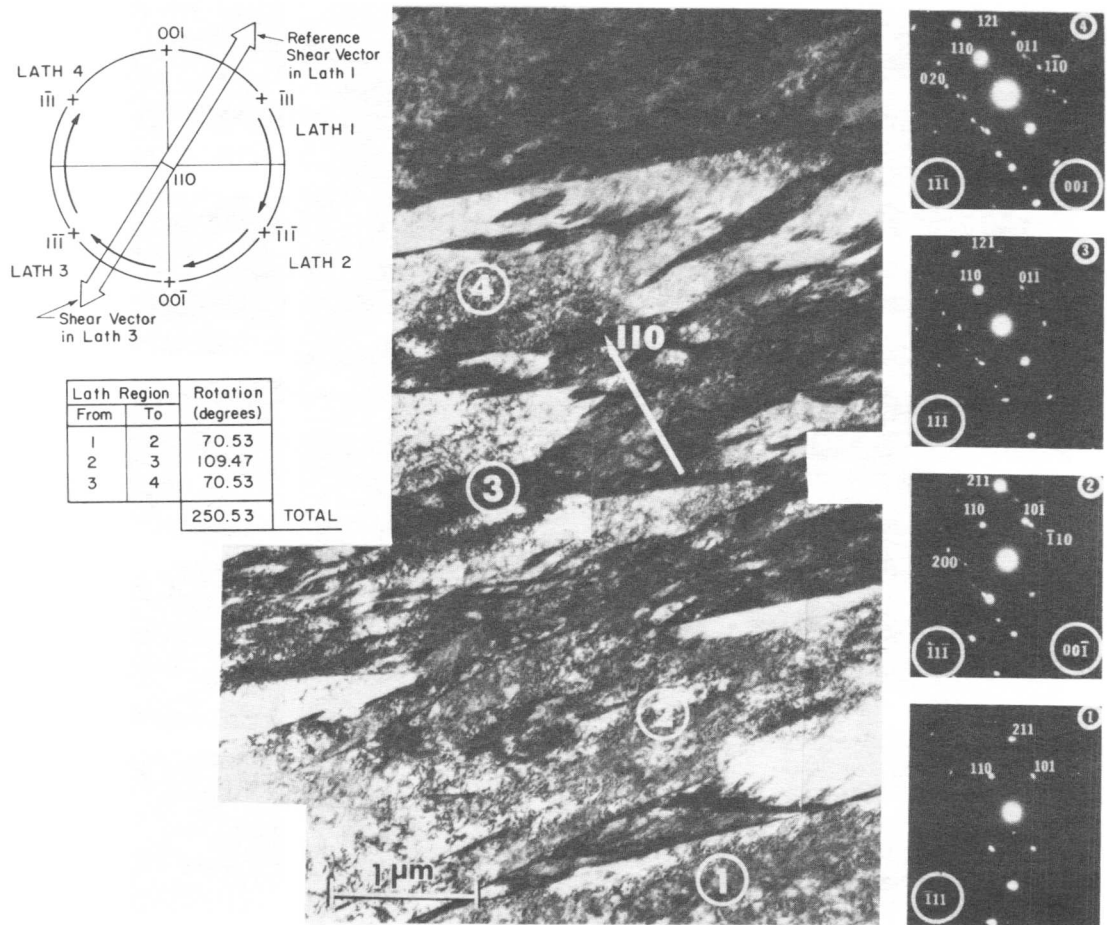
Fig. 2 Detailed analyses of a group of martensite laths in a packet of Fe/3Cr/2Mn/0.5Mo/0.3C alloy: a) Bright-field micrograph and the corresponding SAD analysis and b) stereographic analysis of rotations of adjacent laths.
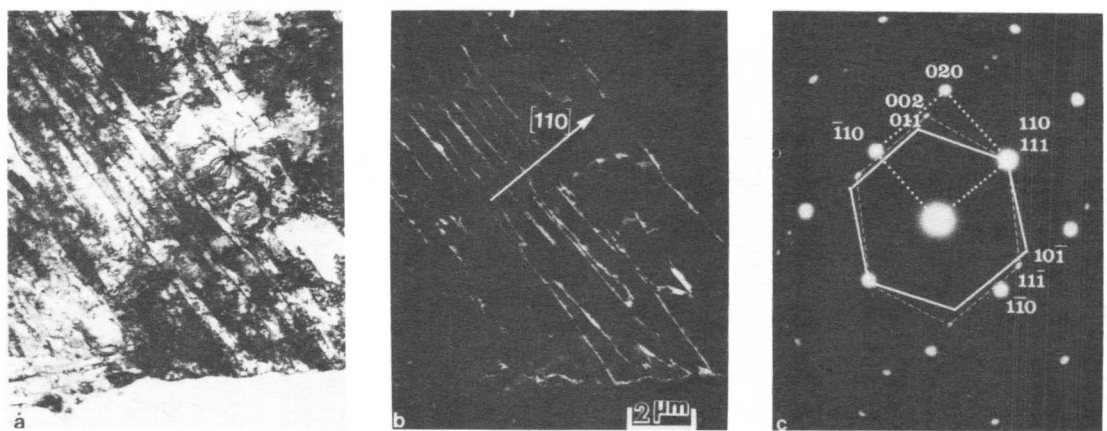
Fig. 3 Bf (a), DF (b) and analyzed SAD pattern (c) showing retained austenite in Fe/3Cr/2Ni/0.5Mo/0.3C alloy.
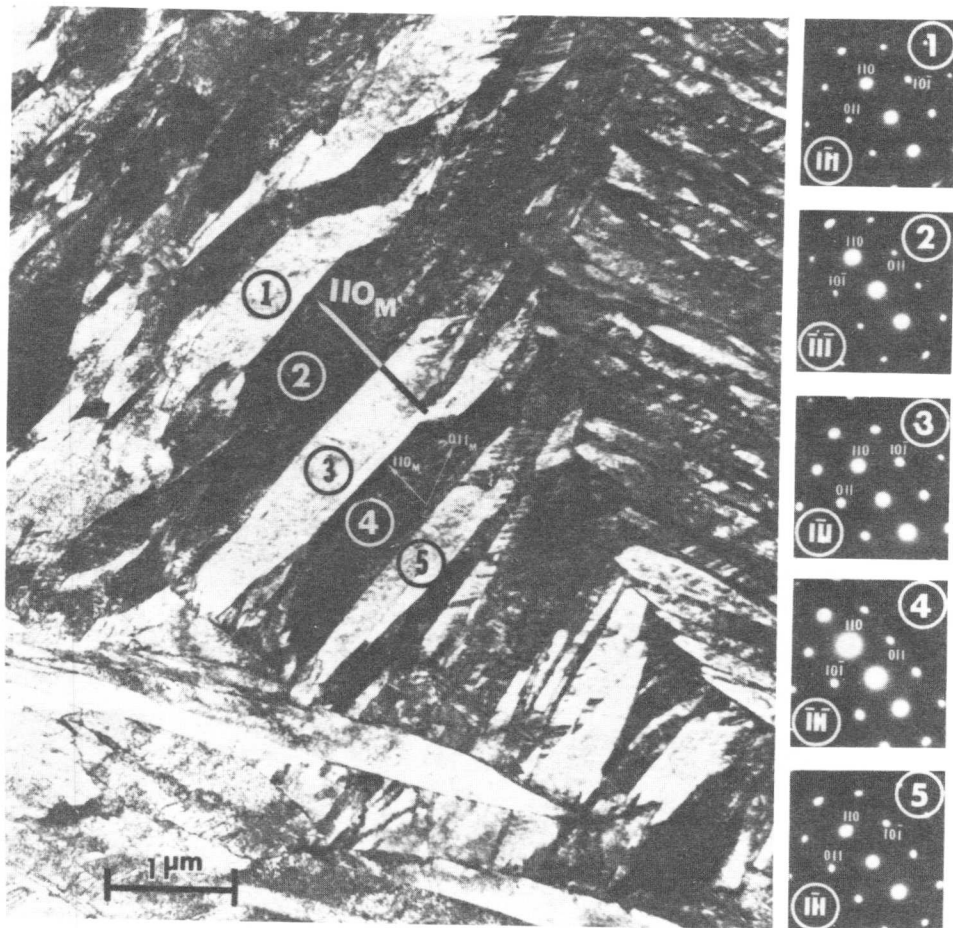
Fig. 4 BF and the corresponding SAD patterns revealing adjacent twin related laths in a packet martensite of Fe/3Cr/2Mn/0.5Mo/0.3C steel.
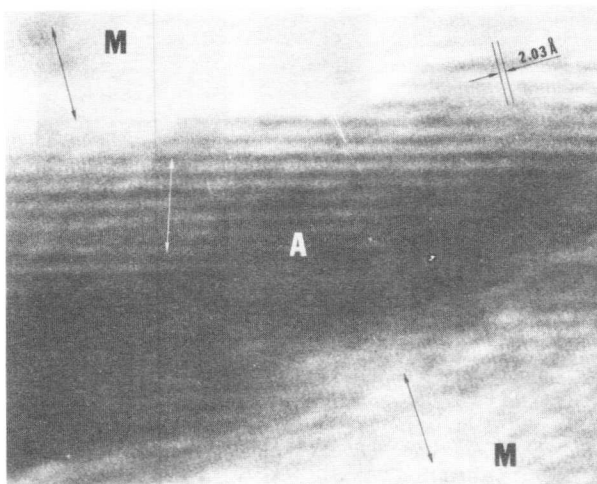
Fig. 5 Lattice image micrograph of retained austenite/lath martensite interface in Fe/4Cr/5Ni/0.3C steel. $\{101\}_m$ fringes are imaged in martensite and $\{111\}_a$ fringes in austenite.
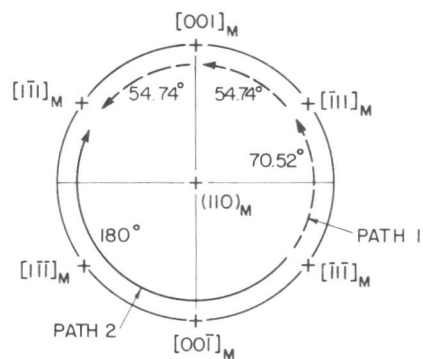
Fig. 6 Stereographic illustration of successive lath rotations in a packet assuming both K-S and N-W relations are obeyed (Path 1). Path 2 corresponds to adjacent twin related laths.

XBL794-6072

Table I. Compositions of the Alloys and Their M_s Temperatures

Alloy #	Nominal Composition Wt.%	M_s, °C
1	Fe-12Ni	300*
2	Fe-15Ni	250*
3	Fe-20Ni	165*
4	Fe-4Cr-0.3C	320
5	Fe-4Cr-5Ni-0.3C	210
6	Fe-4Cr-2Mn-0.3C	253
7	Fe-3Cr-0.5Mo-2Mn-0.3C	320
8	Fe-3Cr-0.5Mo-2Ni-0.3C	330
9	Fe-4Cr-0.4C	320

* Calculated temperatures

Table II. Calculation of Retained Austenite Carbon Content (wt.%) in Fe/4Cr/5Ni/0.27C alloys from lattice images

Martensite d-spacing in 0.27%C Steel at room temp.	Direct Measurement	Optical Diffractogram Measurement
$d_{110_m} = 2.0244\text{Å}$	0.55 wt.%	--
$d_{011_m} = 2.0366\text{Å}$	1.04 wt.%	0.41 wt.%

Formation Process and Construction of Lath Martensite Structure in Fe-C and Fe-Ni Alloys

Tadashi Maki[*], Kaneaki Tsuzaki[**] and Imao Tamura[*]

It has been known that the lath martensite structure in low carbon steels and Fe-Ni alloys is characterized by packets and blocks within a prior austenite grain. In the present study, lath martensite structure in several Fe-C and Fe-Ni-(C) alloys was studied in detail and found to change with alloying content. Based on the microstructure observations, the construction of lath martensite structure could be classified in four types. Furthermore, the formation process of lath martensite structure was studied by applying the well known Greninger-Troiano heat treatment. Observation results indicated that the side-by-side nucleation which has been believed previously is not essential and each martensite lath is independently nucleated, although the formation manner of the lath martensite structure is different among alloys which exhibit different types of lath martensite morphologies.

I. Introduction

It is well known that the Fe-C (up to about 0.6%C) and Fe-Ni (up to about 28%Ni) are typical alloys to exhibit lath martensite. Marder et al. [1,2] have investigated in detail the morphology of Fe-0.2%C and Fe-15 ~ 25%Ni lath martensite and found that the lath martensite structure in these alloys is characterized by packets and blocks within an austenite grain. An austenite grain is partitioned into several packets which consist of parallel laths with the same habit plane. Each packet contains several blocks which are made up of parallel laths having essentially the same orientation, and then blocks are separated by high-angle boundaries each other. Furthermore, they have studied the formation process of lath martensite in Fe-0.2%C and Fe-24.5%Ni by hot-stage cinephotomicrography and concluded that the formation of lath martensite occurs by two types of nucleation: (a) a side-by-side nucleation of laths that gives the effect of a phase front moving through the austenite matrix, and (b) nucleation of non-adjacent laths which partition the parent austenite.

The detailed studies on the lath martensite morphology, however, have been done only in the limited alloys and steels. Recently, the present authors [3] studying a series of Fe-C alloys have found that the construction of lath martensite structure markedly changes with carbon content ranging from 0.1 to 0.8%C. The purpose of this investigation was to classify the construction of lath martensite structure in Fe-C and Fe-Ni-(C) alloys and to study the formation process of these characteristic microstructures.

---

* Department of Metal Science and Technology, Kyoto University, Kyoto 606, Japan. ** Graduate Student of Kyoto University.

II. Experimental Procedure

Fe-C alloys (0.13, 0.21, 0.43, 0.55 and 0.82 wt%C), Fe-Ni alloys (10.2, 18.1 and 23.5 wt%Ni) and Fe-14.7%Ni-0.24%C alloy, which were prepared by vacuum induction melting, and commercial plain carbon steels containing 0.1 to 0.8%C and a 18Ni maraging steel (300ksi grade) were used. Specimens for optical micrography were austenitized in vacuum at suitable temperatures between 1100° and 1250°C for 1 h and quenched into iced brine or water. Furthermore, in order to study the formation process of lath martensite, partially transformed microstructures in 0.6%C steel, 18Ni maraging steel and Fe-14.7%Ni-0.24%C alloy were observed by applying the well known Greninger-Troiano heat treatment, which followed the austenitizing treatment previously given and quenched in salt bath at various temperatures T_1 (between Ms and Mf) for 5 s then up-quenched in salt bath at proper temperatures T_2 (for tempering martensite) and then quenched in water. By this heat treatment, only the martensites formed at-or-above T_1 were darkened by the proper etching.

III. Results and Discussion

(1) Constructions of four types of lath martensite structure

Photo.1 shows the optical micrographs taken from the same area in 18Ni maraging steel etched with different etching solutions. Specimen was quenched from 1200°C followed by aging at 500°C for 20 min. Aging treatment was necessary to reveal each component of lath martensite structure. Packets (Photo.1(a), electrically etched with CrO_3 10g + H_2O 90cc), Blocks (Photo.1(b), etched with $FeCl_3$ 10g + HCl 30cc + H_2O 120cc) and martensite laths (Photo.1(c), etched with 20% nital) are clearly observed. As can be seen, in 18Ni maraging steel, an austenite grain contains several packets which consist of parallel laths, and each packet is made up of parallel blocks. These morphological features of lath martensite are identical to the results in Fe-15～25%Ni lath marten-site observed by Marder et al. [1].

However, it was found in this investigation that the construction of lath martensite is not always unique as described above but changes with alloying content in Fe-C and Fe-Ni alloys. Representative optical micrographs of lath martensite structure are shown in Photo.2.

In a series of Fe-Ni alloys, the lath martensite structure of Fe-18%Ni and Fe-24%Ni alloys is very similar to that of 18Ni maraging steel and characterized by well-developed parallel blocks as shown in Photo.2 (a). On the other hand, in case of Fe-10%Ni martensite, blocks are generally wedge-shaped (similar to Photo.2(b)).

In Fe-C alloys and plain carbon steels, the lath martensite structure changes with carbon content. In case of low carbon content below about 0.3%C, packets and blocks are clearly observed within a prior austenite grain. However, as shown in Photo.2(b), the blocks are wedge-shaped and often segmented unlike Fe-18～25%Ni martensite in which the blocks are well developed and partition a packet. In Fe-0.43%C marten-site (Photo.2(c)), packets are somewhat clearly observed, but blocks within a packet are hardly found. When the carbon content increases to

0.55%C (Photo.2(d)), the regions which are made up of irrationally arranged laths are frequently observed within an austenite grain and thus the packets and blocks become difficult to define. While small regions with aligned laths (i.e., correspond to packets) are locally observed, their boundaries are obscure. In Fe-0.82%C alloy, the lenticular martensites occasionally formed, although the lath martensites predominated. Lenticular martensite plates were easily identified not only by their size but also by the midrib and microcracks. The lath martensite regions of Fe-0.82%C exhibited the similar morphology as Fe-0.55%C lath martensite. In the case of Fe-15%Ni-0.24%C alloy, the martensite structure was very similar to Fe-0.43%C martensite (Photo.2(c)).

The present microstructure observations described above indicated that the construction of lath martensite structure can be classified roughly in following four types.

Type 1 : (Photo.2(a)) Packets are well defined and blocks are well developed within a packet. Packet is almost completely partitioned by blocks in parallel.
(Fe-18%Ni, Fe-24%Ni, 18Ni maraging steel)

Type 2 : (Photo.2(b)) Packets are well defined and blocks are generally wedge-shaped and often segmented.
(Fe-10%Ni, Fe-0.13%C, Fe-0.21%C, plain carbon steels containing 0.1~0.3%C)

Type 3 : (Photo.2(c)) Packets are able to define but blocks are hardly found.
(Fe-0.43%C, 0.4% carbon steel, Fe-15%Ni-0.24%C)

Type 4 : (Photo.2(d)) Martensite laths are irrationally arranged, and thus packets and blocks are difficult to define.
(Fe-0.55%C, Fe-0.82%C, 0.6 and 0.8% carbon steels)

(2) Formation process of lath martensite structure

Formation process of lath martensite structure was studied in 18Ni maraging steel (type 1), Fe-15%Ni-0.24%C (type 3) and 0.6% carbon steel (type 4) which exhibit different types of lath martensite morphologies. Optical micrographs of the specimens held at various temperatures T_1 of the Greninger-Troiano heat treatment in 18Ni maraging steel and 0.6%C steel are shown in Photos.3 and 4, respectively. Martensites formed at-or-above the temperature T_1 are observed to be darkened in these photographs. It appears that the amount of martensites transformed is increased with lowering the T_1 temperature. In both steels, lath martensites form preferentially at the austenite grain boundaries in the initial stage of transformation.

In 18Ni maraging steel which exhibits well-defined packets and blocks, parallel laths form within certain portions of austenite grain. It is noted that these parallel laths have a tendency to form in clusters to some extent (Photo.3(b)). These clustered regions with parallel laths partition an austenite grain. On further cooling, transformation progresses by the subsequent formation of new parallel laths in an untrans-

formed austenite matrix (Photo.3(c)), and the complete transformation produces a characteristic martensite packet. Marder et al. [1,2] have described on the basis of their in situ observations with hot-stage cinephotomicroscopy that the packets in Fe-24.5%Ni and Fe-0.2%C martensite develops mainly by means of side-by-side nucleation (i.e., formation of laths one adjacent to another) that gives the effect of a phase front moving through the austenite matrix. However, the present observation indicates that no clear front of completely transformed region is observed, although parallel laths are apt to form in clusters. It is to be emphasized that, as shown in Photo.5(a), the formation of non-adjacent parallel laths predominates and, even in the clustered regions with parallel laths, much untransformed austenite remain. This suggests that the side-by-side nucleation may not be an essential process of lath martensite formation and each martensite lath within a packet seems to be independently nucleated, as pointed out by Thomas [4]. It can be considered that the surface relief observed with hot-stage microscopy may correspond to the clustered region of many parallel laths such as shown in Photo.3(b), and hence might mask the detailed microstructure.

In case of 0.6%C martensite, in contrast to 18Ni maraging steel, the transformation progresses mainly by the formation of non-parallel laths within an austenite grain as shown in Photo.4(b) and (c), although the parallel laths seem to form locally. As shown in Photo.5(b), non-parallel laths form throughout an austenite grain and finely partition an austenite grain and thus the clear packets do not form. Marder and Krauss [1,2] have shown that the habit plane of Fe-0.6%C martensite is identical to that of Fe-0.2%C and Fe-12%Ni alloys (i.e., close to $\{111\}_\gamma$). Therefore, the difference of formation process observed in 18Ni maraging steel and 0.6%C steel is not considered to be due to the change of martensite habit plane itself (e.g., $\{111\}_\gamma \rightarrow \{225\}_\gamma$). The reason why the formation process and arrangement of lath martensite change with alloying content is not clear at present.

Photo.5(c) shows the optical micrograph of partially transformed martensites in Fe-15%Ni-0.24%C alloy in which the final structure consists of well-developed packets but blocks are hardly observed within a packet. Parallel laths form at certain regions in austenite grain as with 18Ni maraging steel. However, it is to be noted that martensite laths are fairly evenly distributed and do not form in clusters. This tendency is different from the 18Ni maraging steel. Therefore, the appearance of clustered regions with parallel laths might be closely related to the formation of blocks.

References

[1] J. M. Marder and A. R. Marder: Trans. ASM, 62(1969), 1.
[2] A. R. Marder and G. Krauss: Trans. ASM, 62(1969), 957.
[3] T. Maki, K. Tsuzaki and I. Tamura: To appear in J. Iron and Steel Inst. of Japan, 65(1979), No.5.
[4] G. Thomas: Met. Trans., 9A(1978), 439.

(a) Packets   (b) Blocks   (c) Martensite laths
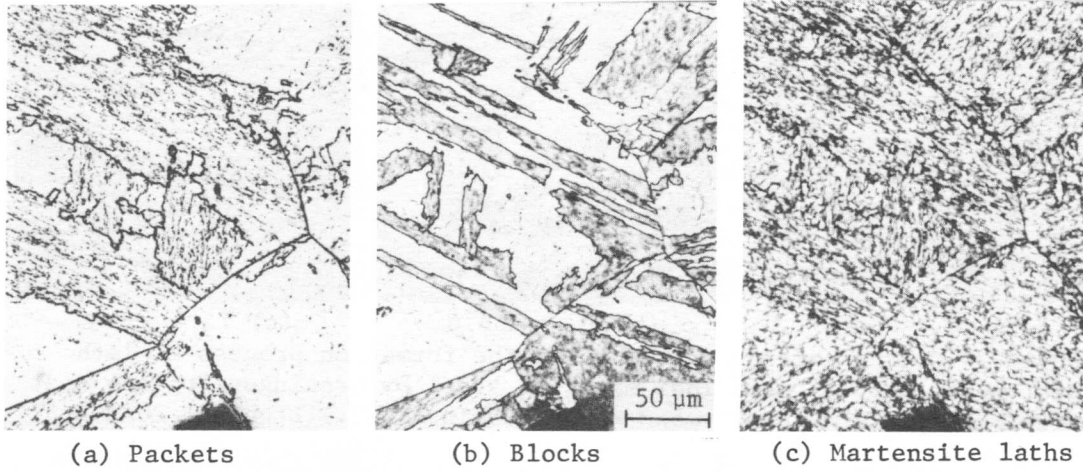
Photo.1   Optical micrographs of lath martensite taken from the same
area in 18Ni maraging steel etched with different etchants.

(a) Fe–18%Ni   (25% nital)   (b) Fe–0.21%C   (2% nital)

(c) Fe–0.43%C   (2% nital)   (d) Fe–0.55%C   (2% nital)
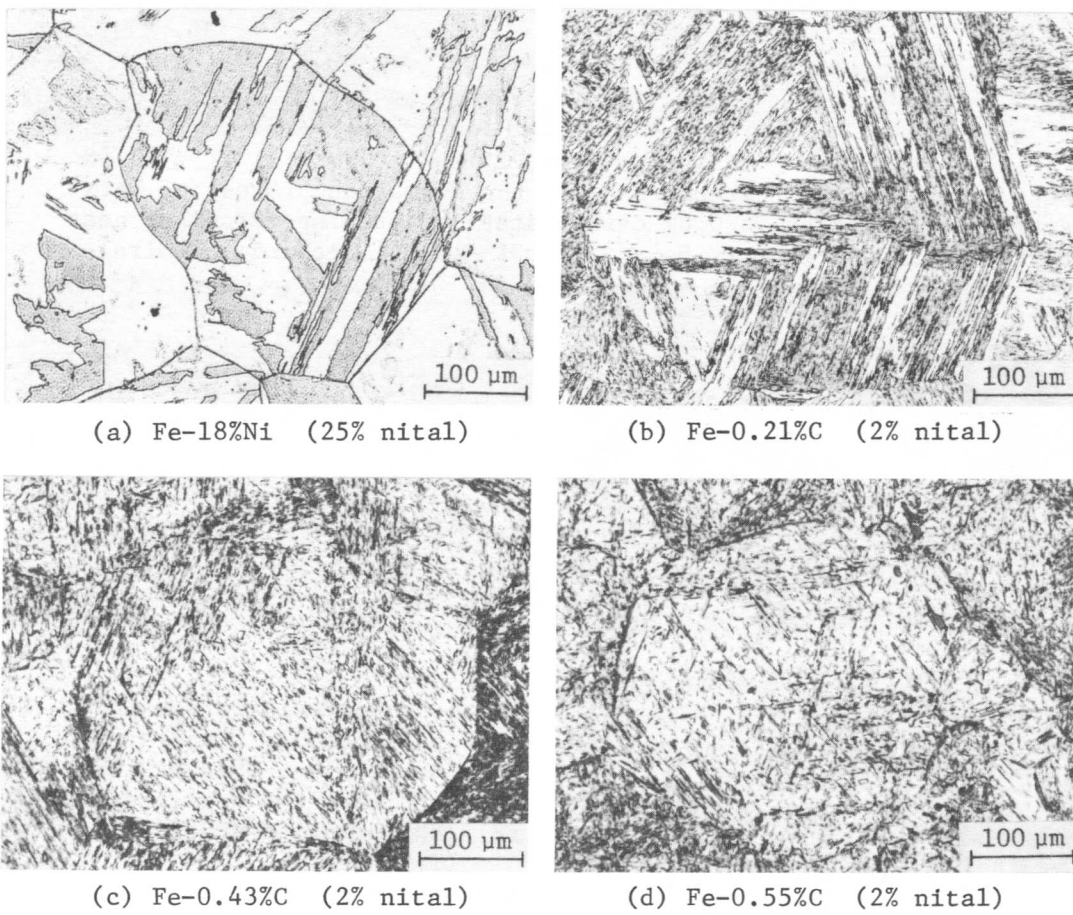
Photo.2   Optical micrographs showing four types of lath martensite
structures.
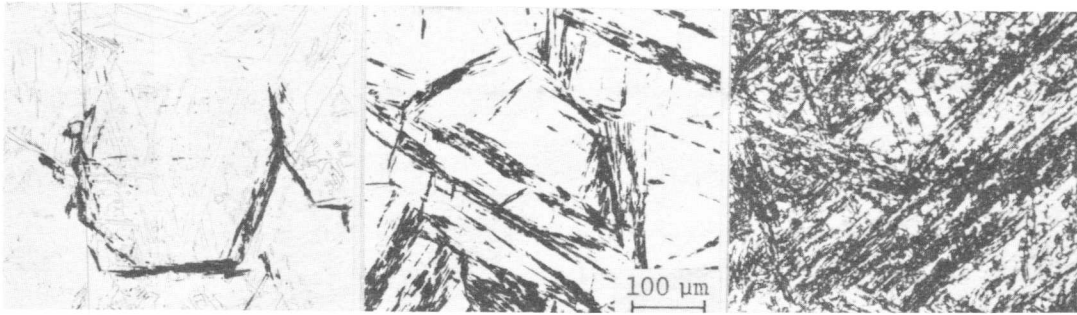
(a) $T_1 = 176°C$ (b) $T_1 = 166°C$ (c) $T_1 = 158°C$

Photo.3 Optical micrographs showing the formation process of lath martensite structure in 18Ni maraging steel by Greninger-Troiano heat treatment (1200°C 1h → T_1 5s → 500°C 20min → W.Q.) Etchant: 20% nital.
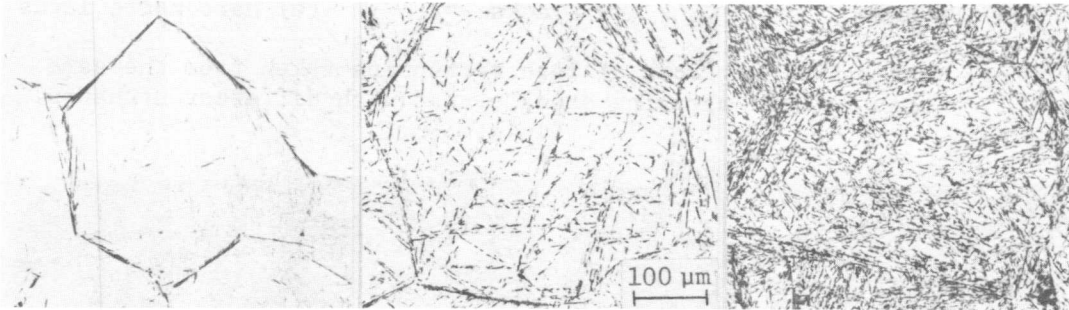
(a) $T_1 = 260°C$ (b) $T_1 = 225°C$ (c) $T_1 = 207°C$

Photo.4 Optical micrographs showing the formation process of lath martensite structure in 0.6% carbon steel by Greninger-Troiano heat treatment (1200°C 1h → T_1 5s → 335°C 3s → W.Q.) Etchant: 5% nital
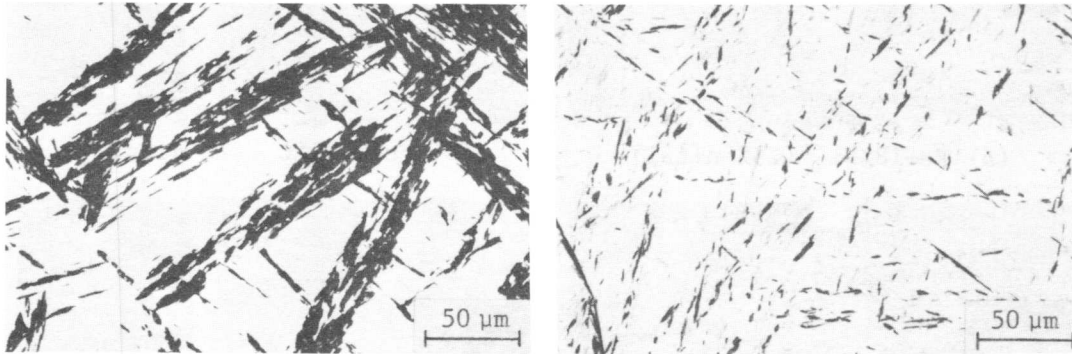
(b)
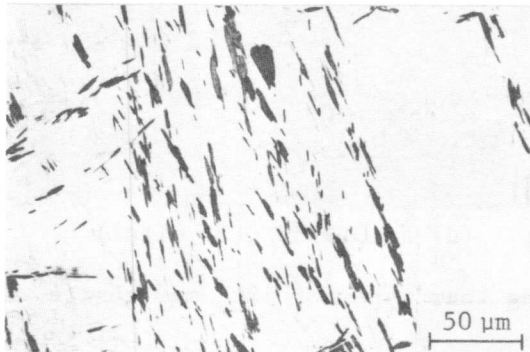
Photo.5 Optical micrographs showing partially transformed lath martensites obtained by Greninger-Troiano heat treatment.
(a) 18Ni maraging steel
    ($T_1 = 166°C$)
(b) 0.6% carbon steel
    ($T_1 = 225°C$)
(C) Fe-15%Ni-0.24%C
    ($T_1 = 173°C$)

The Distribution of Retained Austenite in Martensite and the Influence of Inter-lath Crystallography

H.K.D.H. Bhadeshia and D.V. Edmonds

A series of steels was examined for thin films of austenite trapped between laths/platelets of martensite. The distribution of these films was found to correlate with the inter-lath crystallography. In those steels with almost continuous films of inter-lath austenite the degree of co-operative martensite formation appeared limited. When limited films of heterogeneously distributed austenite were observed, not only was the incidence of twin related laths higher, but austenite was not in general observed between the twin-related laths. In other steels, austenite could not be detected. In these steels the lath packets consisted entirely of twin-related laths. The results are analysed in terms of the degree of mutual accommodation of transformation strains associated with the formation of adjacent martensite variants and the influence of mechanical stabilisation of residual austenite in the absence of mutually compensating accommodation effects.

I. Introduction

In recent years, the study of retained austenite films associated with martensite in low alloy steels has assumed new significance, primarily due to its apparent effect on the mechanical properties of quenched and tempered high-strength steels [1-4]. Due to the relatively high Ms temperatures of low alloy martensites, only thin films of inter-lath austenite are retained at room temperature. However, the reasons for the lack of complete transformation are not clear - even cooling to -196°C often fails to finish the transformation [5,6]. Since such refrigeration fails to give a significant decrease in the amount of retained austenite, chemical or thermal stabilisation has been ruled out as the possible reasons for the anomalous stability of the retained austenite films [6]. Indeed, Mossbauer spectroscopy [7] and X-ray diffraction experiments [5] give no evidence for chemical stabilisation by carbon enrichment of the austenite. While no such enrichment is expected on the basis of the displacive nature of the martensite transformation, partitioning of carbon is feasible either during the quench (i.e. after formation of some martensite) or during subsequent tempering. Hence, although no direct evidence is available, the stability of the retained austenite films has been attributed to mechanical stabilisation [6].

The aim of the present work was to gain a better understanding of the stability of films of retained austenite with the help of transmission electron microscopy. The detailed experimental procedure is discussed elsewhere [4] and is not considered further.

Department of Metallurgy and Materials Science, University of Cambridge, Cambridge, U.K.

II. Results and Discussion

(1) Fe-4Ni-0.4C

A microstructure of lath/platelet martensite was obtained upon quenching from the austenitising temperature. Examination of over 60 electron micrograph/diffraction pattern pairs revealed that approximately 55% of adjacent martensite units had twin related lattices. The structure appeared to be partitioned by large platelets with finer martensite in the partitioned areas (fig.1). The twin related martensite was found mainly in the partitioned regions and occured in two distinct formations. In one situation, the adjacent platelets alternated in twin orientation and formed as clearly defined packets and it was found that retained austenite could not be imaged within these packets (fig.2). When irregular groups of platelets with only some adjacent martensite units being twin related were observed, retained austenite could be imaged between units in the same crystallographic orientation and only to a very limited extent at the interfaces between twin related units. In all cases the retained austenite films were rather discontinuous (fig.3) and it was estimated that the quantity of retained austenite involved is less than 1%. The inhomogeneous distribution of retained austenite can be rationalised if it is considered that the twin related martensite units form in a mutually accommodating manner. In this case mechanical stabilisation of austenite is expected to be mitigated relative to the situation where adjacent variants form in the same crystallographic orientation, when their accommodation effects would be expected to be additive rather than self compensating. Clearly, the compensating effects would be maximised when the twin related platelets can form in regular groups with alternating units. The formation of twin related variants in the regions partitioned by the larger platelets is consistent with the above arguments since such regions would be under the constraint of an already formed rigid martensite frame and a greater degree of mutually compensating accommodation would minimise strains.

(2) Fe-3.9Mo-0.18C

Considerable quantities of inter-martensite retained austenite films could be imaged and it was found that the martensite platelets tended to be in the same crystallographic orientation in space. It is probable that very little mutually compensating accommodation is involved in the formation of such groupings since the shape deformation is expected to be the same for adjacent platelets. In such circumstances the residual austenite would be deformed to a greater extent by the larger resultant accommodation strains, leading to mechanical stabilisation. However, the films of retained austenite proved to be too fine to be able to characterise easily their microstructure (fig.4).

(3) Fe-0.08C-1.1Mn-0.2Si-5.5Ni-14.5Cr-2.1Mo-0.7Nb-1.9Cu

With this alloy the martensite groups again formed in the same crystallographic orientation and the high alloy content allowed the retention of larger quantities of austenite (fig.5). The microstructure

of the latter austenite could be clearly resolved and it was interesting to note that the austenite was heavily faulted, with a dominant fault plane aligned with respect to the martensite habit plane trace, as expected when the austenite absorbs a significant proportion of the accommodation strain. Such extensive faulting can be expected to mechanically stabilise the residual austenite to further transformation.

(4) Fe-0.31C-2.0Si

Since retained austenite could not be detected upon direct quenching, an attempt was made to enhance the retention of austenite by thermal stabilisation. The specimen was austenitised at 1100°C for 5 mins followed by a quench to 335°C (a temperature below the calculated Ms of 410°C) where it was held for 1 hour before finally quenching to room temperature. However, retained austenite could not be detected and it was found that the martensite was in classical lath formation (fig.6) with alternate laths being twin related. The lath packets were extremely regular, as illustrated in fig.7. These results are again consistent with twin related martensite forming in a mutually compensating manner.

In view of the above observations, it is concluded that mechanical stabilisation is one of the key factors responsible for the retention of thin films of austenite. In situations where accommodation effects are minimised (as when adjacent twin related martensite formation occurs), the propensity to retain austenite appears to be reduced. Intuitively one would expect a high strain energy interaction, and hence a lower probability of retaining inter-lath austenite, between twin related variants of martensite. This cannot be supported theoretically without a knowledge of the displacement vector (d_1) associated with the shape deformation of each twin variant. The latter may be obtained after application of the phenomenological theory of martensite, when relevant detailed crystallographic data becomes available. However, in the case of alpha martensite found in high alloy steel [8], it is known that twin related laths have shear components of their shape strains that can cancel each other.

III. Summary

The propensity for austenite retention has been rationalised in terms of the local inter-martensite crystallography, and it was found that twin-related martensite variants do not favour the retention of austenite. Inter-martensite retained austenite films were most profuse when the adjacent martensite variants were in the same crystallographic orientation and the results were found to be consistent with a mechanical stabilisation effect which hindered and often prevented complete transformation to martensite.

References

[1] G. Thomas: Iron and Steel International, 46(1973), 2267.

[2] E.R. Parker: Met. Trans., 8A(1977), 1025.

[3] G. Thomas: Met. Trans., 9(1978), 439.

[4] H.K.D.H. Bhadeshia and D.V. Edmonds: Metal Science: 1979, in press.

[5] H.K.D.H. Bhadeshia and D.V. Edmonds: Unpublished research.

[6] B.V. Narasimha Roa, R.W. Miller, G. Thomas: Proc. Int. Conf. Heat Treatment, 1976, The Metals Society, London.

[7] A.L.T. Azevedo and E.G. da Silva: Scripta Met., 12(1978), 113.

[8] P.M. Kelly: Acta Met., 13(1965), 635.

TWIN RELATED $(011)_\alpha$ ZONES
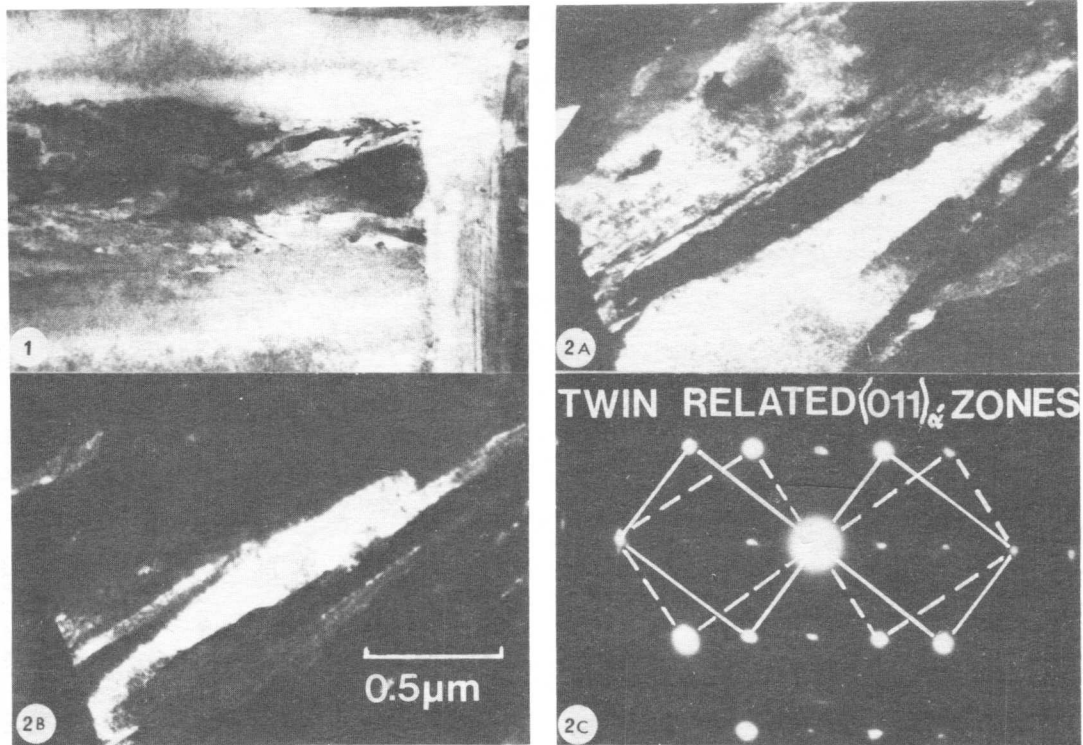
Fig.1 Bright field image of quenched Fe-4Ni-0.4C. Fig.2a,b, c, twin, matrix dark field images and corresponding diffraction pattern. Fig.3a,b,c,d twin, matrix, retained austenite dark field images and corresponding diffraction pattern.

002γ
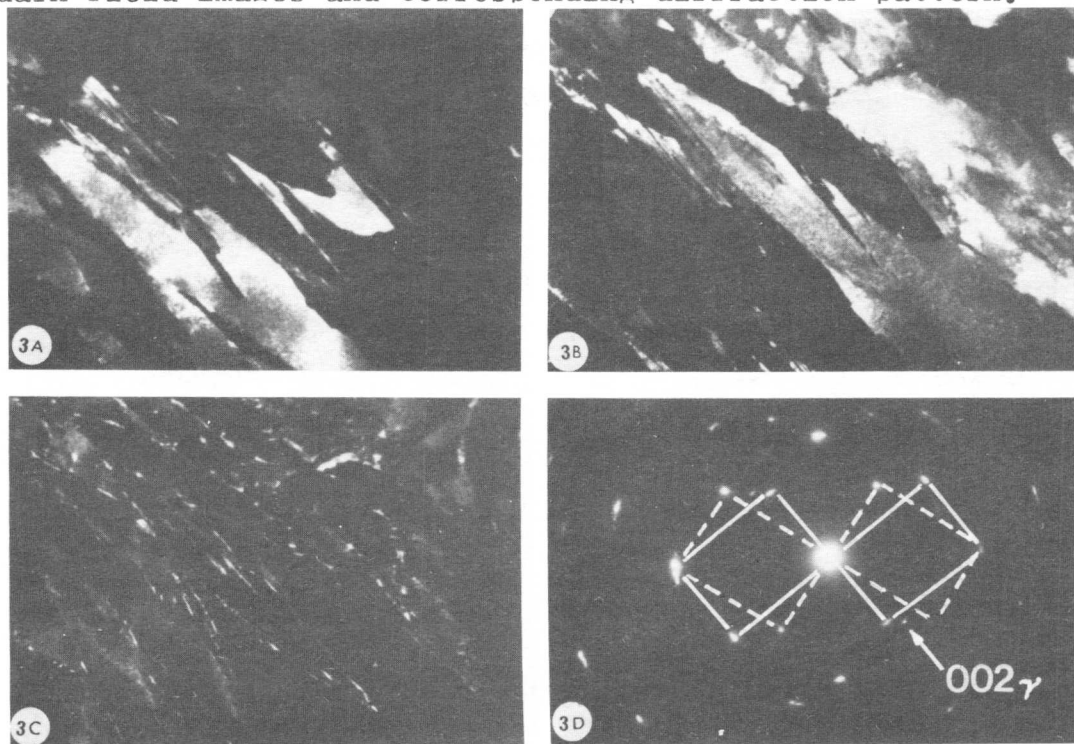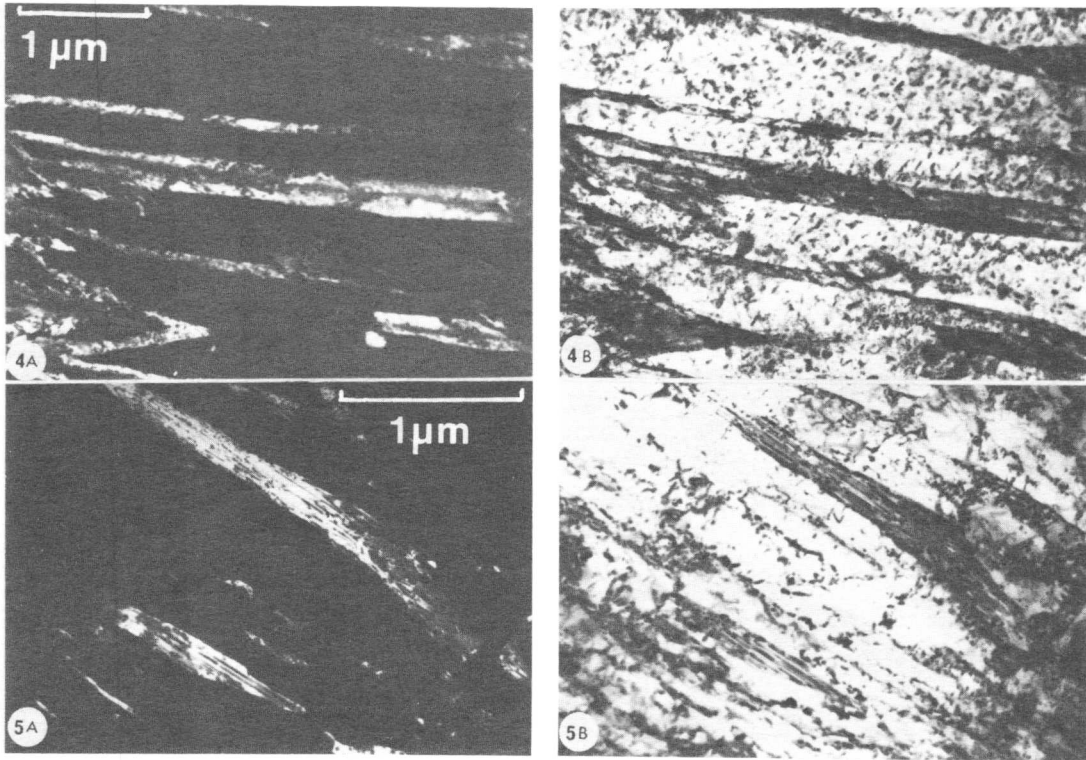
Fig.4a,b γ dark field and bright field images. Fig.5a,b γ
dark field and bright field images. Fig.6 Quenched Fe-0.31C
2Si alloy. Fig.7a,b,c twin, matrix dark field images and
DP.

The Crystallography and Morphology of Lath Martensite in Fe-20Ni-5Mn
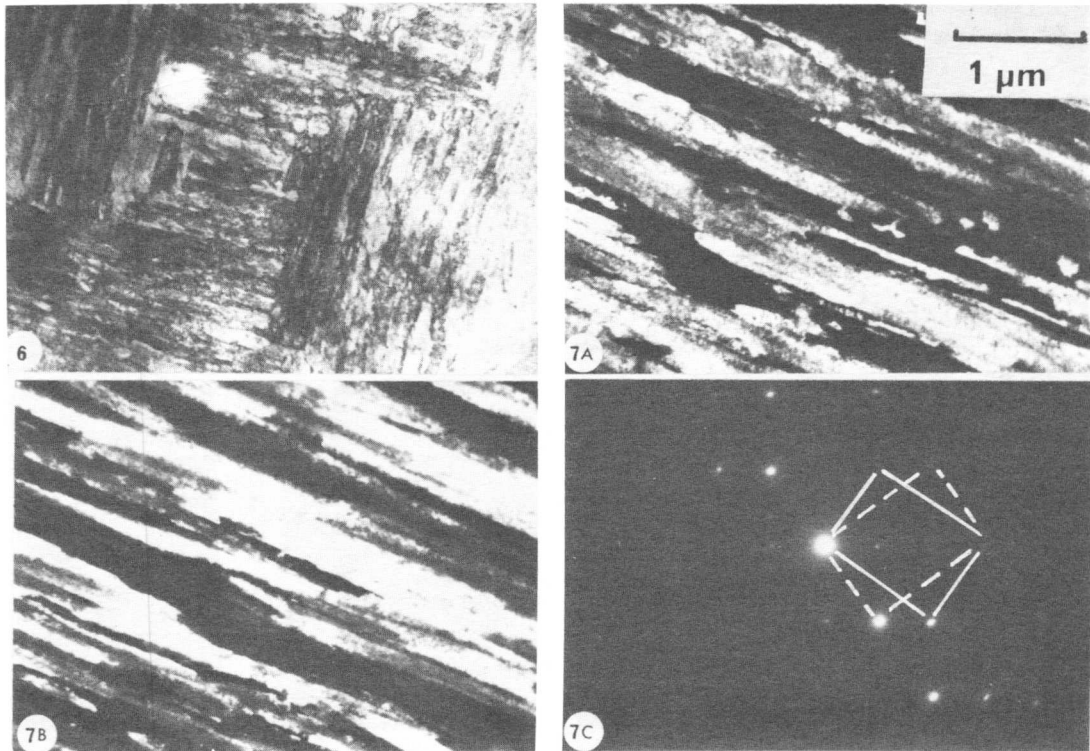
K. Wakasa* and C. M. Wayman*

Alloys of nominal composition Fe-20Ni-5Mn (wt.%) have a low M_s temperature and transform isothermally to lath martensite. Typical lath dimensions are 0.3 x 2.8 x 100 μm with the longitudinal direction being about 4° from $\langle 110 \rangle_A$. Films of retained austenite are found between adjacent laths, which exhibit the Kurdjumov-Sachs orientation relationship with respect to the parent. Adjacent laths are of the same orientation, variant of the K-S relation, and habit plane. The austenite-martensite and martensite-martensite interfaces are about 4.5° from $\{111\}_A$. In one case, where a detailed examination was made, a given grain divided by an annealing twin exhibited 7 martensite variants on one side and 9 on the other. As the surface was progressively removed to a depth of 8 μm, groups (packets) of laths with the same habit plane and variant of the orientation relationship were observed.

I. Introduction

It has been reported that an Fe-20Ni-5Mn alloy may be suitable for producing directionally aligned martensite, following austenite texturing and transformation under tensile strain at low temperature [1]. This result is empirical, and requires a detailed analysis of the crystallographic features of the isothermal lath martensite for clarification. This is the purpose of the present investigation.

In general, the crystallography of ferrous lath martensite is not well or universally understood. In quenched Fe-C alloys containing 0.20 and 0.60 wt.% C (no retained austenite) the habit planes have been determined to be $\{557\}_A$ by two-surface analysis [2]. (Subscripts A and M refer to austenite and martensite, respectively.) For quenched and tempered lath martensites in medium carbon steels and Fe-Ni alloys, the internally dislocated laths are reported to have $\{011\}_M(\{111\}_A)$ and $\{331\}_M$ habit planes, and retained austenite films are found in the medium carbon steels [3,4]. Differing opinions exist concerning the mutual orientation of adjacent martensite laths which comprise packets [3,5].

II. Experimental Procedure

Three different alloys were studied: Fe-20.1Ni-4.78Mn-0.007C (Alloy I), Fe-19.8Ni-5.25Mn-0.009C (Alloy II) and Fe-20.2Ni-5.65Mn-0.009C (Alloy III). These were austenitized at 1423°K for 6 hr, water

---

* University of Illinois at Urbana-Champaign, Urbana, IL 61801

quenched, and then further cooled to 233°K to produce isothermal lath martensite. The lath morphology was most clearly revealed after a two-stage etch, first with 25% HNO_3 in methanol, followed by a solution containing 2 gms of $NaHSO_4$ in 100 ml H_2O. The austenite-martensite and martensite-martensite impingement interface planes were determined by two-surface analysis. Different martensite variants were conveniently studied by choosing various austenite grains with $\{111\}_A$ surfaces and removing successive layers 0.1-0.4 μm thick by chemical polishing. The lath dimensions and morphology, retained austenite between laths, austenite-martensite orientation relationship, martensite-martensite relationships were studied by optical microscopy (including interference microscopy), and scanning and transmission electron microscopy.

III.   Results and Discussion

1. Morphology

After austenitizing and water quenching to room temperature, it was observed that Alloy I showed 90-100% martensite, Alloy II contained 20-40% martensite, and Alloy III showed no transformation. The retained austenite in Alloy II and the austenite in Alloy III transformed isothermally below room temperature with "C" curve behavior, the nose of the "C" curve being about 233°K in both cases. After transforming these alloys from 4-7 hours at 233°K some surface relief features could be obtained, and the relief from an apparent single lath as observed on a $\{111\}_A$ plane was about 0.27 μm as deduced from interference fringes. By careful chemical polishing and etching, this relief was found to correspond to a single lath. Figures 1(a) and (b) show optical micrographs of martensite laths in Alloy III. Figure 1(a) was obtained after removal of 1.0 μm from the $(111)_A$ surface of the specimen, which was held at 233°K for 7 hr. The laths designated as A_1 and A_2, B_1 and B_2, and C (in the $(111)_A$ surface) had habit planes near $(1\bar{1}1)_A$, $(11\bar{1})_A$ and $(\bar{1}11)_A$, respectively, and correspond to single laths (see Section III.3). Variants A_1 and A_2 correspond to $(1\bar{1}1)[011]_A$ and $(1\bar{1}1)[110]_A$, respectively (see Section III.4). Each of these laths is "going down in" from the surface and lies approximately in $(1\bar{1}1)_A$, $(11\bar{1})_A$ and $(\bar{1}11)_A$ planes. In other words, the specimen surface forms the base of a Thompson tetrahedron, and the laths "going down in" are approximately along the $\langle 110 \rangle_A$ directions which point to the apex.

2. Retained austenite

Retained austenite films have recently been noted in quenched and tempered lath martensites in medium carbon steels [3]. Figure 2 for Alloy III is a transmission electron micrograph showing retained austenite between adjacent martensite laths. Figure 2(a) shows that the thickness of the retained austenite layer is about 0.035 μm. In Fig. 2(b), A shows $(1\bar{1}0)_A$ and $(100)_M$ diffraction patterns (B shows only a $(100)_M$ pattern) and the austenite-martensite orientation relationship was analyzed to be of the Kurdjumov-Sachs type after considering other possibilities such as the Bain, Nishiyama and Pitsch relations. The K-S relation was also confirmed for an isolated lath of martensite.

-35-

Diffraction patterns from regions B, C, D, E and F were also the same (i.e., a $(100)_M$ orientation). This is also verified in Fig. 2(c), a dark field image taken using an $(002)_M$ reflection.

The above result is in contrast to previous reports on the relative orientation between adjacent laths which include a twin relationship and an off-twin relation [5], and a gradual 180° rotation with respect to a $[110]_M$ axis [3]. The first of these is consistent with the present findings, but the second is not in that $[110]_M$ and $[110]_T$ (T refers to twin) are not parallel. Thus, in the present alloy which shows retained austenite between the martensite laths, all adjacent laths had the same $(002)_M$ orientation, $(111)_A$ habit plane, and variant of the K-S orientation relationship.

3. Habit plane

According to reports [2-4] there is a substantial scatter in the lath martensite habit plane, ranging from $\{557\}_A$ (optical microscopy) to $\{331\}_M$ (transmission electron microscopy). These are respectively 7.5 and 13.1° from $\{011\}_M(\{111\}_A)$. In the former case, the habit plane was not determined for a single lath, but for packets of small laths, and in the latter case, trace analysis and not two-surface analysis was employed. The lack of retained austenite may be responsible for some of these differences. As shown in Fig. 1, it was possible to obtain isolated laths in Alloy III, allowing the austenite-martensite and martensite-martensite (impingement) interfaces to be determined without difficulty.

In the present work, the traces of austenite annealing twins on two orthogonal surfaces were used to determine the martensite habit plane, which was determined relative to a given $\{111\}_A$ twin plane. Using seven different austenite grains in Alloy III, the habit plane for both isolated laths and laths comprising packets was commonly 4.5° from $\{111\}_A$ with variations ranging from 2.5 to 8.0 degrees. This result was also confirmed by transmission electron microscopy, where the following additional information was also obtained. 1) The martensite interfaces were not necessarily "flat" and were frequently stepped. This was observed in a $(100)_M$ orientation. 2) In specimens or foils with $\{111\}_A$ normals one side of the laths was straight while the other was wavy (optical microscopy and TEM).

4. Number of variants

Figures 3(a) and (b) show optical micrographs of martensite laths in Alloy III. (a) and (b) were obtained after removal of 0.7 and 2.0 μm from the surface of the initial surface relief specimen. The initial surface before transformation was prepared by careful mechanical polishing, and layers 0.2-0.4 μm in thickness were successively removed by chemical polishing. During chemical polishing, reference to fiducial etch pits was used to assess the lath direction as successive layers were removed, i.e., whether the laths were "going down in," parallel to the surface, etc.

-36-

In Fig. 3(a) and (b), the surfaces to the left and right are twin-related relative to the $(\bar{1}11)_A$ twin plane. In the right-hand region of Fig. 3(a), six distinct variants could be identified, which are arbitrarily designated as 1, 2, 3, 7, 8 and 12. These correspond to 1: $(1\bar{1}1)[0\bar{1}1]$; 2: $(111)[10\bar{1}]$; 3: $(111)[\bar{1}01]$; 7: $(\bar{1}11)[110]$; 8: $(1\bar{1}1)[110]$; and 12: $(11\bar{1})[011]$. Variants 7, 8 and 12 are "going down in," while 1, 2 and 3, appearing flat, are nearly parallel to the surface. Variant 4, $(1\bar{1}1)[10\bar{1}]$, appeared at a depth of 1.3 μm from the specimen surface. At the right of the twin, seven variants still exist at 2.0 μm below the initial surface (Fig. 3(b)). On the other hand, to the left of the twin (the T orientation), the corresponding situation at 2.0 μm below the initial surface is that nine martensite variants 1^T, 2^T, 3^T, 6^T, 7^T, 8^T, 9^T, 10^T and 12^T formed (6^T: $(11\bar{1})[101]^T$, 9^T: $(\bar{1}11)[101]^T$, and 10^T: $(11\bar{1})[101]^T$, where T indicates a twin with respect to the $(\bar{1}11)_A$. Variants 9^T and 10^T are "going down in" from the surface and variant 6^T is nearly parallel to the $(11\bar{1})_A$ plane. Variants 3^T and 6^T appeared first at 0.8 and 1.3 μm depths, respectively, from the initial $(111)_A$ surface. In Fig. 3, six martensite variants, $1(1^T)$, $2(2^T)$, $3(3^T)$, $7(7^T)$, $8(8^T)$ and $12(12^T)$ were commonly found in the left and right regions, except variant 4 (right) and variants 6^T, 9^T and 10^T (left). A similar distribution of variants was found after an examination of some 10 other austenite grains with $\{111\}_A$ surface normals. Laths of variants 1 and 1^T which were along the twin boundary were found in all grains. Upon removal of 8 μm from the $\{111\}_A$ surface for 2 of 11 specimens, packets of laths were found, and observed by optical microscopy and SEM. These correspond to laths with the same habit plane and K-S variants which were going down in.

<div align="center">References</div>

1. M. Khobaib, R. Quattrone and C. M. Wayman, Met. Trans., 9A (1978) 1431.
2. A. R. Marder and G. Krauss, Trans. ASM, 62 (1969) 957.
3. G. Thomas and B. V. N. Rao, presented at Intl. Conf. on Martensitic Transformations, Kiev, USSR, May 1977.
4. G. Thomas, Met. Trans., 9A (1978) 439.
5. J. M. Chilton, C. J. Barton and G. R. Speich, JISI, 208 (1970) 184.
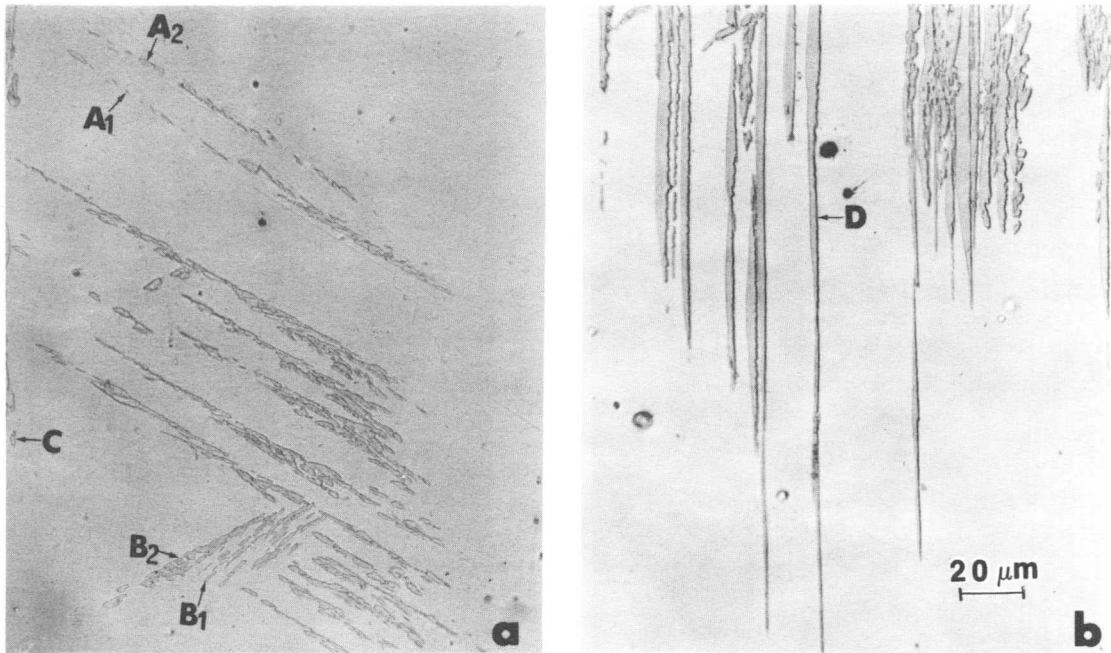
Fig. 1. Lath martensite in Alloy III isothermally treated at 233°K for 7 hr: (a) Laths A_1, A_2, B_1, B_2 and C are "going down in" (see text); (b) Laths D are approximately parallel to the surface.
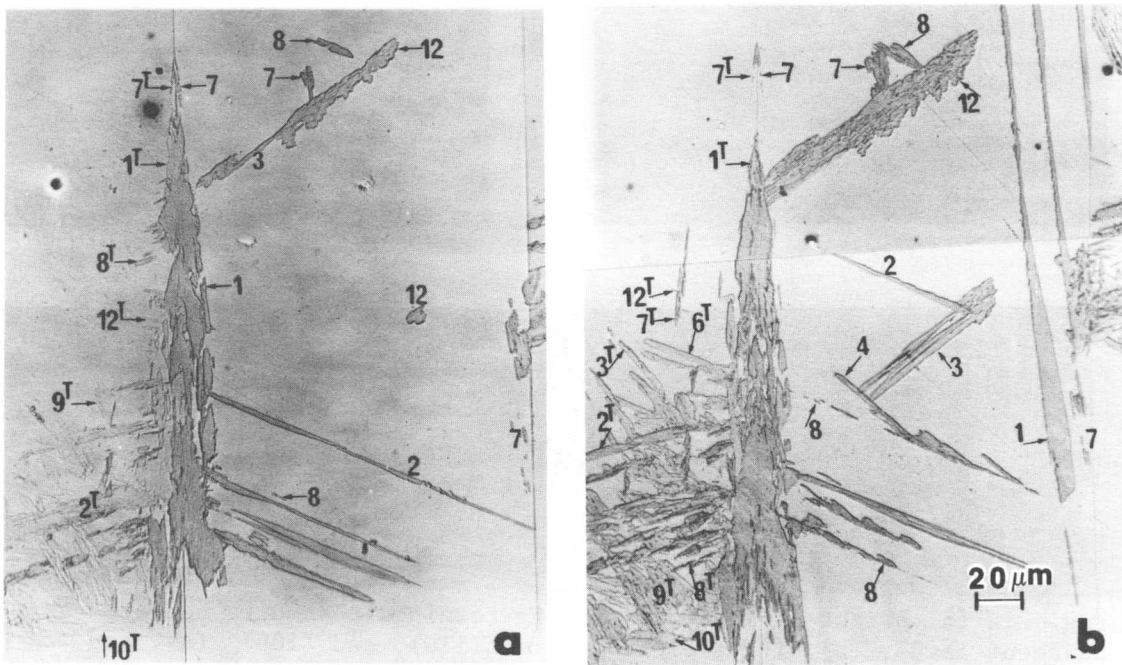
Fig. 3. Optical micrographs of isothermal lath martensite in Alloy III(233°K for 7hr): (a) 0.7 μm and (b) 2.0 μm removed from initial $(111)_A$ specimen surface.
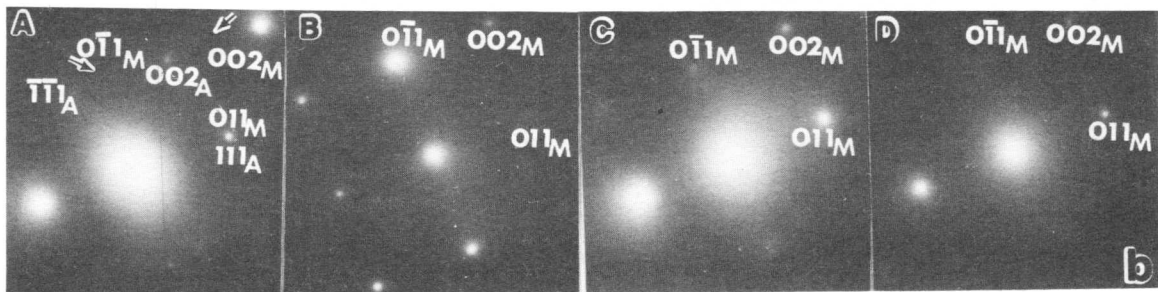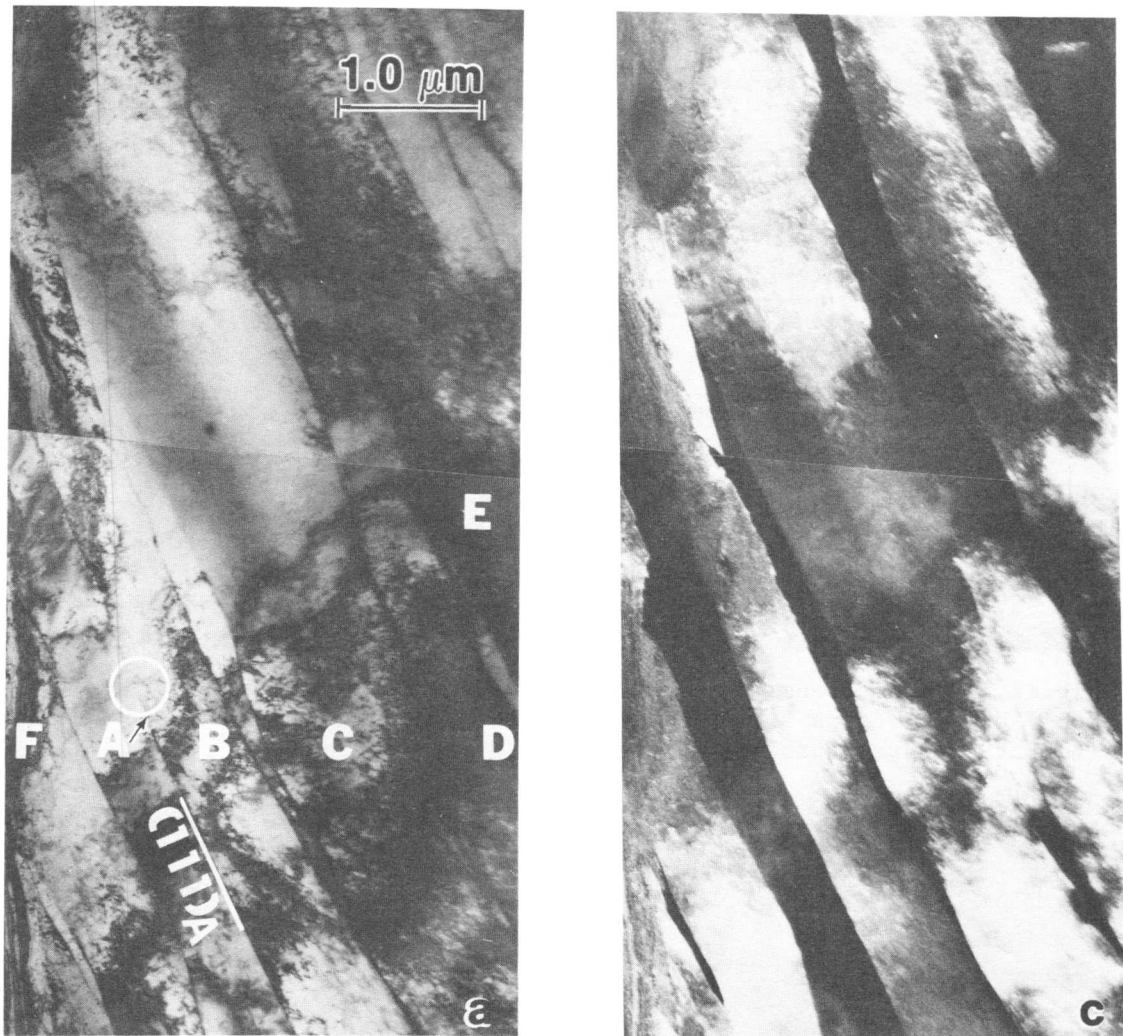
Fig. 2. (a) Bright field image showing retained austenite between adjacent laths; (b) Diffraction patterns $(1\bar{1}0)_A$ and $(100)_M$ (A), and $(100)_M$ (B, C and D); (c) Dark field image using 002_M reflection in B, C and D.

Strain-Induced Martensite in Fe-Ni-C Alloys

T. Nuri Durlu

Several aspects of strain-induced martensite formation were examined in thin foil and bulk samples of three different Fe-Ni-C alloy austenites. Two different types of martensites were found during deformation-induced transformations. The first type is described as stress-assisted martensite and appeared between M_S and $\sim(M_S + 50)^{\circ}$C temperatures. The second martensite was observed near to the upper temperature limit of stress-assisted martensite formation, which is here designated as M_d, and well above this temperature. **In situ** observations of strain-induced martensite formation in high voltage transmission electron microscope revealed that the formation characteristics of this martensite is similar to that of slip formation. Crystallographic and morphologic properties of strain-induced martensite were also investigated during the work and although the habit plane and orientation relationships were found different, substructure of strain-induced martensite was observed as similar to that of thermally induced plate martensites of the same alloys.

I. Introduction

The influence of the applied stresses on the formation of martensite in Fe-Ni-C and Fe-Ni-Cr-C alloys was investigated by Bolling and Richman [1-3]. They studied the martensite formation under applied stresses in two different groups which were distinguished by a definite temperature, M_S^{σ}, above the usual M_S temperature. The transformation below M_S^{σ} is influenced by the elastic stresses and the product is called stress-assisted martensite. Applied plastic deformation above M_S^{σ} temperature also caused the formation of martensite which has different structural characteristics than those of plate martensites and is described as strain-induced martensite. Guimaraes [4], Guimaraes and Shyne [5,6] and Maxwell et al [7] also studied several aspects of the deformation-induced transformations in different Fe-Ni-C alloys and described the crystallography and morphology of these martensites as well as the mechanical properties of the transformed materials.

Although the morphology of strain-induced martensite was investigated in different Fe-Ni-C alloys [7,8] and described as parallel "bands" in the austenite matrix,

Science Faculty of Ankara University, Department of Physics, Beşevler, Ankara, TURKEY .

Onodera and Tamura [9] opposed to the formation of strain-induced martensite "bands" under applied external stresses and described the observed "bands" as deformation twins formed after the application of plastic deformation.

In the present investigation a detailed study of strain-induced martensite in thin foil and bulk austenite samples of Fe-Ni-C alloys is described by means of high voltage transmission and scanning electron microscopy, and the results are compared with those of normal plate martensites of the same alloys reported earlier [8].

II. Experimental Procedure

Three Fe-Ni-C alloys which all had **sub-zero** M_S temperatures were supplied by the United Steel Co.Ltd: Fe-26.4%Ni-0.24%C ($M_S \approx -45^{\circ}$C), Fe-24%Ni-0.45%C ($M_S \approx -50^{\circ}$C) and Fe-17.1%Ni-0.81%C ($M_S \approx -65^{\circ}$C). Specimens were annealed in evacuated silica tubes for 12 h at 1200°C; after the annealing process, the structures were completely austenitic. The bulk austenitic samples were deformed plastically by rolling and examined with a Cambridge Stereoscan MK1 scanning electron microscope. The same instrument was also used to obtain selected area channelling patterns for crystallographic determinations.

The thin tensile specimens were machined from sheet samples in 5x16x0.2 mm dimensions and were annealed to austenite as described above, then dished and electropolished to obtain sufficiently thin areas around the center regions for **in situ** observations of strain-induced martensite formation in high voltage electron microscope. Tensile tests in an AEI EM7 high voltage transmission electron microscope was carried out by using a specially designed stage, and the formation of martensite was followed and recorded with a TV screen connected to a video-monitor attached to the microscope. The high voltage microscope was operated at 500 kV to avoid radiation damage.

III. Results and Discussion

(1) Formation of strain-induced martensite

Although the occurence of strain-induced martensite has been known since Otte's[10] studies on stainless steel, no satisfactory explanation has been given on its nucleation and growth mechanism. The formation of strain-induced martensite was observed at temperatures ~200°C above the usual M_S temperature of ferrous alloys and very large stresses would be required to raise the M_S temperature to this limit with a constant driving force [11]. However Maxwell et al [7] observed strain-induced martensite formation in some Fe-Ni-C alloys even at temperatures

-41-

well above the early predicted T_0 temperature at which the transformation free energy is zero,and found that ~1% strain-induced martensite is formed after ~35% deformation at +260°C.Although this discrepancy can be explained with the new data given by Apple and Krauss [12] for the T_0 temperature as+270°C (i.e. ~M_s+240°C),still the formation of the observed strain-induced martensite or its resemblance to athermally formed plate martensites needs more explanation because of the required high amount of applied stress to raise M_s until these upper temperature limits. Studies on the formation of lath martensites in small iron precipitate particles in a copper matrix [13,14] showed that martensite in iron can be nucleated by interaction of the slip dislocations of the copper matrix with the iron precipitates.This suggests a possible similar mechanism for the formation of strain-induced martensite which involves simple dislocation interactions in the deformed austenite.

In the present investigation several austenitic specimens of the three Fe-Ni-C alloys were deformed in the microscope in tension and the structural changes during the tests were recorded with a video-monitor within 1/25 sec. intervals.Tests were carried out at room temperature and it was observed that the formation of strain-induced martensite occurs in some austenite grains under a given applied stress whilst in others there is no transformation.This presumably indicates that a critical amount of strain is required to produce strain-induced martensite.The time taken to form an individual plate was found to be smaller than 1/25 sec.Fig. 1 is an electron micrograph of a group of strain-induced martensite formed simultaneously during the test in an Fe-17.1%Ni-0.81%C alloy sample.As is shown in the micrograph,strain-induced martensite may form in parallel groups on a common crystallographic system of the austenite matrix which is more likely determined by the tensile axis.In each grain,more parallel groups of strain-induced martensites were formed after the application of additional strains.A scanning electron micrograph of such groups formed in bulk austenite sample of Fe-26.4%Ni-0.24%C alloy and corresponding selected area channelling patterns of the matrix and product phases are shown in **Fig. 2** . Indexing of channelling patterns in conjuction with the scanning electron microscope pictures revealed that strain-induced martensites have {111} type habit plane and Kurdjumov-Sachs orientation relationship with the matrix austenite.From the observations of austenite to strain-induced martensite transformations in Fe-Ni-C alloys it can be predicted that the formation mechanism shows similarities with that of slip lines in metal crystals and this support the idea that strain-induced martensite may have a different nature rather than simply resembling athermal plate martensites.

Electron microscope observations of the matrix auste-

nite prior to the transformation revealed that Fe-Ni-C aus-
tenites contain only dislocation type lattice imperfections.
Dislocations appeared in the form of tangles and further
plastic deformation of austenite increased the dislocation
densities at room temperature.Since the dislocations were
the only crystal fault to appear before the formation of
strain-induced martensite,they may be responsible to create
the new nucleation sites or embryos mentioned in the strain-
induced martensite nucleation theory developed by Olson and
Cohen [15].

The overall strain-induced martensite volume fractions
in bulk samples were determined as a function of deforma-
tion at room temperature for Fe-26.4%Ni-0.24%C and Fe-
17.1%Ni-0.81%C alloys.Since the maximum stress-assisted
martensite formation temperature of Fe-Ni-C alloys was
found as +10°C [8] ,this type of martensite were not for-
med during the tests.Austenitic samples were deformed in
compression to various strains and strain-induced martensite
volume fractions were determined with resistance measure-
ments [8].The volume fractions of strain-induced martensites
of two Fe-Ni-C alloys are shown in Fig. 3 as a function of
deformation.

(2) The morphology of strain-induced martensite

The substructures of strain-induced martensites were
also examined for the three Fe-Ni-C alloys used during the
studies and it was found that martensitic regions contain
very high densities of dislocations as reported earlier [8].
Fig. 4 is an electron micrograph of the observed disloca-
tions in an Fe-17.1%Ni-0.81%C alloy martensite.However
after the careful tilting of the electron microscope spe-
cimens it was found that strain-induced martensite also
exhibits twinned substructure.Fig. 5 shows a high magni-
fication electron micrograph of a strain-induced marten-
site containing twins which extend across the entire
martensite structure in Fe-24%Ni-0.45%C.The appearence of
the twins depends on their orientation with respect to the
specimen surface.In situ observations of the strain-indu-
ced martensite formation revealed that martensites are
formed with twinned substructure.Therefore the observed
twins are transformation twins and they are caused by
internal stresses arising from the transformation strain
rather than the further deformation of the samples after
the martensite formation.Fig. 6 shows a dark-field elec-
tron micrograph and corresponding diffraction pattern of
twinned strain-induced martensite of alloy Fe-26.4%Ni-
0.24%C .The dark-field image was taken with a twin ref-
lection and indexing of diffraction pattern revealed that
transformation twins are formed on {112}⟨111⟩ system of
the strain-induced martensite.The orientation relation-
ship between strain-induced martensite and austenite was
determined from the same electron diffraction pattern and

it was found to be consistent with that of Kurdjumov-Sachs. The habit plane of martensite was also determined in thin foils and found as {111} planes of the matrix austenite. These results indicate that strain-induced martensites formed in thin foil and bulk samples of Fe-Ni-C austenites have unique habit plane and orientation relationships in both conditions.

The results obtained after the examination of strain-induced martensite formation in thin foil and bulk samples of Fe-Ni-C alloys show that the formation characteristics of strain-induced martensite are similar to those of slip formation with a formation time smaller than 1/25 sec . On the other hand, this martensite has unique habit plane and orientation relationship with the matrix austenite and exhibits twinned substructure as observed in the athermally formed plate martensites of Fe-Ni-C alloys with the same compositions [8].

Author would like to thank Prof. J. W. Christian for many helpful discussions.

References

[1] G. F. Bolling and R. H. Richman: Phil Mag.,19(1969),247.
[2] G. F. Bolling and R. H. Richman: Scripta Met.,4(1970), 569 .
[3] G. F. Bolling and R. H. Richman: Acta Met.,18(1970),673.
[4] J. R. C. Guimaraes: PhD Thesis,Stanford University , (1969) .
[5] J. R. C. Guimaraes and J. C. Shyne: Scripta Met., 4(1970),1019 .
[6] J. R. C. Guimaraes and J. C. Shyne: Met.Trans., 2(1971),2063 .
[7] P. C. Maxwell, J. C. Shyne and A. Goldberg: The TRIP Effect in Fe-Ni-C Alloys,California University,(1972) .
[8] T. N. Durlu: DPhil Thesis,Oxford University,(1974).
[9] H. Onodera and I. Tamura: Scripta Met.,11(1977),1057 .
[10] H. M. Otte: Acta Met.,5(1957),614 .
[11] J. R. Patel and M. Cohen: Acta Met.,1(1953),531 .
[12] C. A. Apple and G. Krauss: Met.Trans.,2(1971),1785 .
[13] K. E. Easterling and G. C. Weatherby: Acta Met., 17(1969),845 .
[14] K. E. Easterling and P. K. Swann: Inst.of Metals Monograph,No.33,(1969).
[15] G. B. Olson and M. Cohen: J.Less-Com.Met.,28(1972),107.
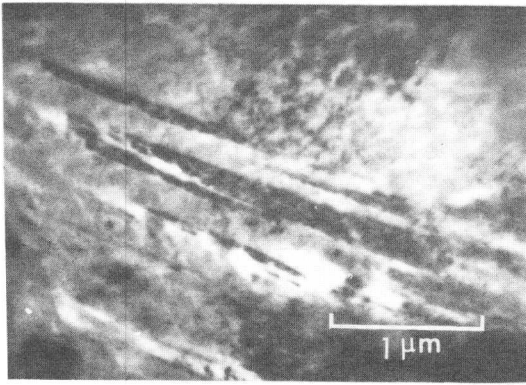
Fig. 1 A group of strain-induced martensites formed in Fe-17.1%Ni-0.81%C alloy.
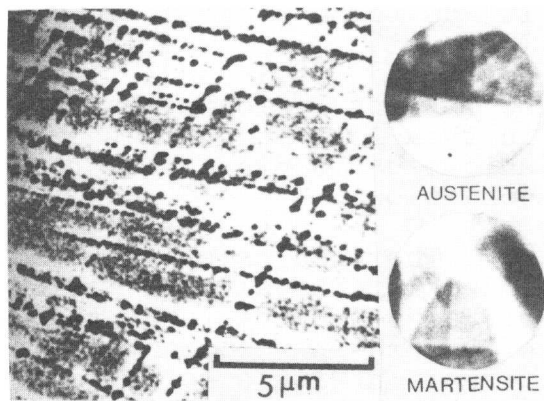
Fig. 2 Scanning electron micrograph of strain-induced martensite groups and channelling patterns of matrix and product phases.
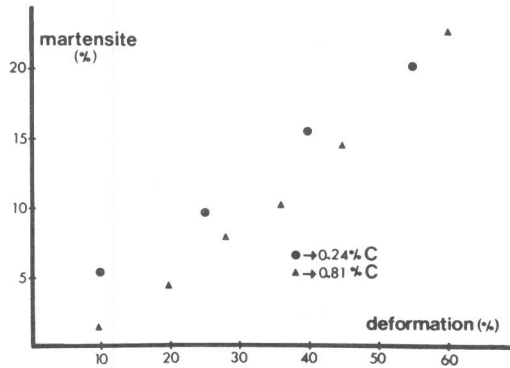
Fig. 3 Martensite volume fraction vs deformation changes for two Fe-Ni-C alloys.
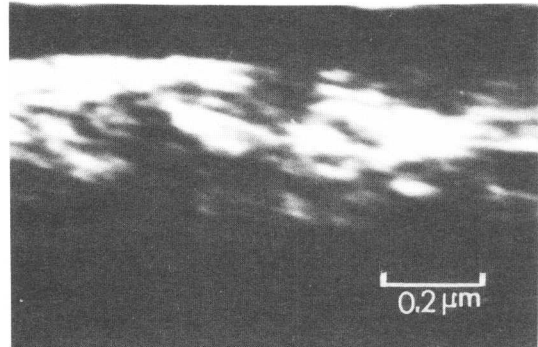
Fig. 4 Dislocations in an Fe-17.1%Ni-0.81%C alloy strain-induced martensite.
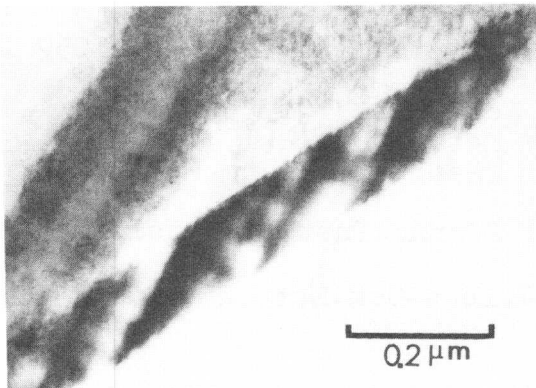
Fig. 5 Transformation twins in an Fe-24%Ni-0.45%C alloy strain-induced martensite.
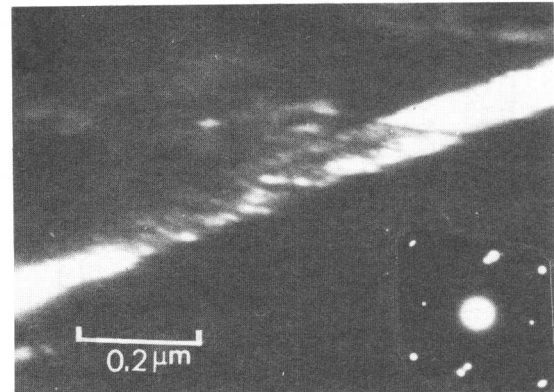
Fig. 6 Dark-field electron micrograph and corresponding electron diffraction pattern of a twinned martensite.

Martensite Morphology in Rapidly Solidified Fe Alloys

Y. Inokuti[*] and B. Cantor[+]

It has been shown that when pure Fe, Fe-Ni, Fe-Mn and Fe-Ni-C alloys are rapidly solidified by splat-quenching techniques, the resulting materials show two surprising features (1,2). Firstly, the M_S temperature is depressed by an amount which increases with increasing alloy content and reaches a value as high as $\sim$ 200K in an Fe-15%Ni alloy; this effect is thought to be caused by a small as-solidified austenite grain size. Secondly, splat-quenched specimens which had become fully martensitic during cooling to room temperature had an extremely high hardness of up to 700Kgmm^{-2}; this has been shown to be a grain size effect also, caused primarily by a small martensite plate size (3). The present paper summarises this previous data and describes the results of a transmission electron microscope investigation of the martensite morphology in splat-quenched Fe-Ni alloys. The splat-quenched microstructure is described in relation to the well-known morphological transition from lath-like to internally twinned martensite in conventional solid-state quenched Fe-Ni.

I Experimental Technique

The alloys were prepared by induction melting in recrystallised alumina crucibles under a dynamic Ar atmosphere. Specimens of $\sim$ 1g each were splat-quenched by a 2-piston technique described previously (4), which involved levitation melting under Ar followed by splat-quenching between 2 magnetically-accelerated polished Cu pistons. The resulting foils were typically 50-150μm thick and 30mm in diameter. The closing velocity of the pistons was 5-13ms^{-1} (4) and the effective cooling rate has been measured as 10^5-10^7Ks$^{-1}$(5). For comparison, specimens of the same alloy stocks were prepared by cold rolling, austenitising, and solid-state quenching into iced brine.

II Depression of M_S

Table 1 shows the phases detected by X-ray diffractometry in splat-quenched and solid-state quenched Fe-Ni, Fe-Mn and Fe-Ni-0.1%C.

---

[*] Kawasaki Steel Corporation, Chiba City, Japan.

[+] School of Engineering and Applied Sciences, University of Sussex, Brighton, UK.

wt% Ni or Mn	Phases Present					
	Fe-Ni		Fe-Ni-C		Fe-Mn	
	SQ	SSQ	SQ	SSQ	SQ	SSQ
0	α	α	α	α	α	α
5	α	α	α	α	α	α
10	α	α	α	α	α+(γ)	α
15	α	α	α	α	α+γ+(ε)	α+ε
20	α+γ	α	α	α	γ+(ε)	α+γ+ε
25	γ	α	γ	α+(γ)		
30	γ	α+γ	γ	(α)+γ		
35	γ	γ	γ	γ		
40	γ	γ	γ	γ		

Table 1: X-ray diffractometer results showing phases present in splat-quenched (SQ) and solid-state quenched (SSQ) Fe-Ni, Fe-Ni-C and Fe-Mn alloys. Phases in brackets were present in traces only.

In each alloy system, the onset of austenite retention in splat-quenched specimens occurred at a lower concentration of solute than in solid-state quenched specimens. Thus for instance, solid-state quenched Fe-25%Ni was fully martensitic ar room temperature whereas splat-quenched Fe-25%Ni was fully austenitic and had not begun to transform. The solid-state quenched data was as expected from previous experiments (8), so the difference in austenite retention implied that M_S had been drastically reduced by splat-quenching, and this has recently been confirmed by calorimetric experiments (6). The martensite was not isothermal because the X-ray diffractograms were independent of ageing at room temperature. As expected, the austenite retention decreased for a lower cooling rate during splat-quenching, or after a subsequent sub-zero cooling treatment. Careful composition analysis showed that splat-quenching caused no increase in trace interstitials such as C,N,O which can all depress M_S strongly.

It seemed possible that depression of M_S and retention of austenite were caused directly during the splat-quenching process, either by the very rapid cooling rate in the solid-state (5) or by stray magnetic fields, shear deformation, or hydrostatic pressure in the specimen between the pistons. However, these possible explanations were shown to be incorrect because M_S remained depressed even after long annealing times in the austenite range (6), (up to $\sim$ 1000 mins at 1000K). This indicated that the depression of M_S had a microstructural origin. The most reasonable explanation was that the as-solidified austenite grain size and dendrite cell size was very small, so that active martensite nucleation catalysts were segregated into

relatively few austenite grains or cells and thus rendered ineffective. This is similar to the classic martensite nucleation experiments of Cech and Turnbull (7) on small particle Fe-Ni powders.

III Martensite Morphology

SEM pictures of splat-quenched martensitic Fe-Ni showed a microstructure which was independent of Ni content (6). A typical example for Fe-10%Ni is shown in fig 1. The martensite appeared very similar to the lath martensite which is found in conventional solid-state quenched Fe-Ni at low Ni content (10,11). However, the martensite laths were on a small scale with widths of $\sim$0.3-0.5µm and lengths of $\sim$ 3-5µm. SEM micrographs of splat-quenched martensitic pure Fe were virtually identical to fig 1 (3).

Figs 2-8 show the results of a TEM investigation of the splat-quenched martensitic microstructure. TEM pictures confirmed that the martensite in splat-quenched pure Fe consisted of small-scale approximately parallel laths (fig 2). The true lath width was $\sim$ 0.1-0.3µm, somewhat smaller than that indicated by SEM pictures. As described elsewhere (9), interlath boundaries were {211} and diffraction patterns frequently showed twin spots, indicating that adjacent laths were sometimes related by twin orientations.

TEM pictures of splat-quenched Fe-Ni alloys (figs 3-6) revealed a microstructure independent of Ni content, but rather different from the laths in splat-quenched pure Fe. The martensite consisted of very fine-scale parallel arrays of twin plates $\sim$ 0.01-0.05µm wide, clearly much smaller than had been indicated by SEM pictures such as fig 1. The morphology differed from that in pure Fe because the plates were narrower, interplate boundaries were straighter, and there was a more regular alternating black-white contrast between adjacent plates. The twin relationship between adjacent plates was shown in several ways. Firstly, selected area diffraction patterns almost always contained two twin-related superimposed arrays of spots, and a typical example is shown for Fe-15%Ni in fig 5. Secondly, trace analysis showed that interplate boundaries were {211} as can be seen in figs 5 and 7. Thirdly, dark field micrographs using one of the less intense twin spots produced a reversal of the black-white contrast as shown in fig 3 for Fe-5%Ni.

The microstructure in figs 3-6 is identical to a fine-scale twinned ferrite. Thus, it might be argued that during splat-quenching the austenite transforms to massive ferrite, which becomes heavily twinned by deformation between the two splat-quenching pistons. Massive ferrite grains have been observed in splat-quenched pure Fe, but they contain no twins (3,9). Moreover, massive ferrite is very unlikely in the higher Ni alloys where martensite forms readily at cooling rates many orders of magnitude below that in splat-quenching. The TEM specimens were prepared by ion-beam thinning and only small areas were electron transparent. Thus, it also might be argued that figs 3-6 show fine twins within martensite laths or plates as is common in high Ni solid-state quenched Fe-Ni (11). However, SEM

-48-

pictures such as fig 1 indicate that the martensite laths or plates are no more than ∿ 0.3-0.5μm wide, so the martensite itself should be seen on figs 3-6 which are ∿ 1-2μm square. In addition, internally-twinned martensite is unlikely in Fe-5 or 10%Ni (11). The most reasonable conclusion is that the martensite produced by splat-quenching consists of arrays of fine scale twins, and that this microstructure is independent of Ni content. In pure Fe, the crystallography is similar but the martensite shows a more conventional lath morphology.

IV Martensite Hardness

Fig 8 shows the Vickers microhardness of splat-quenched and solid-state quenched Fe-Ni as a function of Ni content. In the martensitic splat-quenched alloys, the hardness was very high, ∿ 700Kgmm^{-2}, and decreased when the microstructure became austenitic. Recent experiments have shown that the high hardness of splat-quenched pure Fe martensite can be explained as a Hall-Petch effect, by assuming that interlath martensite boundaries act as dislocation barriers (3,9). On this basis martensitic splat-quenched Fe-Ni shsould have an even higher hardness, because of the finer scale of the microstructure as described in the last section. It is not clear why an increased hardness is not seen experimentally. A very high hardness is also seen in splat-quenched Fe-Mn and Fe-Ni-0.1%C, but the hardness increases with increasing alloy content (2). The martensite morphology is presently being investigated in Fe-Mn. In addition in-situ straining experiments in the TEM are being performed on splat-quenched Fe-Ni to determine directly the deformation mechanisms.

References

1   Y Inokuti & B Cantor, Scripta Met 10 (1976) 655
2   Y Inokuti & B Cantor, J Mat Sci 12 (1977) 946
3   F Duflos & B Cantor in"Rapidly Quenched Metals III" ed B Cantor
    (Metals Society, London, 1978) vol 1   p 110
4   R W Cahn, K D Krishnanand, M Laridjani, M Greenholz & R Hill,
    Mat Sci Eng 23 (1976) 83
5   F Duflos & B Cantor to be published
6   Y Inokuti & B Cantor to be published
7   R E Cech & D Turnbull, TMS-AIME 206 (1956) 124
8   L Kaufman & M Cohen, TMS-AIME 206 (1956) 1393
9   Y Inokuti, F Duflos & B Cantor in "Phase Transformations" Institu-
    tion of Metallurgists Spring Conference, York, 1979 (Chameleon
    Press, London, in press)
10   R G Bryans, T Bell & V M Thomas in "The Mechanism of Phase Trans-
    formations in Crystalline Solids" (BPC Letterpress, London, 1969)
    p 181
11   T Bell in "Martensite" ed E R Petty (Longman, London, 1970) ch 4
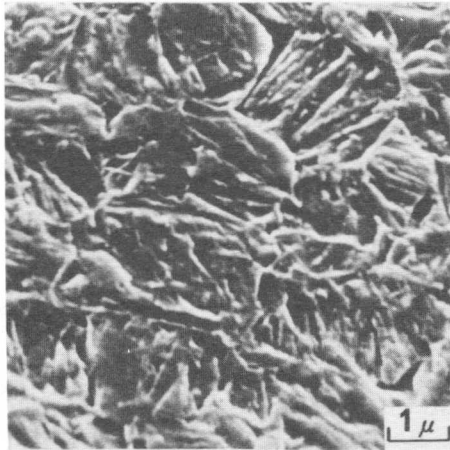
Figure 1: SEM of splat-quenched
Fe-10%Ni
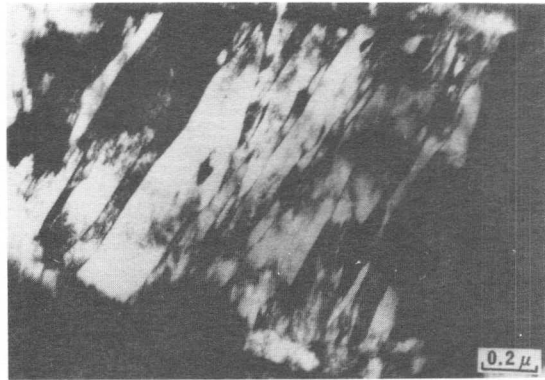
Figure 2: Bright-field TEM of
splat-quenched pure Fe
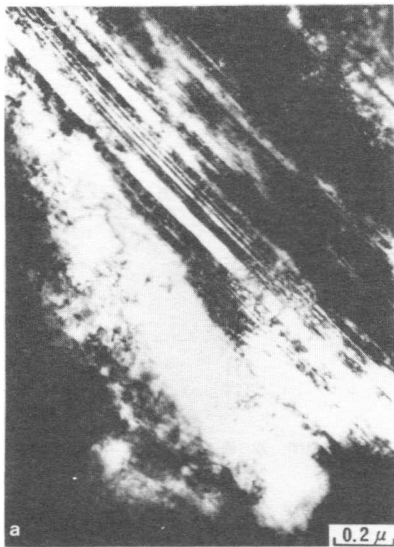
Figure 3: TEM of splat-quenched Fe-5%Ni

(a) bright-field   (b) dark-field
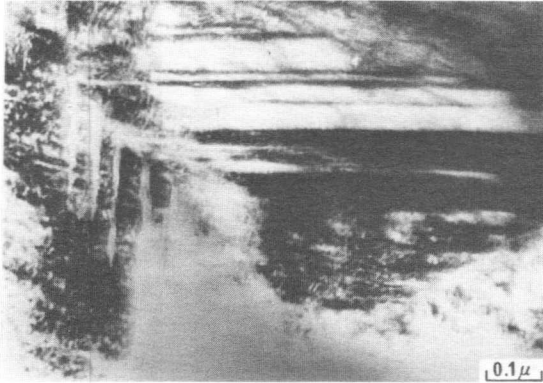
Figure 4: Bright-field TEM of
splat-quenched Fe-10%Ni
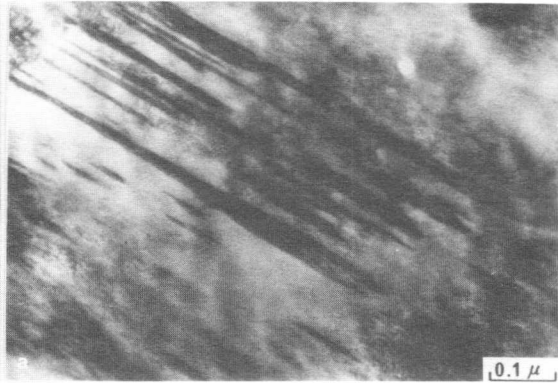
Figure 5: TEM of splat-quenched
Fe-15%Ni
(a) bright-field
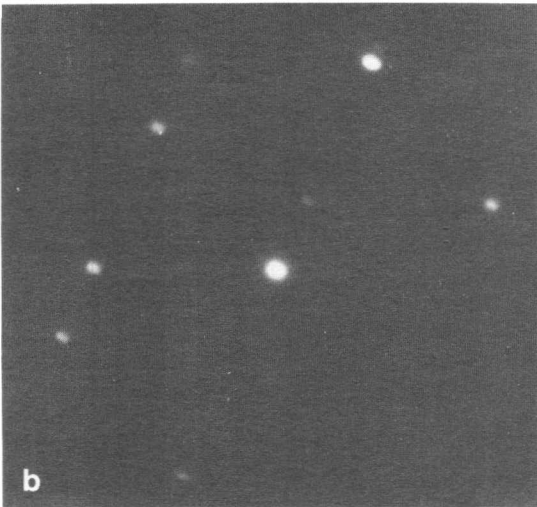
Figure 5: TEM of splat-quenched
Fe-15%Ni
(b) diffraction pattern
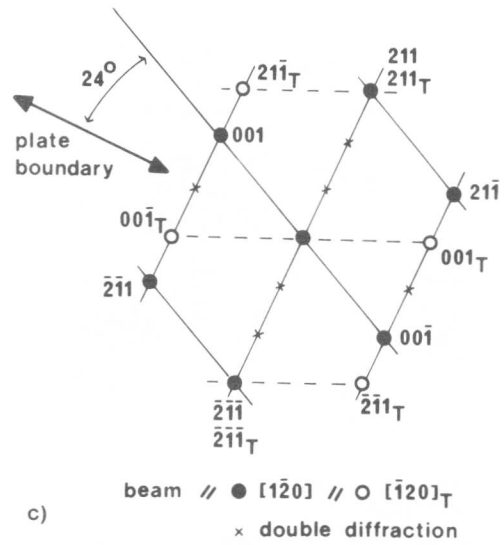
Figure 5: TEM of splat-quenched
Fe-15%Ni
(c) diffraction analysis
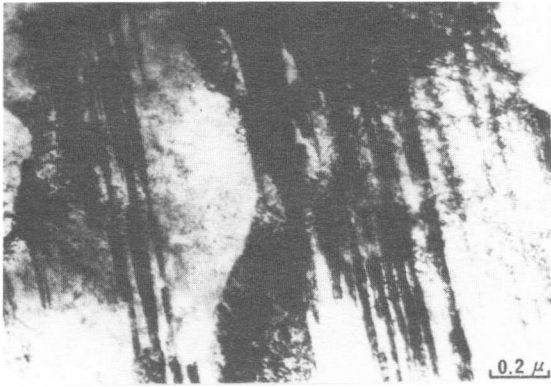
Figure 6: Bright-field TEM
of splat-quenched
Fe-20%Ni
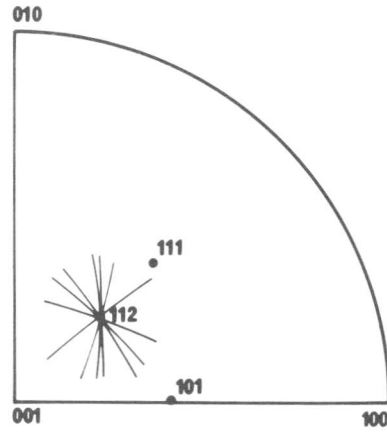
Figure 7: Trace analysis of
martensite boundaries
in splat-quenched Fe-Ni

Fe-20%Ni Alloy
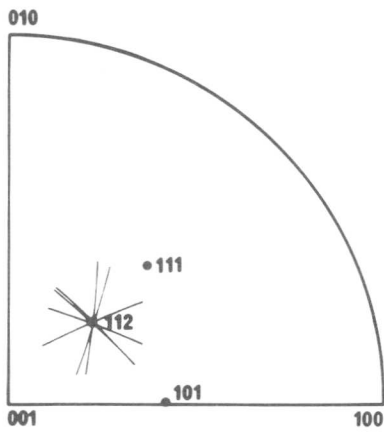
Figure 7: Trace analysis of
splat-quenched
Fe-Ni
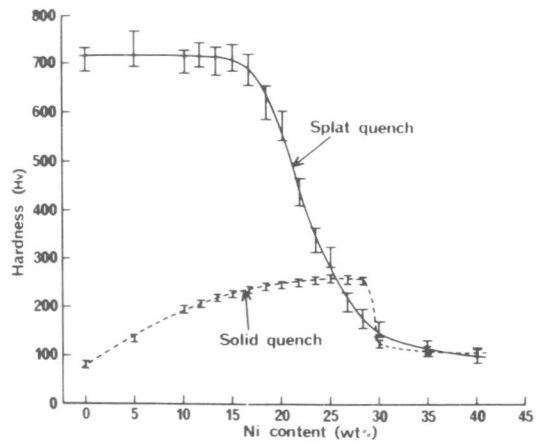
Figure 8: Hardness of splat-
quenched and solid-
state quenched Fe-Ni

-52-

M. Umemoto and I. Tamura

The morphological and crystallographic characteristics of butterfly martensite were studied in Fe-Ni-C alloys using mainly optical microscopy. There are two types of butterfly martensites formed by cooling. One is characterized by narrow wings, smooth and straight α'-γ interface and without a mid-rib. Another is characterized by thicker wings and an existence of a mid-rib with a twinned region around it. As a three-dimensional picture, a butterfly martensite has a shape like as if one put together two half circle converging lenses with an obtuse angle. The habit plane of butterfly martensite is close to $\{225\}_f$ and if one wing is $(hh1)_f$ another wing is either $(\bar{h}h1)_f$ or $(h\bar{h}1)_f$. Butterfly martensite also forms on a specimen surface during polishing. This butterfly martensite is characterized by thick and short wings, irregular α'-γ interface and there is a clear straight junction plane trace at the boundary of two wings.

I. Introduction

In ferrous alloys four different morphologies of bcc(bct) martensites have been recognized, ie. lath, lenticular, thin plate and butterfly martensites. Lath and lenticular martensites [1] are the most popular morphologies and observed in many ferrous alloys other than Fe-Ni-C alloys. Thin plate martensite, which is first observed in Fe-Ni-C alloys [2] and characterized as completely twinned without a mid-rib, was less popular than the lath or lenticular but recently becoming popular with the findings of this type morphology in other ferrous alloys such as Fe-Al-C [3] and Fe-Pt [4]. Butterfly martensite, which is named from its appearance [5] and sometimes called "angle profile" [6], "chevron" [7], or "bracket" [8] martensite, is the least popular morphology among the four morphologies. Most of this reason seem to be arised from experimental difficulties to obtain it. In Fe-Ni-C alloys martensite morphology strongly depends on its formation temperature and butterfly martensite forms above 273 K irrespective of carbon content [9]. To obtain butterfly martensite in a partially transformed condition (around 10% is best) by cooling between room temperature and 273 K, M_s temperature have to be well controlled at around room temperature. In the specimen of M_s temperature close to room temperature or specimens cooled just below room temperature, martensites are easily induced on a specimen surface by mechanical polishing. This causes another difficulty in the observation of butterfly martensite which has never happened in the study of lenticular or thin plate martensite. In spite of these experimental difficulties, it is considered to be important to study butterfly

Department of Metal Science & Technology, Faculty of Engineering, Kyoto University, Sakyo-ku, Kyoto, 606, Japan.

martensite since it is not a peculiar but a regular morphology like lath, lenticular or thin plate. Moreover since butterfly martensite is considered to be the one in between lath and lenticular martensite, its investigation will make clear the relation between lath and lenticular martensite. Thus the purpose of this paper is to present the experimental results about morphological and crystallographic characteristics of butterfly martensite.

II. Experimental Procedure

Fe-19.50Ni-0.73C and Fe-18.32Ni-0.74Cr-0.50C (wt%) alloys used were prepared by vacuum induction melting. The ingots were hot-forged at 1373 K to produce sheets about 10 mm in thickness, and then homogenized in vacuum at 1473 K for 20 h. After being homogenized, they were cold-rolled down to 1.5 mm thick and then cut into pieces of 8 X 15 mm. Specimens were austenitized in vacuum at 1473 K for 1 h and air-cooled to room temperature. The M_s temperature in these two alloys were close to room temperature. Optical microscopic observation was done with an etching solution of 35% $Na_2S_2O_5$. In present paper most of the results were presented in an alloy containing 0.74% Cr but situations were completely the same for the case of Cr free Fe-Ni-C alloy.

III. Results and Discussion

(1) Morphology of Butterfly Martensite

Photograph 1 shows a representative micrograph of butterfly martensites. A butterfly martensite consists of two plates forming an obtuse angle. Those plates are not extended through out a grain (like lenticular or thin plate martensite). The size of butterfly martensite is much smaller than that of lenticular or thin plate and the average span of two wings is about 30 μm and the maximum of it is at most 100 μm. It is noted that there are two different types of butterfly martensites transform by cooling as marked type A and B in Photo.1. Photographs 2(a) and (b) show high magnification micrographs of typical type A and B butterfly martensites. Type A which is more frequently observed than B, has a thickness of the wing only 1 to 3 μm and characterized by a smooth and straight α'-γ interface. While type B, which is larger than type A, is characterized by a thicker wings around 10 μm and somewhat curved α'-γ interface and most importantly characterized by the existence of a mid-rib in the center of each wing along the longitudinal direction. It is noted that in every case the mid-ribs in the two wings are continuous at the junction of two wings. Photographs 3(a) and (b) show further example of type B butterfly martensite. (a) shows an example when two butterfly martensites forms in a zig-zag fashion. In this case mid-ribs are also continuous through out these two butterflies. This feature of mid-ribs is quite similar to those observed in lenticular martensite when several plates form in a zig-zag fashion. Photograph 3(b) is an example when one of the wings is close to parallel to the specimen surface and showing the detail of the region around a mid-rib. Along the mid-rib it is clearly seen a twinned structure similar to the one observed around a mid-rib of lenticular martensite. From these observations it can be concluded that type B butterfly martensite has a mid-rib with a twinned region around it.

To develop a three-dimensional picture of butterfly martensite, a serial-sectioning experiment has been performed. Photograph 4(a) shows the initial polished and etched surface, and Photo.4(b) and (c) show, respectively the same area after 76 µm and 128 µm have been removed. The two wings of butterfly martensite in Photo.4 become shorter with increasing depth. Figure 1 is a three-dimensional diagram of the butterfly martensite observed in Photo.4. From this and other experiments it is considered that a butterfly martensite (both type A and B) has a shape like as if one put together two half circle converging lenses with an obtuse angle as shown schematically in Fig.2.

(2) Crystallography of Butterfly Martensite

The habit plane and combination of two variants forming a butterfly martensite were determined by the following experiment. First, a grain having four different $\{111\}_f$ annealing twin traces was selected (Photo.5). The specimen normal and the indices of four twin traces were calculated following a reported procedure [10]. After measuring the directions of α'-γ interface plane traces, the specimen was mechanically and chemically polished for a certain distance parallel to the initial surface. The slope of interface plane with specimen surface was calculated from the polished depth and the distance of displacement on the plane parallel to the specimen surface. Using this technique the indices of interface plane were determined for 8 wings of 4 butterfly martensites marked in Photo.5 (where No.1 and 4 are type B and No.2 and 3 are type A). Figure 3 is a stereographic unit triangle showing measured interface plane normals. It is clear that butterfly martensite has a habit plane very close to the $[\bar{1}10]_f$ zone (irrespective of the types of butterfly martensite) and within the limitation of experimental accuracy can be considered as $(hh1)_f$. The mean habit plane is given by $p_1' = (0.3481, 0.3878, 0.8540)$. This average result is 3.7 deg from $(112)_f$, 2.4 deg from $(225)_f$. The habit plane normal obtained in present investigation is consistent with that reported by Brook et al [11]. It is interesting to note that the habit plane of Fe-Ni-C alloys changes with the decrease in M_s temperature from $\{111\}_f$ (lath) $\rightarrow$ $\{225\}_f$ (butterfly) $\rightarrow$ $\{259\}_f$ (lenticular) $\rightarrow$ $\{3,10, 15\}_f$ (thin plate). This type of change in habit plane is also observed in Fe-C alloys in which the habit plane changes from $\{111\}_f \rightarrow \{225\}_f \rightarrow \{259\}_f$ with increase in carbon content and equally with decrease in M_s temperature [12]. The combination of two variants forming a butterfly martensite can be seen in Fig.4 in which habit plane normals (a and b) and direction of intersection of two habit planes (R) of four butterfly martensites in Photo.5 are plotted on a standered stereographic projection. In this particular case all the four intersections lying on $(010)_f$ plane and butterfly martensites are symmetric along the $(010)_f$ plane. In general, two variants of a butterfly martensite are selected so that if the habit plane of one variant is $(hh1)_f$ the habit plane of another variant is either $(\bar{h}h1)_f$ or $(h\bar{h}1)_f$ but not others.

(3) Butterfly Martensite Formed by Mechanical Polishing

In addition to the above two types of butterfly martensites transformed by cooling, there is another type of a butterfly martensite. Photograph 6 shows an example of this type of butterfly martensite. This type of butterfly martensite (call type C) is characterized by thick and

short wings, irregular α'-γ interface and an existence of a clear line trace at the junction of two wings. From a serial-sectioning experiments, this butterfly martensite is found to exist only near the specimen surface (5-50 μm) and there are indications that this type of butterfly martensite are stimulated by plastic deformation since their density is low in carefully polished specimens (using very light pressure), but increases considerably in less carefully polished specimens. From these it is quite probable that this type of butterfly martensites are formed on the specimen surface during mechanical polishing at room temperature. To make this point clear the following experiment has been performed. An austenitized specimen was subzero cooled to transform martensite and then tempered at 373 K for 2 h. After that specimen was mechanically polished and etched. Since tempered martensite can be etched much deeper than that of untempered, if martensites are formed during polishing these can be distinguished by etched contrast from those transformed by initial subzero cooling. Photo.7 is an example of the result of this experiment and showing that the martensites etched complete dark are all either type A or B and all type C butterfly martensites were etched lightly. In addition to this, surface relief observation in which martensites are transformed by cooling on a prepolished austenite surface also indicate that all the surface relieves correspond to either type A or B and not C. From these it is concluded that type C butterfly martensites are formed on a specimen surface during mechanical polishing at room temperature. It is also noted that type C butterfly martensites form in the specimen of which M_s temperature is close to room temperature. Once specimen is cooled to below 253 K, type C butterfly martensites are scarcely observed.

The habit plane of type C butterfly martensite is not clear but it is considered to be same as that of type A or B butterfly martensite (since in many cases wings appear parallel to those of type A or B butterfly martensites). The straight line at the junction of two wings is considered to be a trace of junction plane of two variants. A one surface analysis revealed that the traces of junction planes correspond to $\{100\}_f$. In an early work, Klostermann [5,6] observed a butterfly martensite (could be classified as type C) in an Fe-30Ni alloy and considered the line structure as a mid-rib. However, comparing it with any mid-rib of lenticular martensite, it is more reasonable to consider it as a junction plane.

Referenses

[1] G.Krauss and A.R.Marder, Met. Trans., 2 (1971) 2343.
[2] I.Tamura, Proc. of First JIM Int. Symp., (1976) 59.
[3] M.Watanabe and C.M.Wayman, Met. Trans., 2 (1971) 2221.
[4] M.Umemoto and C.M.Wayman, Acta Met., 26 (1978) 1529.
[5] J.A.Klostermann and W.G.Burgers, Acta Met., 12 (1964) 355.
[6] J.A.Klostermann, ISI Spe. Rep. No.93, (1965) 43.
[7] M.J.Carr, J.R.Strife and G.S.Ansell, Met. Trans., 9A (1978) 857.
[8] O.P.Maksimova et al, Prob. Metalloved. Fiz. Metal., 44 (1955) 123.
[9] M.Umemoto and I.Tamura, to be published.
[10] Y.Shugo, K.Sakazume, S.Kato and T.Honma, Research Inst. of Mineral Dressing and Met. Rep. Tohoku University, 32 (1976) 109.
[11] R.Brook and A.R.Entwisle, JISI,203 (1965) 905.
[12] C.M.Wayman, "Introduction to the Crystallography of Martensitic Transformation", MacMillan Company, New York, 1964.

Photo.1 Optical micrograph of butterfly martensites in Fe-18Ni-0.7Cr-0.5C alloy cooled to 263 K.
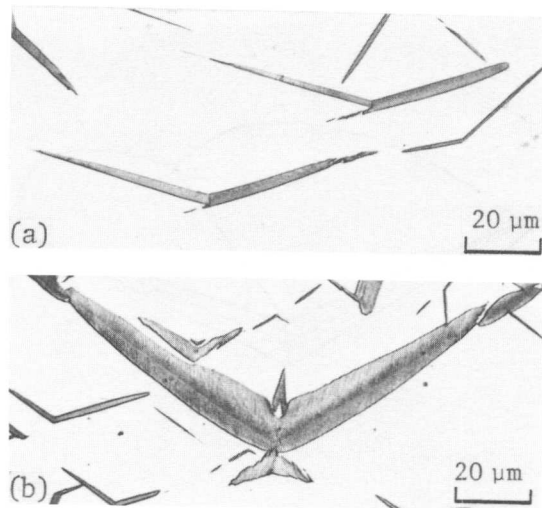
Photo.2 Optical micrographs of type A (a) and type B (b) butterfly martensites in Fe-18Ni-0.7Cr-0.5C.
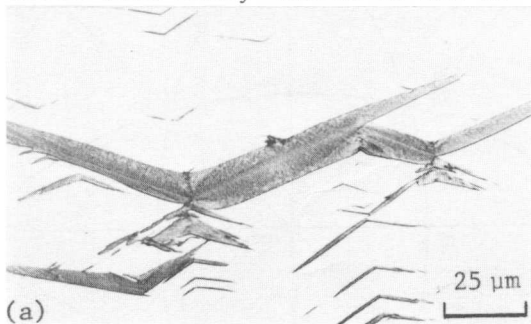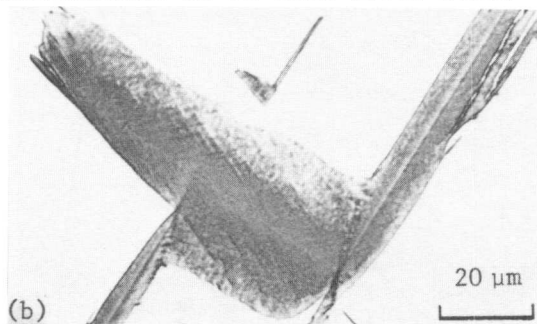
Photo.3 Optical micrographs of type B butterfly martensites.
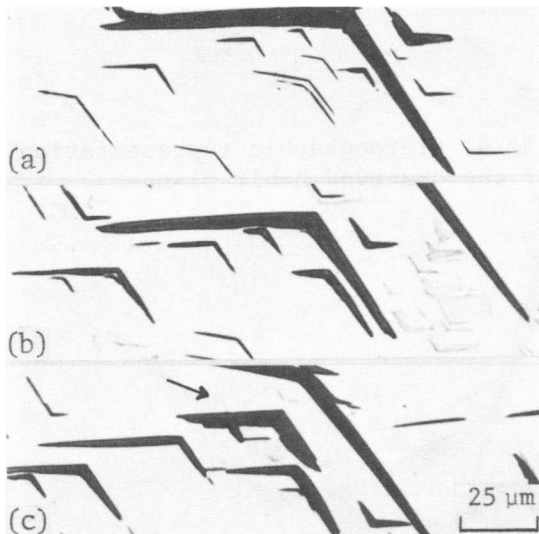
Photo.4 Serial sectioning of a butterfly martensite in Fe-18Ni-0.7Cr-0.5C alloy cooled to 263 K. (a) initial surface;(b) 76 μm below (a); (c) 128 μm below (a).
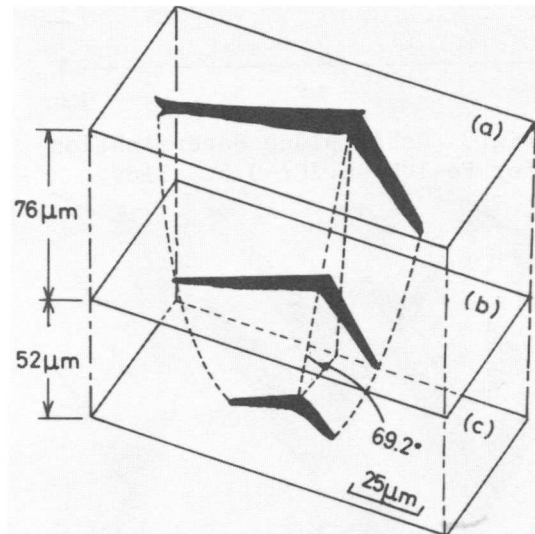
Fig.1 Three dimensional diagram of the butterfly martensite in Photo.4.
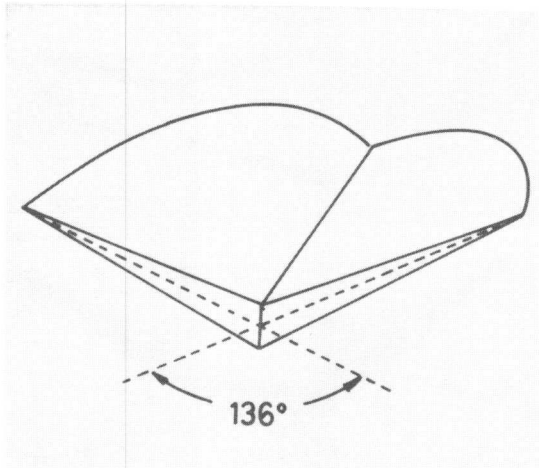
Fig.2 Schematic diagram of a butterfly martensite.
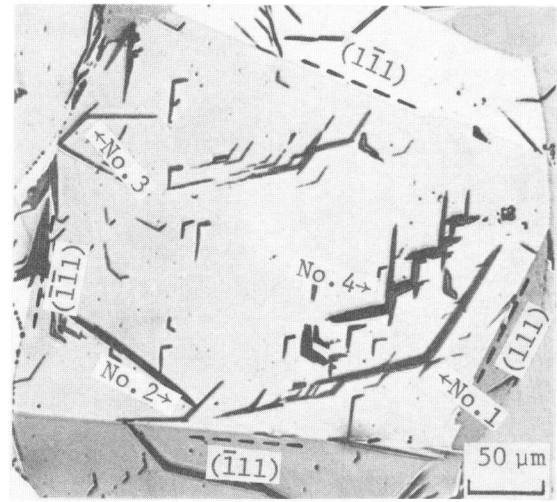
Photo.5 Optical micrograph of Fe-18Ni-0.7Cr-0.5C cooled to 263 K.
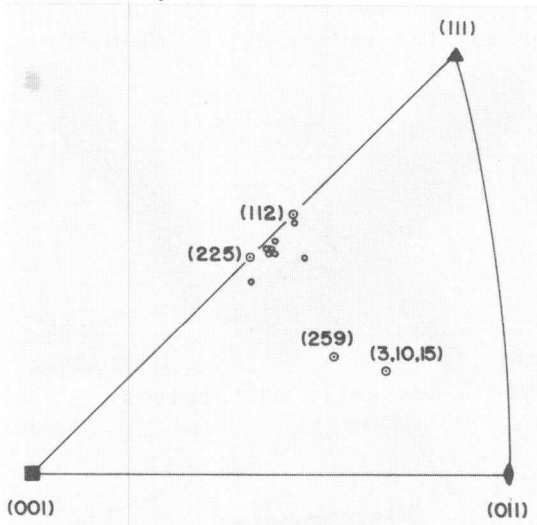
Fig.3 Habit plane determination for Fe-18Ni-0.7Cr-0.5C alloy.
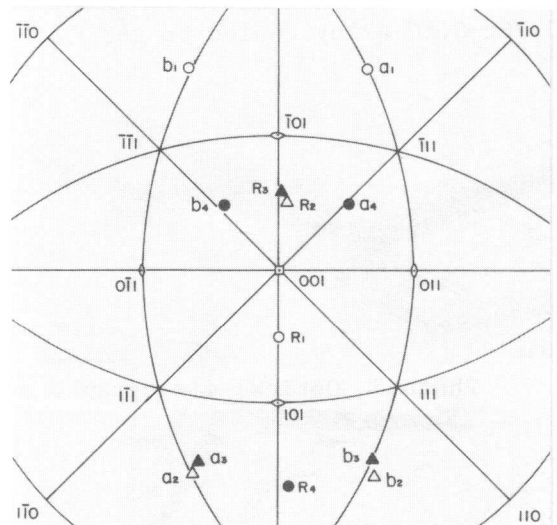
Fig.4 Stereographic representation of the observed habit planes.
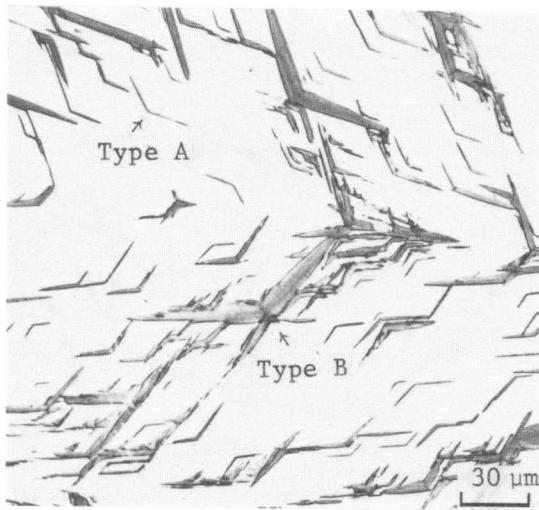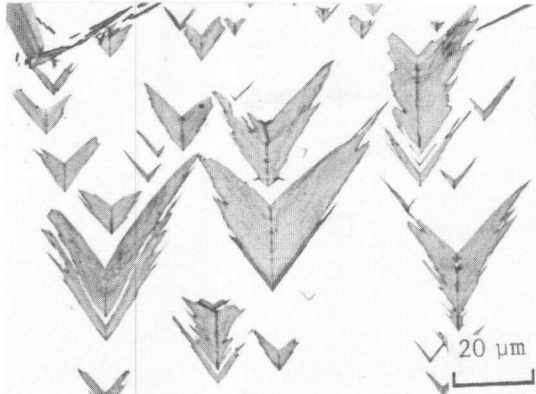

Photo.6 Optical micrograph of type C butterfly martensites in Fe-18Ni-0.7Cr-0.5C alloy cooled to 263 K.
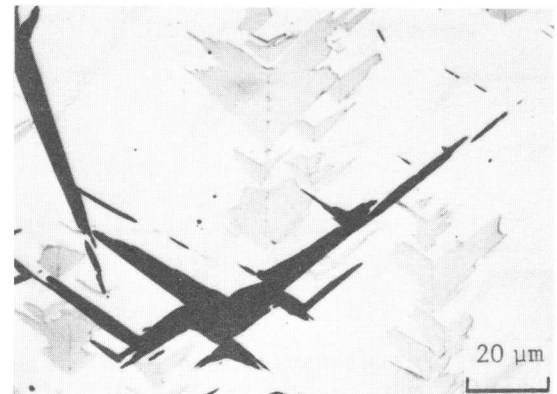
Photo.7 Fe-18Ni-0.7Cr-0.5C alloy cooled to 263 K and tempered at 373 K for 2 h.

Martensitic Plate Dimensions and Their Relationship to Austenitic Grain Size

J.R.C. Guimarães and J.C. Gomes

The evolution of the microstructure of Fe-31.1%Ni-0.02%C during martensitic transformation was studied by quantitative metallography. It was disclosed that the transformation in coarse-grained austenite leads to progressively smaller plates, whereas in finer-grained austenites the mean plate dimensions, particularly their volume, do not change appreciably. The aspect ratio of the martensitic plates ($\overline{t}/\overline{r}$) does not appear to depend upon the austenitic grain size. The applicability of available partitioning models is discussed in view of these experimental findings.

I. Introduction

In a previous paper (1), we have dealt with the influence of the austenitic grain size upon the processes of "spreading" (from grain to grain) and "fill-in" of the martensitic transformation (2,3) which are relevant to an understanding of the martensite kinetics. More recently (4) the adequacy of available partitioning models (5,6) in discribing the transformation behaviour of a coarse-grained Fe-Ni-C austenite was discussed. In the present work, we will consider the influence of the austenitic grain size on the martensite microstructure as a function of the volume fraction transformed. It should be pointed out, however that the lack of a thorough understanding of the microstructural evolution at this stage permits only an exploratory, rather than analytical, study.

II. Experimental Methods

The alloy sellected for this study was Fe-31.1%Ni-0.02%C. The routines followed in the preparation of the material are described elsewhere (1,4) and need not be repeated here.

The basic experimental approach was quantitative metallography (7). Volume fraction of martensite (V_v) and the surface area per unit volume of specimen of internal boundaries (S_v) were determined by point-counting and lineal analysis, respectively. The average volume of the martensitic plates was obtained with the aid of Fullman's equation (8) and the mean plate thickness ($\overline{t}$) from the ratio S_v^m/V_v, where S_v^m is surface area per unit volume of martensite mid-plane (6). This procedure was adopted in

---

Instituto Militar de Engenharia, Pça. Gen. Tibúrcio s/nº 22290 - Rio de Janeiro, RJ, Brazil.

preference to the one suggested by Fullman in order to alleviate the extent of the operator's influence. The determinations were systematically repeated to keep the statistical error of the mean below 20%.

III. Results and Discussion

(a) The Burst

The martensitic transformation in this alloy starts by a burst at sub-zero temperature. Both the temperature of the burst (M_b) and its magnitude are affected by changing the austenitic grain size (1). However the morphology of the burst is far more sensitive than the M_b to such a change, and this allowed an investigation of the burst as a function of grain size without much change in M_b as described in ref. (1). The material studied for this purpose had an average M_b of 221 K.

Reducing the austenitic grain size increases the heterogeneity of the burst on a microstructural scale, and decreases the fraction of transformed, Fig. 1(a), but the martensitic plate morphology is not noticeably affected. We describe the heterogeneity of the transformation by the parameter G_g which expresses the volume fraction of the alloy comprised of austenitic grains which have undergone some transformation (1). The data indicate that decreasing the austenitic grain size restricts the transformation to a relatively few grains grouped in "pockets".

The data of Fig. 1(b) show that decreasing the austenitic grain size produces a decrease in the mean radius of the plates formed in a burst. A mean radius ($\bar{r}$) of about 10 μm appears to be attained as a lower limit with decreasing grain size. The plot indicates that $\bar{r}$ might be about 40 μm in a single crystal, other things being equal. Moreover, $\bar{r}$ tends to be smaller than the austenitic mean linear intercept ($\equiv 2/S_v$), particularly at the largest grain sizes which suggests that obstacles other than austenitic grain and twin boundaries, exist in the matrix. However, in all the specimens, the largest plates were found to be generally limited in size by the austenitic grain and twin boundaries.

Another microstructural characteristic which appears relevant to a rationalization of the mode of the martensitic plate arrangement in the material is the extent of martensitic plates in surface contact with each other. The extent of such plate association (EPA) was found to be suitably described by:

$$EPA = x\ 100\ (1 - \frac{S_v^{m-a}}{2S_v^m}) \qquad (1)$$

which varies from zero ($S_v^{m-a} = 2S_v^m$ for separated disk-like plates) up to 100 at $V_v = 1$. Actually, EPA is analogous to Gurland's contiguity ratio discussed in ref. (7). An appreciable value of EPA at a small V_v is indicative of

MEAN LINEAR INTERCEPT LENGTH (µm)

MARTENSITE BURST CHARACTERISTICS

(a)

VOLUME FRACTION

g_g

V_v

(b)

MEAN PLATE RADIUS ($\bar{r}$) µm

$\langle M_b \rangle = 221$ K

(c)

E.P.A. %

DENSITY OF AUSTENITIC GRAIN AND TWIN BOUNDARIES (S_v) mm⁻¹
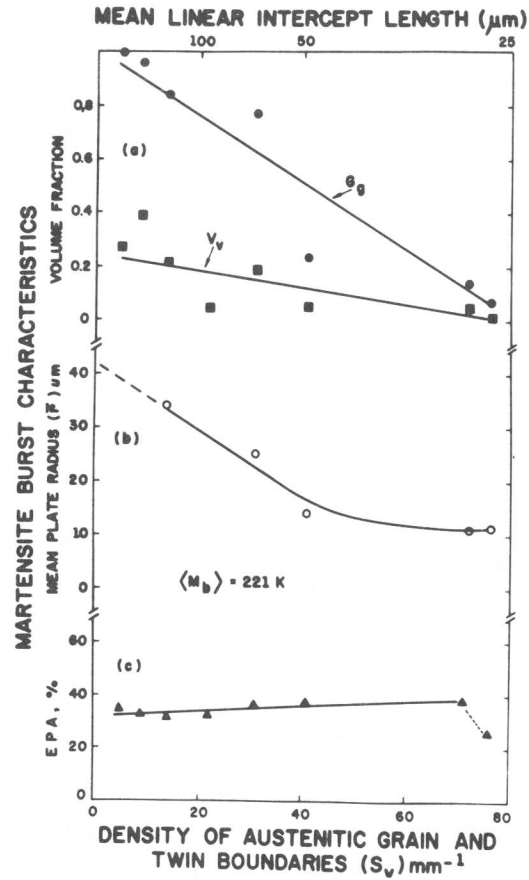
Fig. 1

Microstructural parameters related to the burst transformation as a function of austenitic grain size.

MARTENSITIC PLATES DIMENSIONS

(a)

MEAN PLATE VOLUME ($\bar{v}$) mm³

$S_v = 14$ mm⁻¹

$S_v = 41$ mm⁻¹

(b)

ASPECT RATIO ($\bar{t}/\bar{r}$)

$\blacksquare \rightarrow S_v = 14$ mm⁻¹
$\bullet \rightarrow S_v = 41$ mm⁻¹

MARTENSITIC VOLUME FRACTION (V_v)

Fig. 2

Variation of the mean plate volume and aspect ratio with the extent of martensitic transformation in coarse and medium grain-size austenites.

contacting martensitic plates due to autocatalysis.

The data of Fig. 1(c) show that EPA in the burst practically remains constant* with decreasing the austenitic grain size while V_V decreases. This can be taken as an indication of a small enhancement of plate association in the finer grained material, since the opposite behavior would be expected from geometrical considerations alone. The single anomalous EPA value observed at the finest grain size does not show this trend but it may be ascribed to higher experimental uncertainty because of the poorly resolved microstructure.

The observation that reducing austenitic grain size makes the spread of the burst from grain to grain more difficult may be interpreted as indicative that the mechanism of that process is related to the stress-field set-up by martensitic plates (1). However, the constancy of the EPA values, observed in the burst of specimens with different austenitic grain-sizes, suggests that in addition to the stress-field provided by martensitic plate there would exist a short-range mechanism of autocatalysis. In summary, it is proposed that in untransformed grains the reaction occurs at pre-existent nucleation sites whereas in the partially transformed grains the nucleation occurs at "autocatalytically produced" sites.

(b) Transformation During Cooling

Like other alloys of its class, the transformation of this Fe-Ni-C, below M_b, is a function of the temperature. The pertinent kinetic curves were presented in ref. (1), and the relevant comment for present purposes is that, like the burst, the transformation becomes more heterogeneous the finer the austenitic grain size. This poses a major experimental obstacle in that the mart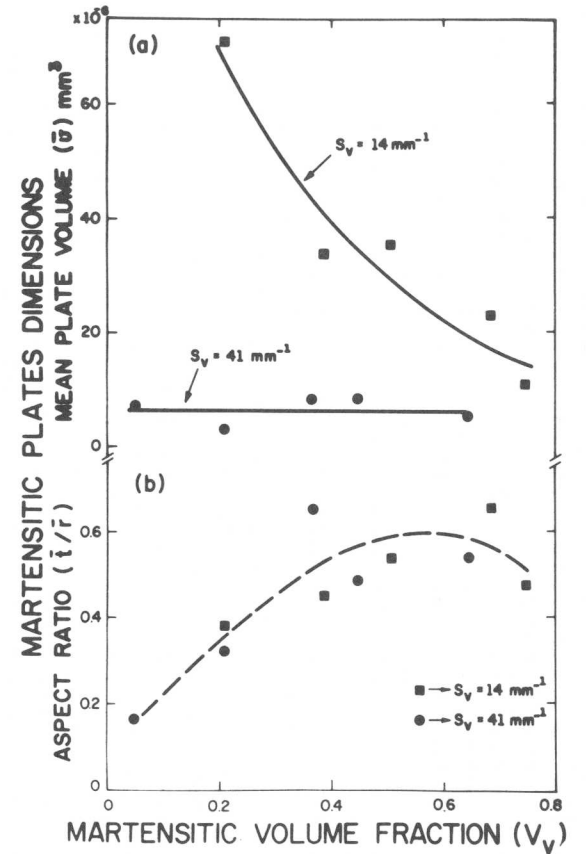ensitic features in the finer grained austenitic tend to be extensively clustered and difficult to resolve by optical microscopy. Consequently, the present study was limited to the medium and coarse grained conditions ($S_V = 41 \text{ mm}^{-1}$ and 14 mm^{-1}, respectively).

The plots of Fig. 2(a) show the variation of the mean martensitic plate volume with increasing fraction transformed. These data show that $\bar{v}$ is practivally constant in the finer grained material whereas it decreases with the progress of the transformation in the coarser grained material. These results are at variance with the findings of McMurtrie and Magee (9) who studied Fe-24/28%Ni-0.4%C with austenitic grains similar to that of our coarser grained austenite. They reported that the mean martensitic plate dimensions and in particular its volume, were independent of V_V up to a significant fraction transformed. Their data also show that the martensitic plates formed were considerably smaller than in our alloy despite the comparable (coarse)

---

*The data show an increasing tendency, however, that should be cautiously interpreted in view of the uncertainties involved in the determination of EPA.

grain sizes. At present it is not possible to provide a suitable explanation for the destinct transformation behaviors.

However it follows from our previous results (1) that the difference in transformation behavior between our finer and coarser grained alloy is surely related to the spread of the transformation through-out the austenitic grains. $G_g < 1$ leads to $\bar{v}$ = constant, while $\bar{v}$ decreasing with V_v is a consequence of $G_g = 1$. This subject matter is an important issue in the development of kinetics models as well as in the interpretation of the morphology and properties of quench-hardened steels.

Fisher et al (5) and Chen and Winchell (6) proposed models to describe the arrangements of the martensitic plates forming in the austenite. They are based upon the assumption of uniform transformation and lead to a dependence of $\bar{v}$ on V_v. On the other hand, Magee (2) suggested that autocatalysis should lead to the invariance of the mean plate volume. The experimental data from our coarser grained material described in ref. (4) and that from the finer grained austenite now described, show that the partitioning concepts (5,6) are not applicable to either case but Magee's hypothesis appears reasonable to describe the transformation behavior of the finer grained material.

The data of Fig. 2(b) indicate that the aspect ratio of the plates, estimated by $\bar{t}/\bar{r}$, varies with V_v but would not depend upon the austenitic grain size.

All these findings cannot be accounted for by the partitioning model described in refs. (5) and (6). Their failure is surely related to autocatalytic nucleation which causes the transformation morphology to depart from randomness both during the "spread" ($G_g < 1$) and "fill-in" stages, Fig. 3. It is germaine to mention that the aspect ratio of the plates can also be affected by autocatalysis through the nucleation of coupled plates.

Fig. 3

Optical photomicrograph. Coarse grained material cooled to 180 K. Notice the existance of parallel plates in extensive side-by-side contact.

In summary, it appears reasonable to conclude that geometrical partitioning concepts alone do not apply to reactions predominantly autocatalytic such as in the alloy studied. The consideration of the autocatalytic process should lead to a better description of the microstructural evolution than is possible through geometry alone.

IV. Conclusions

1. Austenitic grain size markedly affect the evolution of the microstructure during martensitic transformation. A small grain size favors the formation of plates of roughly constant (mean) volume. Coarser-grained austenites lead to a more uniform transformation with the formation of progressively smaller plates.

2. The aspect ratio of the martensitic plates is found to be practically grain-size independent; however, it varies significantly with the volume fraction transformed.

3. The findings are not compatible with the concept of geometric partitioning. It is suggested that considerations of autocatalytic nucleation may lead to a better description of the microstructural evolution.

References

(1) J.R.C. Guimarães and J.C. Gomes, Acta Met., 26, (1978) 1591.
(2) C.L. Magee in Phase Transformations, ASM, Metals Park (1968) p. 115.
(3) V. Raghavan, Acta Met., 17, (1969) 1299.
(4) J.R.C. Guimarães and J.C. Gomes, Met. Trans., 10A, (1979).
(5) J.C. Fisher, J.H. Hollomon and D. Turnbull, Trans.AIME, 185, (1949) 691.
(6) W.Y.C. Chen and P.G. Winchell, Met. Trans., 7A, (1976) 1177.
(7) R.T. DeHoff and F.N. Rhines, Quantitative Metallography, editors, McGraw-Hill, New York (1968).
(8) R.L. Fullman, Trans. AIME, 197, (1953) 447.
(9) D.G. McMurtrie and C.L. Magee, Met.Trans., 1, (1970) 3185.

Effect of Carbon on the c/r Ratio of Martensitic Plates

S. K. Gupta and V. Raghavan

This paper describes our experimental results of the effect of small variations in carbon content of an Fe-Ni-Mn alloy on the c/r ratio of martensitic plates formed during isothermal transformation. Specimens were doped with small quantities of carbon at 850°C. The grain size established by a prior annealing treatment at 1000°C did not change during doping. The lengths and thicknesses of plates in the transformed specimens were measured by quantitative metallography and the mean c/r ratios were computed using Fullman's relations. The c/r ratio decreases from 0.059 to 0.025 for an increase in the carbon content of the alloy from 0.019 to 0.033%. The corresponding isothermal transformation curves indicate that the transformation rate is drastically reduced due to the small increase in carbon content. Using the currently available models of the isothermal transformation kinetics, it is shown that the effect of carbon on the kinetics arises from the associated variation in c/r.

Introduction

It is well known that, in ferrous alloys of very low carbon content, the martensite start temperature M_s is particularly sensitive to carbon content. For example, in an Fe-30Ni alloy, the M_s decreases by as much as 12°C for a small increase of 0.01% in the carbon content of the alloy [1]. It is also known [2] that the growth rate of martensitic laths is drastically decreased for small increases in the carbon concentration. Here, we present some of our results on the effect of small variations in carbon content on the kinetics of isothermal martensitic transformation. The isothermal mode is particularly suitable for such studies, as the effect can be studied at a constant transformation temperature, thereby keeping the thermal effects constant.

Experimental Results

Specimens in the form of a wire of 1.5 mm diameter and 30 mm long of an Fe-22.4Ni-3.6Mn alloy were used in the experiments. They were sealed in an evacuated vycor tube and austenitized for 10 min at 1000°C. After the anneal, the sealed tube was cooled in air to yield a fully austenitic structure at room temperature. The grain size of the aus-

---

Materials Science Laboratory, Applied Mechanics Department, Indian Institute of Technology, New Delhi 110 029, India.

tenite after this treatment was 0.064 mm. This grain size did not change during the subsequent anneal at a lower temperature. The specimens were resealed in the vycor tube with a carbon source and reannealed at 850°C for various lengths of time ranging from 7 min to 240 min. During this anneal, the specimens were doped with different amounts of carbon.

The isothermal experiments were carried out at -192°C, which is below the nose of the C-curve for isothermal martensitic transformation in this alloy. The progress of the transformation was recorded by measuring the resistance of the specimen with an autobalance bridge (Wayne Kerr B642) with a four-terminal arrangement. The resistance values were calibrated by point counting to yield the fraction of martensite formed as a function of time at the reaction temperature. The isothermal transformation curves corresponding to different carbon contents are shown in Fig.1.

Micrographs of the transformed specimens were obtained from various parts spanning the entire cross-section of the wire. Typical micrographs from three specimens of different carbon contents are shown in Fig.2. The martensite has plate morphology. The mean reciprocal ($\bar{E}$) of the plate lengths, the mean reciprocal ($\bar{F}$) of the plate thicknesses and the mean ratio ($\bar{G}$) of the thickness-to-length of the plates were obtained by making at least 50 pairwise random measurements on each specimen. Assuming the plates to be thin cylindrical discs with radius $r \gg$ thickness $2c$, the mean semithickness-to-radius ratio ($\overline{c/r}$) is computed using the relation [3]:

$$(\overline{c/r}) = \frac{16\,\bar{E}}{3\,\pi^2\,\bar{F}} \tag{1}$$

The measured ($\overline{c/r}$) ratios are plotted as a function of carbon content in Fig.3.

Discussion

Fig.1 shows that the isothermal transformation rate decreases drastically for small increases in the carbon content of the alloy. After three hr of isothermal transformation, the martensite formed in a 0.019% carbon alloy is 32%, whereas in a 0.033% carbon alloy, the corresponding martensite content is only 2%. This big decrease in the transformation rate is in accord with the steep decrease in M_s observed in the athermal mode for small increases in carbon concentration.

A visual comparison of the microstructures of Fig.2 clearly indicates that, for the same plate length, the thickness decreases with increasing carbon concentration. Also, two different sets of 50 pairwise measurements of lengths and thicknesses of the plates yielded the same ($\overline{c/r}$), even though the average radius of the plates turned out to

-66-

be different for the two cases. Therefore, at least as a first approximation, it can be concluded that the $(\overline{c/r})$ ratio is a function of only the carbon content and not of the plate lengths. As shown in Fig.3, this ratio decreases by more than a factor of 2 from 0.059 to 0.025, as the carbon content is increased from 0.019 to 0.033%.

Schoen and Owen [2] observed a big decrease in the growth rate of lath martensite, for a small increase of carbon content in low carbon alloys. They explained this on the basis of a drag effect exerted by the carbon atmosphere on the movement of the dislocations at the austenite-martensite interface. A similar explanation is not feasible here, as the mobility of carbon atoms at -192°C is too small to account for the effect. At any rate, the plates in isothermal transformation at subzero temperatures grow very rapidly. The overall transformation kinetics here is controlled only by the nucleation rate and the mean volume of the plate per nucleation event. Furthermore, the decrease in the driving force for the transformation due to this small increase in carbon content is only about 2% [4]. It is insufficient to account for the decrease in the transformation kinetics or for the thinner plates. Likewise, the variation in the shear modulus is also too small to account for this effect. It is not known whether the yield strength of austenite or martensite can be the controlling factor. In view of these, we now turn our attention to the possible correlations between the transformation kinetics and the variation in the mean volume $\overline{v}$ of the martensitic plates that arises from the observed decrease in the $(\overline{c/r})$ ratio of the plates.

The isothermal martensitic transformation curves have been previously computed [5,6] by numerically integrating the following equation:

$$df/dt = \left[n_i + f(p-1/\overline{v}) \right] \nu \, \exp(-\Delta W_a/RT) \, v \qquad (2)$$

where f is the fraction of martensite formed,
       t is time,
       n_i is the initial number of nucleation sites,
       p is the autocatalytic parameter,
    ΔW_a is the activation energy for nucleation, and
       v is the instantaneous volume of the plates forming at martensitic fraction f.

Pati and Cohen [6] determined the average volume of the martensitic plates $\overline{v}$ metallographically and assumed a linear variation of $\overline{v}$ with f. The autocatalytic parameter p is found from the best fitting curve.

Using a similar approach, we have measured $\overline{v}$ at known values of martensitic fraction f. The transformation curves have been computed for different carbon contents, varying the $\overline{v}$ values only. Assuming a linear variation of $\overline{v}$ with f,

($\bar{v}=a-bf$), and noting that

$$v = \bar{v}^2/(\bar{v} - f \, d\bar{v}/df) \tag{3}$$

equation (2) can be integrated to yield

$$t = A \left[\ln \frac{\bar{v}}{n_i+pf-f/\bar{v}} + \frac{B}{\sqrt{Q}} \ln \frac{\sqrt{Q}+D+2pbf}{\sqrt{Q}-D-2pbf} - C \right] \tag{4}$$

where $A = 1/[2\,\nu \exp(-\Delta W_a/RT)]$,
       $B = n_i b+pa+1$,
       $D = n_i b-pa+1$,
       $Q = D^2+4n_i bpa$, and
       C is the constant of integration.

The curves computed from equation (4) are shown in Fig.4. These curves are similar in shape but not identical to the experimental curves shown in Fig.1. This deviation might be due to the assumption of a linear variation of $\bar{v}$ with f. More precise determinations of $\bar{v}$ at different fractions of martensite may resolve this point. The computed curves in Fig.4 clearly show that the decrease in the transformation rate arises mainly from the decrease in the $(\overline{c/r})$. For 3 hr of transformation time, the martensitic content computed for a 0.019% carbon alloy is 34%. This decreases to 2% for 0.033% carbon, closely agreeing with those found experimentally.

Conclusions

1. Small increases in the carbon content of an Fe-Ni-Mn alloy drastically reduces the rate of isothermal transformation of martensite.

2. Quantitative metallographic measurements show that the $(\overline{c/r})$ ratio of the martensitic plates decreases by more than a factor of 2 when carbon content increases from 0.019 to 0.033%.

3. The computed transformation curves indicate that the decrease in the transformation kinetics arises from the associated decrease in the $(\overline{c/r})$ ratio.

References

[1] V. Raghavan: Ph.D. Thesis, University of Sheffield,(1964).
[2] F.J. Schoen and W.S. Owen: Met. Trans., 2(1971), 2431.
[3] R.L. Fullman: Trans. AIME, 197(1953), 447.
[4] M.M. Rao, R.J. Russell and P.G. Winchell: Trans. AIME, 239(1962), 634.
[5] V. Raghavan and A.R. Entwisle: The Physical Properties of Martensite and Bainite, ISI, London, Special Report No. 93(1965), 29.
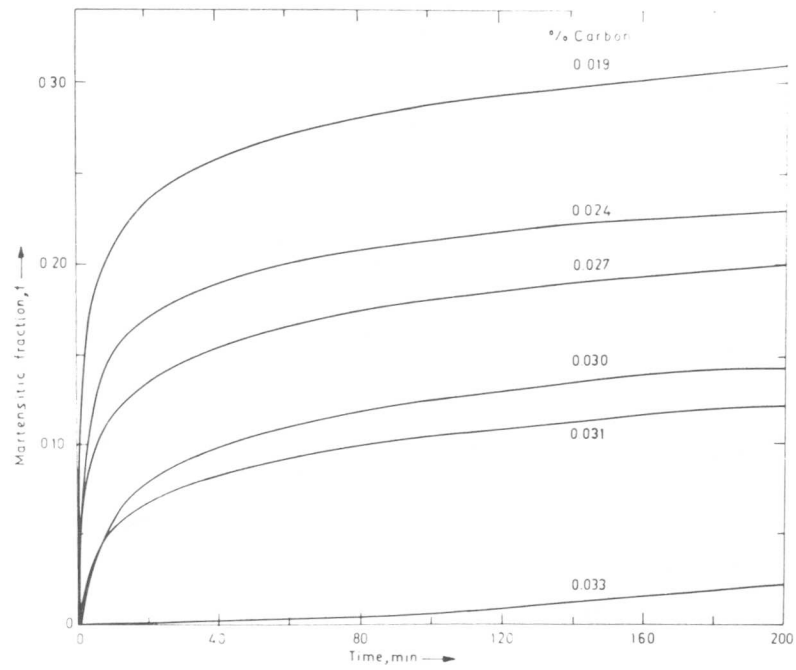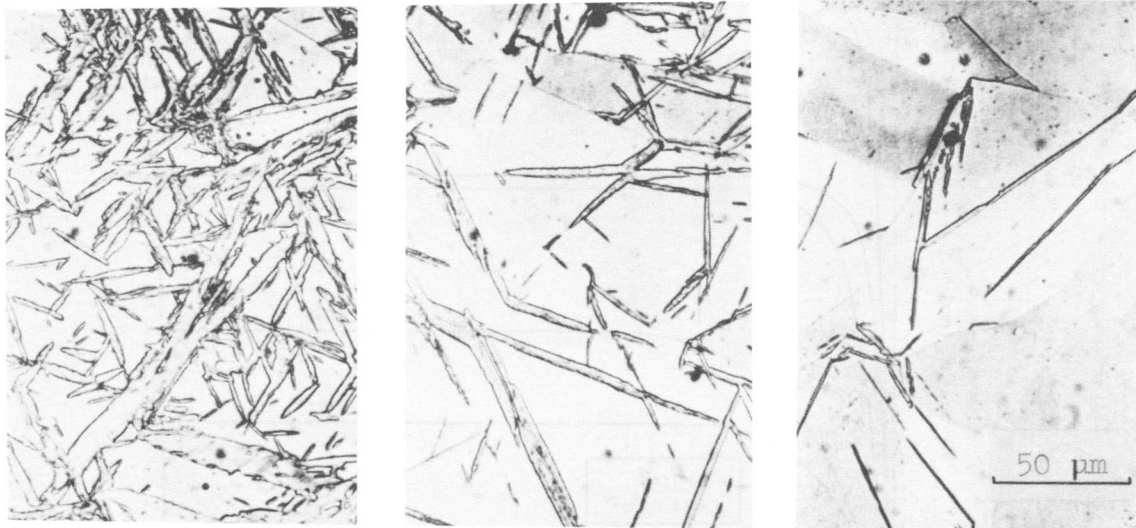[6] S.R. Pati and M. Cohen: Acta Met. 19(1971), 1327.

Figure 1 Isothermal transformation curves for an Fe-22.4Ni-3.6Mn alloy at -192°C for the carbon % indicated.

(a) 0.019% carbon   (b) 0.027% carbon   (c) 0.033% carbon

Figure 2 Microstructures obtained after isothermal transformation at -192°C.
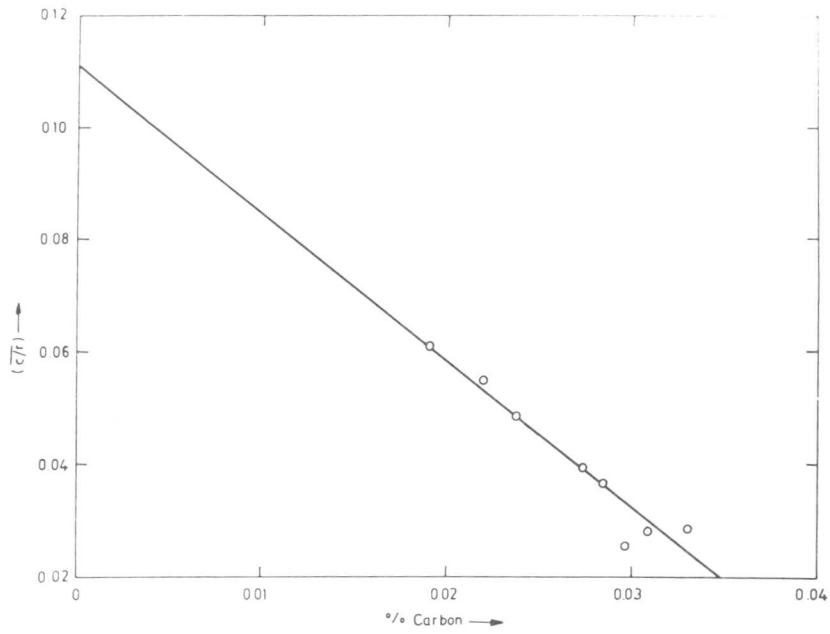
Figure 3 The $(\overline{c/r})$ ratio of isothermally formed martensitic plates as a function of carbon content of an Fe-22.4Ni-3.6Mn alloy.
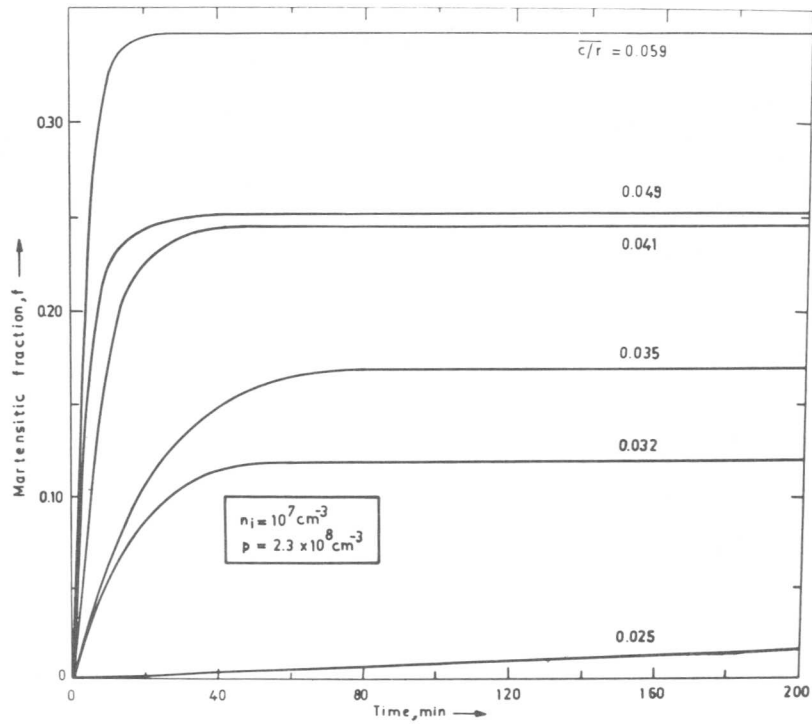

Figure 4 Computed transformation curves.

AXIAL RATIO ABNORMALITIES AND

MORPHOLOGY OF MARTENSITIC CRYSTALS IN STEEL

by

A. G. Khachaturyan,[*] A. F. Rumynina, and G. V. Kurdjumov[**]

1.   Introduction

X-ray studies of the crystal lattice parameters of austenite sin-
gle crystals of manganese steel show that the crystal lattice of
freshly formed martensite (κ' martensite) is orthostrombic rather than
tetragonal [1 to 3]. Heating to the rooms temperature results in the
increase of c parameters and decrease of b parameter which tends to the
parameter a. According to [4] these effects arise because C-atoms in
freshly formed martensite occupy O_x and O_y octahedral interstices as
well as O_z. The same conclusion has been made in the neutron diffrac-
tion study of Fe-8%Ni-1%C martensite [5].

The other interesting aspect concerning the structure of freshly
formed martensite of Fe-6%Ni-1%C steel has been reported by Oshima and
Wayman [6] and Oshima, Azuma, Fujita [7]. They observed the extra
spots on the electron diffraction pattern situated on the directions
[101] of either sites of the fundamental reflections. The distance be-
tween extra spots and fundamental reflections corresponds 5 to 6 inter-
planar distances $d_{(101)}$. This effect seems to be produced by the peri-
odical layer distribution of C-atoms. The phenomenological theories of
the martensitic transformation proposed by Wechsler-Lieberman-Reed [8]
and Bowler-Mackenzie [9] based on the Bain $\gamma \to \alpha$ rearrangement cannot
explain these phenomena as well nor can they give the satisfactory ex-
planation of the $(225)_A$ habit which has been observed in many alloys
and in the particular case [10] Fe-Mn-C alloy as well [11].

In this paper we shall try to give the explanation of all above-
mentioned phenomena introducing the heterogeneous mechanism of $\gamma \to \alpha$ re-
arrangement. The quantitative treatment will be based on the crystal
lattice rearrangement which is the combination of the conventional Bain
distortion and $[0\bar{1}1](011)_M$ slip and occurs in each mth $(011)_M$ plane of
the martensitic crystal.

We shall proceed from the conventional invariant plane conception
[8,9] according to which the habit plane is a macroscopically invariant
plane.

[*] Institute of Crystallography, Academy of Sciences of the USSR, Moscow
11733

[**] Solid State Physics Institute, Academy of Sciences of the USSR, Moscow

Employing this conception we shall explain the following results from the unique point of view:

(i) orthorhombic lattice of as-quenched Fe-Mn-C martensite and calculate its crystal lattice

(ii) increase of the axial ratio at heating to the room temperature.

(iii) the position of extra spots on the selected area diffraction pattern.

(iv) the $(225)_A$ habit and Kurdjumov-Sacks orientational relationships.

2. The habit plane orientation and orientational relationships

As mentioned above the proposed mechanism of $\gamma \rightarrow \alpha$ rearrangement is based on the combination of the Bain distortion and the elementary $\langle 0\bar{1}1\rangle(011)_M$ translation slip. This slip corresponds to the $\langle 11\bar{2}\rangle(111)_A$ shear in austenite. The accepted model is very close to the dislocation mechanism of the formation of martensite in Fe-Mn-C alloys with abnormally low axial ratio which has been proposed by Oshima and Wayman [6].

In this case the total change of the shape of austenite volume after accomplishment of $\gamma \rightarrow \alpha$ rearrangement id described by the matrix $\hat{A}$ which is a product of two matrices: the Bain distortion $\hat{B}$ and the $[0\bar{1}1](011)_M$ elementary slip $\hat{D}$. The result is

$$\hat{A} = \hat{D}\hat{B} \tag{1}$$

Since the $\gamma \rightarrow \alpha$ rearrangement in Fe-Mn-C steel produce the orthorhombic martensite the corresponding Bain distortion has also the orthorhombic symmetry

$$\hat{B} = \begin{pmatrix} n_1 & 0 & 0 \\ 0 & n_2 & 0 \\ 0 & 0 & n_3 \end{pmatrix} \tag{2}$$

where $\quad n_1 = \sqrt{2}\,\dfrac{a_M}{a_A}, \quad n_2 = \sqrt{2}\,\dfrac{b_M}{a_A}, \quad n_3 = \dfrac{c_M}{a_A}; \quad a_M, b_M, c_M \quad$ are

crystal lattice parameters of martensite, a_A-crystal lattice parameter of austenite, x,y,z axes are $[100]_A$, $[010]_A$, $[001]_A$ directions.

The matrix $\hat{D}$ describing the macroscopic shape change mode in martensite crystal is